CANADIAN THESES ON MICROFICHE

THÈSES CANADIENNES SUR MICROFICHE

National Library of Canada
Collections Development Branch

Canadian Theses on
Microfiche Service

Ottawa, Canada
K1A 0N4

Bibliothèque nationale du Canada
Direction du développement des collections

Service des thèses canadiennes
sur microfiche

NOTICE

The quality of this microfiche is heavily dependent upon the quality of the original thesis submitted for microfilming. Every effort has been made to ensure the highest quality of reproduction possible.

If pages are missing, contact the university which granted the degree.

Some pages may have indistinct print especially if the original pages were typed with a poor typewriter ribbon or if the university sent us an inferior photocopy.

Previously copyrighted materials (journal articles, published tests, etc.) are not filmed.

Reproduction in full or in part of this film is governed by the Canadian Copyright Act, R.S.C. 1970, c. C-30. Please read the authorization forms which accompany this thesis.

AVIS

La qualité de cette microfiche dépend grandement de la qualité de la thèse soumise au microfilmage. Nous avons tout fait pour assurer une qualité supérieure de reproduction.

S'il manque des pages, veuillez communiquer avec l'université qui a conféré le grade.

La qualité d'impression de certaines pages peut laisser à désirer, surtout si les pages originales ont été dactylographiées à l'aide d'un ruban usé ou si l'université nous a fait parvenir une photocopie de qualité inférieure.

Les documents qui font déjà l'objet d'un droit d'auteur (articles de revue, examens publiés, etc.) ne sont pas microfilmés.

La reproduction, même partielle, de ce microfilm est soumise à la Loi canadienne sur le droit d'auteur, SRC 1970, c. C-30. Veuillez prendre connaissance des formules d'autorisation qui accompagnent cette thèse.

THIS DISSERTATION
HAS BEEN MICROFILMED
EXACTLY AS RECEIVED

LA THÈSE A ÉTÉ
MICROFILMÉE TELLE QUE
NOUS L'AVONS REÇUE

Canada

NL 339 (r. 86/09)

DESIGN AND REALIZATION OF
A 17 GHz SINGLE BALANCED MIXER
IN INTEGRATED QUASI-PLANAR TECHNIQUE

by

Ihn S. Kim

A Thesis
presented to the University of Ottawa
in partial fulfillment of the
requirements for the degree of
Master of Applied Science
in
Department of Electrical Engineering

UNIVERSITÉ D'OTTAWA
UNIVERSITY OF OTTAWA

University of Ottawa requires the signatures of all persons using or photocopying this thesis. Please sign below, and give address and date.

ABSTRACT

This thesis describes the design and performance of a single balanced mixer realized in quasi-planar technology. Two beam lead GaAs Schottky barrier diodes, microstrip and fin line make the mixer circuit in planar form.

In the mixer, a 17 GHz signal is downconverted to 900 MHz intermediate frequency with 1 GHz bandwidth, pumped by 13 dBm of local oscillator power at 16.1 GHz. It has a conversion loss of typically 4 dB, reaching a minimum of 3.7 dB, and a 6.6 dB noise figure at the center frequency.

The mixer is realized on 0.03 in. thick RT/duroid 5880 substrate ($\varepsilon_r = 2.22$) which is suspended in the E-plane of a split-housing with inner dimensions of WR (62) waveguide. Both signal and LO ports contain exponential fin line tapers for broadband traisition to WR (62). A fin line-microstrip 180° hybrid assures frequency-independent in-phase signal excitation and out-of-phase LO excitation of the mixer diodes. The module also contains two microstrip filters: a band pass filter for the LO frequency and a low pass filter for the intermediate frequency. The diodes can be matched to the signal input using tunable microstrip stubs.

The purpose of this experimental design was to build a component which can be realized at low cost and in large quantities without loss of performance as compared with more conventional design.

ACKNOWLEDGEMENT

I would like to express my deep appreciation to my supervisor, Dr. W.J.R. Hoefer, for his continuous encouragement and expert guidance throughout this work. Thanks are also due to all the members of the Department of Electrical Engineering. I am also indebted to Mr. K. Verver and his staffs in CRC, Ottawa, for material assistance during measurements. Finally I would like to dedicate this thesis to Sookhe whose patience and support have made this effort possible.

GENERAL INTRODUCTION

Microwave and mm-wave receivers, in common use in communication, radar and even radiometric receivers, are invariably of the superheterodyne type. A mixer is an essential part in such a receiver. The function of a mixer is to pick up the signal with as little noise and interference as possible and convert it into a signal at a lower frequency (intermediate frequency) which can be subjected to a conversion from RF to baseband.

This thesis is directed toward realizing a 17 GHz single balanced mixer by using planar technology. Beam lead device technology and planar transmission media are bases for our mixer integration. The mixer has been designed to convert a signal at 17 GHz down to an intermediate frequency of 900 MHz with a bandwidth of ±500 MHz. It requires 13 dBm of local oscillator power at 16.1 GHz. Equipped with two GaAs Schottky barrier beam lead diodes, 4 dB conversion loss and 6.6 dB noise figure are obtained by measurements.

In Chapter 1, mixer principles are summarized. Following these we shall discuss mixer design. The chapter ends with an operation theory and summarizes the advantages of a single balanced mixer using a 180° hybrid.

Chapter 2 deals with technologies suitable for making a planar mixer. Beam lead GaAs Schottky barrier diodes, fin line and microstrip line providing not only simple and cost effective design but also very

good performance, are briefly discussed. Mixer diode selection criteria for low noise and conversion loss designs and basic E-field configurations of the two planar transmission media are also presented.

Chapter 3 presents design and realization details of the mixer. The design starts with a low frequency equivalent circuit for the overall configuration. Design information on components forming the unilateral and antipodal fin line transitions, microstrip filters, and planar 180° hybrid are explained. The computer generated circuit layout is also presented.

Chapter 4 reports measurement methods and results of the mixer performance realized in the technologies provided in Chapter 2. Two filter responses separating the IF and LO signals are briefly discussed. All measured mixer performances including transfer characteristic are displayed.

Chapter 5 concludes this thesis with brief comments about the mixer features and with suggestions and trends for mixer design and applications.

Finally, the appendix contains a fin line synthesis formula developed at the University of Ottawa for convenience.

TABLE OF CONTENTS

CHAPTER 1

MIXER PRINCIPLES

This chapter describes the physical mechanism of the mixing process and presents analytical expressions useful in mixer design. It also defines the most important concepts and parameters used to describe mixer performance.

1.1 Introduction

All microwave and mm-wave front-ends of the heterodyne type use some form or variation of nonlinear operation upon the desired input signal to produce a lower frequency output, which is ultimately demodulated further along the receiver chain. It is possible to use transistors (FET's) or diodes as the nonlinear element, depending upon application, but we shall restrict this thesis to quasi-planar single balanced mixers with two GaAs Schottky barrier diodes.

In this chapter we shall discuss the basic concepts related to a mixer in the receiver front-end.

1.2 Frequency Conversion

Mixing may be broadly defined as the conversion of a low power signal (RF) from one frequency to another by combining it with a local oscillator (high power) signal in a device which has a nonlinear i(v) transfer function. The nonlinear device is essential to the mixing process. By the principle of superposition, the addition of two frequencies in a "linear" device never results in additional (beat) frequencies: only the two original frequencies will exist in the Fourier spectrum of the resulting signal. If, however, the device is nonlinear, it will generate the sum and difference frequencies of the applied signals. These newly created frequencies will, in turn, beat with each other and with the originally applied signals, to create still more frequencies, and so on ad infinitum. The spectrum of the output voltage from such a nonlinear device may, therefore, be exceedingly

complex.

The usual requirement for a mixer is that it convert energy at an RF signal frequency to a lower intermediate frequency. (See Figure 1-1(a)). In practice the incoming signal, mixing with the local oscillator and its harmonics, generates a whole spectrum of mixing products. (See Figure 1-1(b)).

The input-output relationship of any general nonlinear element can be expressed by a Maclaurin series

$$B_{out} = \sum_{n=0}^{\infty} K_n B_{in}^n \tag{1.1}$$

where B_{out} is the output quantity and B_{in} is the input quantity.

Most devices used as mixing elements in frequency converters do not have exact square-law characteristics, i.e. their transfer function contains higher than second order terms. Nevertheless, for the sake of analysis we will assume throughout Chapter 1 that mixer diodes have an ideal square-law characteristic.

When a voltage is applied across a nonlinear resistance, the current through the nonlinear resistance, can then be expressed as a Maclaurin series of voltage

$$i = \sum_{n=0}^{\infty} K_n V^n \tag{1.2}$$

The voltage is the sum of the local oscillator and signal voltages, V_{LO} and V_s. If $V_s = A_s \cos\omega_s t$ and $V_{LO} = A_{LO}\cos\omega_{LO} t$,

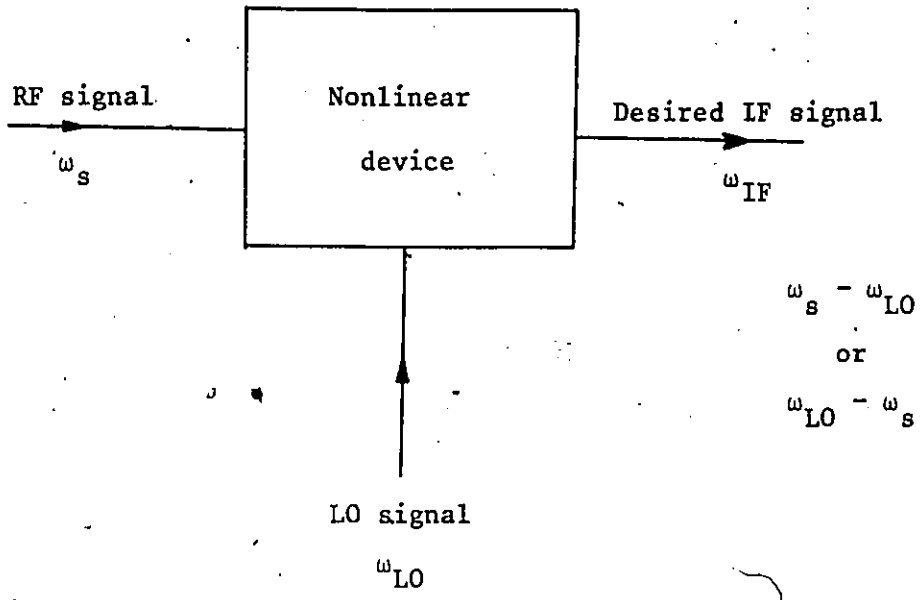

Figure 1-1(a). Block diagram of a mixer.

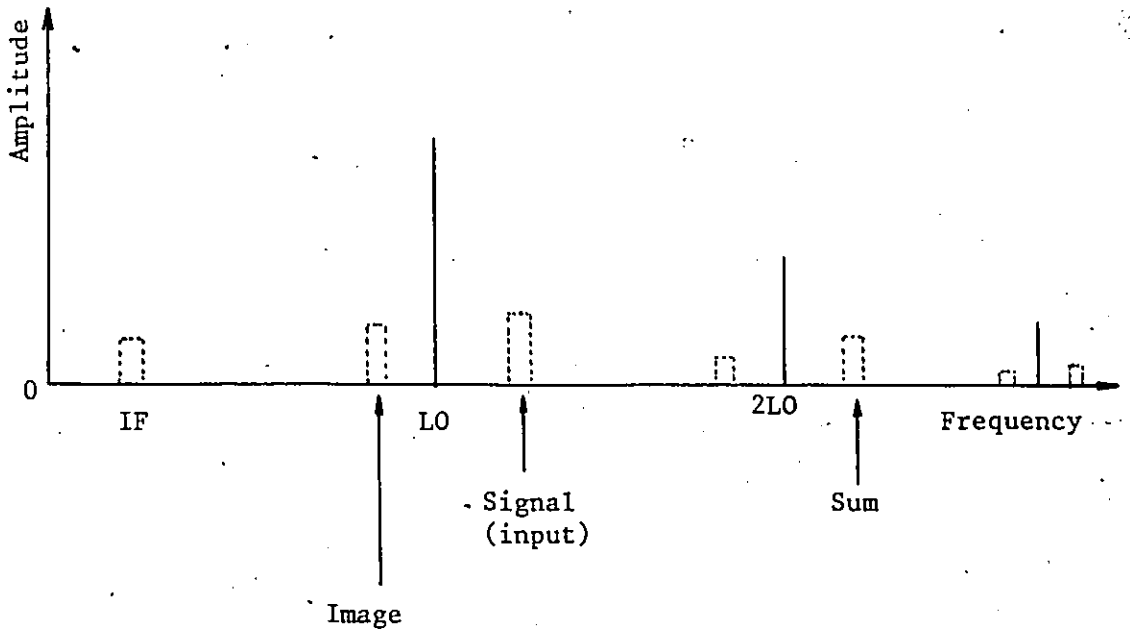

Figure 1-1(b). Spectrum diagram showing the lower order mixing products in a mixer.

then

$$V = V_s + V_{LO} = A_s \cos\omega_s t + A_{LO}\cos\omega_{LO} t \tag{1.3}$$

where A_s --- amplitude of signal voltage

A_{LO} -- amplitude of local oscillator voltage

ω_s --- signal frequency

ω_{LO} -- local oscillator frequency

Substituting (1.3) into (1.2), (1.4) yields

$$i = \sum_{n=1}^{\infty} K_n (A_s \cos\omega_s t + A_{LO}\cos\omega_{LO} t)^n \tag{1.4}$$

where the DC term is neglected. Eqn.(1.4) is an expression combining the various currents flowing at the different frequencies in the nonlinear element. The amplitudes of all the harmonics are proportional to their coefficients of the polynomial. From (1.4) the general frequency content of the mixing product can be characterized by

$$\omega_{m,n} = n\omega_s \pm m\omega_{LO}$$

where $n,m \geq 1$

While the higher order terms contribute intermodulation and cross modulation terms, i.e., second and higher order terms generate higher order harmonics, mixer analysis uses the principle that the second order term is responsible for generation of the desired converted

output. Thus the fundamental mixing products $\omega_s \pm \omega_{LO}$ are represented by the second term

$$K_n[A_s^2(1 + \cos 2\omega_s t) + 2A_s A_{LO}(\cos(\omega_s - \omega_{LO})t + \cos(\omega_s + \omega_{LO})t) + A_{LO}^2(1 + \cos 2\omega_{LO} t)]/2 \qquad (1.5)$$

where $\omega_s - \omega_{LO}$ = IF FREQUENCY

$\omega_s + \omega_{LO}$ = SUM FREQUENCY

In practice the third and higher order terms are usually neglected because the amplitudes of those harmonics are small. However, the mixing product of the second LO harmonic and the RF signal should be considered. The two products of this mixing process are given by

$$a \cos\omega_s t \cdot b \cos 2\omega_{LO} t = \frac{\overline{ab}}{2}[\cos(2\omega_{LO} - \omega_s)t + \cos(2\omega_{LO} + \omega_s)t] \qquad (1.6)$$

The two frequencies produced are $\omega_I = 2\omega_{LO} - \omega_s$ (the "image frequency") and $2\omega_{LO} + \omega_s$. See Figure 1-2.

Thus only a fraction of the incoming energy is transferred to the IF. It follows that, if the generation of these unwanted mixing products can be prevented, a larger fraction of the incoming energy may be converted to the IF. This can be achieved by designing the mixer circuitry such that it presents reactive terminations at the frequencies of these unwanted products. If the circuitry is correctly designed, more energy is transferred to the IF and thus conversion loss is

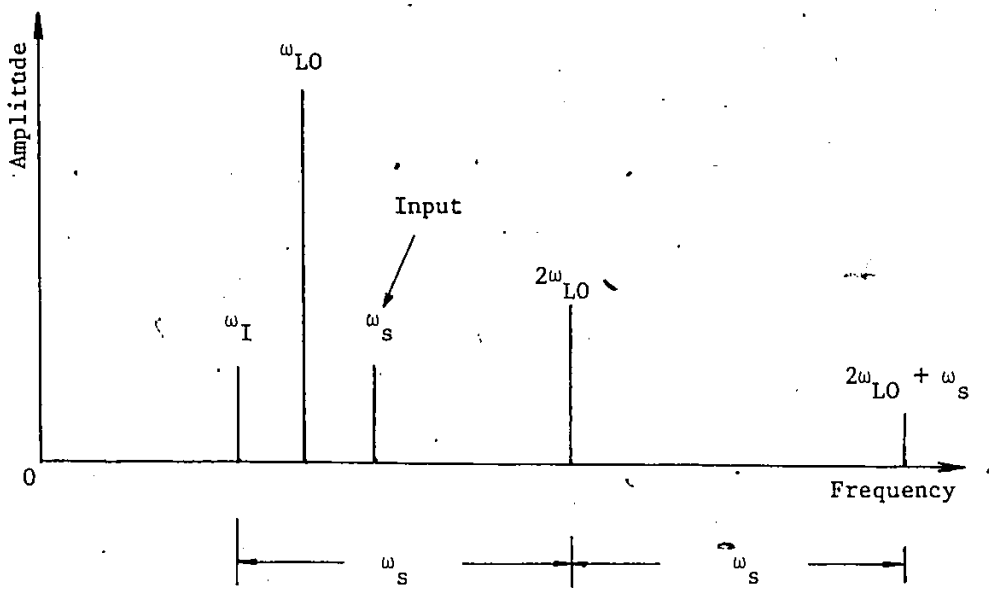

Figure 1-2. Spectrum diagram showing the two mixing products generated by the signal input and the LO second harmonic.

reduced [1].

If the mixer in question presents a matched termination at all frequencies considered, and if the diode has a cut-off frequency well above this frequency range, it is reasonable to assume that identical amounts of energy are transferred at the sum frequency and the IF. Thus, if energy at the sum frequency can be fully recovered and converted to IF, the conversion loss is reduced by 3 dB.

1.3 Conversion Loss

The frequency conversion process in a mixer is accompanied by power loss and the generation of excess noise. The noise problem will be explained in the next section.

The conversion loss L_c of a mixer is defined as follow [1]:

$$L_c = \frac{P_s}{P_{IF}} = \frac{\text{power available from signal source}}{\text{power delivered to IF load}}$$

It is one of the most important parameters since it measures the efficiency with which a mixer converts RF energy to IF energy.

Theoretically, the conversion loss in a balanced mixer is not smaller than in a single-ended mixer. Balanced and single-ended mixers have identical conversion loss if each diode in the balanced mixer has an impedance equal to that in the single-ended mixer. Therefore, the following analysis concerns single-ended mixers, but the results are directly applicable to the balanced configuration as well.

The conversion loss in microwave and mm-wave mixers is influenced by many factors. But if a suitable diode is selected, its optimum

conversion loss in general is degraded and can be represented approximately by the product of the three types of losses as follows:

L_1 diode parasitic loss due to its junction capacitance and spreading resistance

L_2 mismatch loss due to impedance mismatch at RF and IF ports

L_3 intrinsic junction loss of the ideal diode.

$$L_c = L_1 \cdot L_2 \cdot L_3 \tag{1.7}$$

The first type of conversion loss L_1, is the loss associated with the parasitic elements of the diode, the junction capacitance, and spreading resistance. Defined as the ratio of the signal power (RF) to the power delivered to the average barrier resistance (the power which is converted) of the diode at the signal frequency [2], with reference to the equivalent circuit of Figure 1-3 [3], it can be seen that at an signal angular frequency ω_s.

$$L_1 = \frac{R_s + R_B/[1 + (\omega_s C_B R_B)^2]}{R_B/[1 + (\omega_s C_B R_B)^2]} \tag{1.8}$$

Thus, when simplified, the diode parasitic conversion loss L_1 is given by

$$L_1 = 1 + \frac{R_s}{R_B} + \omega_s^2 C_B^2 R_s R_B \tag{1.9}$$

where R_B is the barrier (junction) resistance, ω_s is the signal angular frequency, C_B is the barrier capacitance, and R_s is the

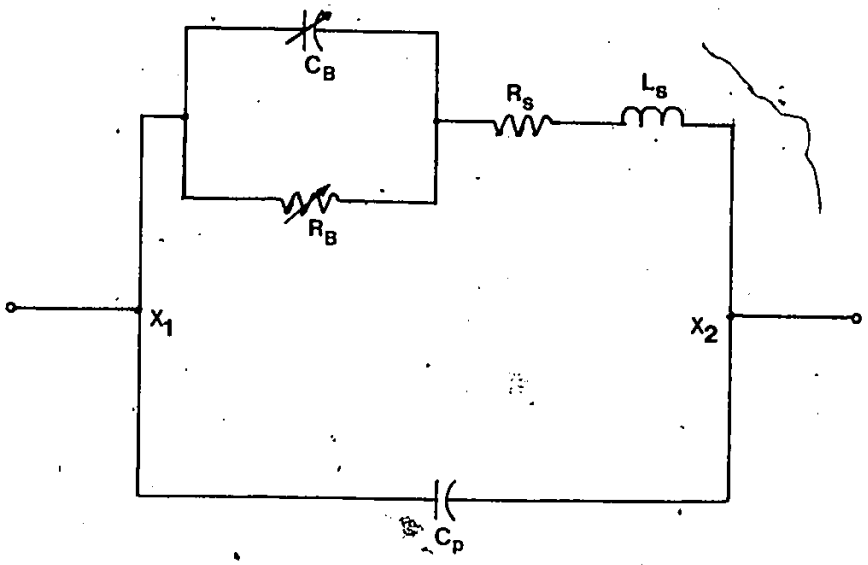

a) Parallel equivalent circuit

b) Series equivalent circuit

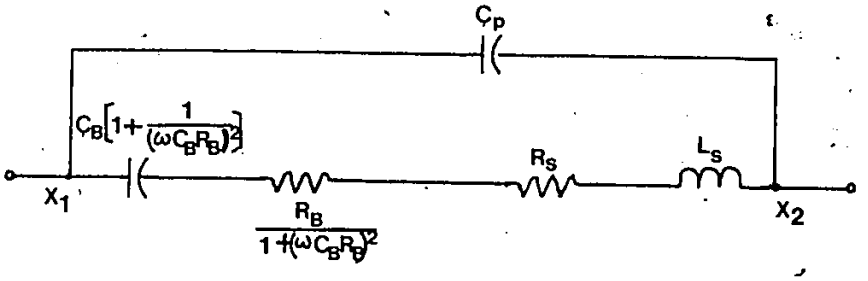

Figure 1-3. Simple equivalent circuits for Schottky-barrier diode.

series (spreading) resistance. The spreading resistance R_s is the resistance resulting from constriction of current flow in the semiconductor near the contact.

If the nonlinear rectifying element is represented by R_B only, the conversion loss decreases and approaches a value of 3 dB (image matched) as the LO power (and therefore the rectified diode current) is increased. However, the effect of C_B on the conversion loss is most pronounced at low values of LO drive; as this is decreased, the value of R_B increases, more current is shunted by C_B, and therefore the conversion loss increases. The effect of R_s on conversion loss, however, is most pronounced at high levels of LO drive; as the LO drive is increased, the value of R_B is decreased, and more power is dissipated in R_s, and again the conversion loss increases. Obviously there is an optimum drive condition for maximum voltage across R_B and maximum power at R_B, and minimum conversion loss will occur when R_B is equal to $\frac{1}{\omega_s C_B}$, or

$$L_{1(\min)} = 1 + 2\omega_s R_s C_B \qquad (1.10)$$

Further increase in the drive results in increased L_1 due to dissipation in R_s, while decreasing drive also increases insertion loss due to the shunting effect of the junction capacitance.

The second type of loss, the mismatch loss L_2, depends on the degree of the impedance match at the RF and the IF ports. The mixer diode is often matched to the LO power in a fixed or tunable mount.

But this LO port match is not critical. However, since only the RF signal power is converted to the intermediate frequency, it is more important to match the diode at the signal frequency and at the IF output frequency. The IF impedance Z_{IF} appears at the mixer output terminals when the diode is biased by a local oscillator. This impedance is a function of the LO driving power level, the diode properties, and the circuit parameters.

When the match is different from optimum match at the RF and the IF ports, the available RF signal power level at the diode and the IF power level are reduced. At the RF port, the mismatch loss L_2 (RF) can therefore be expressed by the following ratio:

$$L_2 \text{ (RF)} = \frac{P_s}{P_s - P_{sR}} \tag{1.11}$$

where P_s is the input signal power and P_{sR} is the reflected signal power due to mismatch. The mismatch loss L_2 (RF) becomes

$$L_2 \text{ (RF)} = \frac{1}{1 - |\Gamma|^2} = \frac{(1 + \rho_s)^2}{4\rho_s} \tag{1.12}$$

where ρ_s is the VSWR at RF port. As at the RF port, the mismatch loss L_2 (IF) at the IF port is

$$L_2 \text{ (IF)} = \frac{(1 + \rho_{IF})^2}{4\rho_{IF}} \tag{1.13}$$

where ρ_{IF} is the VSWR at the IF port. The total mismatch loss L_2 of a mixer is given by

$$L_2 = L_2\,(RF) \cdot L_2\,(IF) = \frac{(1+\rho_s)^2}{4\rho_s} \cdot \frac{(1+\rho_{IF})^2}{4\rho_{IF}} \qquad (1.14)$$

The third type of loss is the intrinsic junction loss of a mixer diode. It depends mainly on the terminating conditions at the image frequency and the form of the diode i(v) characteristic. It can be shown that L_{3min} approaches a limiting value of 3 dB under broadband condition. This means that one half of the RF power goes to the IF port and the remaining power is dissipated in the resistance (loss) at the image frequency. Therefore, it is possible to provide the image frequency with a reactive (lossless) termination such that the image frequency power recombines with the LO power at the diode in such a way as to reduce the overall conversion loss. Theoretically a minimum conversion loss of 0 dB is obtainable for open or short-circuited image. A mixer of this type is called an image-enhanced mixer.

A resistive diode, i.e., a diode in which energy storage effects are minimal, is typically characterized by

$$i = I_{sat}\,(e^{\alpha v} - 1) \qquad (1.15)$$

The small signal conductance for this diode is given by

$$g = \frac{di}{dv} = \alpha I_{sat} e^{\alpha v} = \alpha(i + I_{sat}) \cong \alpha i \qquad (1.16)$$

where $i >> I_{sat}$.

In the above equation I_{sat} is the diode saturation current and $\alpha = q/KT \cong 40\ \text{Volt}^{-1}$ at room temperature.

In practice, g(t) is obtained by pumping the diode with the local oscillator, and usually, V_{LO} is much greater than V_s. Then the signal at ω_s sees the diode approximately as a linear, periodically time-varying resistance [4] although nonlinear distortion always exists to some extent.

The voltage across the diode imposed by the local oscillator is

$$V_d = V_{LO} \cos\omega_{LO}t \tag{1.17}$$

The current through the diode can contain any harmonic of ω_{LO}. Eqn.(1.15) gives

$$i_d = I_{sat}[e^{\alpha(V_{LO} \cos\omega_{LO}t)} - 1] \tag{1.18}$$

The pumping voltage across the diode is a sinusoidal signal while i_d can contain all harmonics since the imbedding network short-circuits all the LO harmonics. Expanding (1.18) in a Fourier series yields

$$\frac{1}{2\pi}\int_0^{2\pi} e^{A\cos X} \cos(nX)\,dX = \mathbb{I}_n(A) \tag{1.19}$$

where $\mathbb{I}_n$ is the modified Bessel function of the first kind of order n. Eqn.(1.18) then becomes

$$i_d = I_{sat}e^{\alpha}[\mathbb{I}_0(\alpha V_{LO}) + 2\mathbb{I}_1(\alpha V_{LO}) \cos\omega_{LO}t + 2\mathbb{I}_2(\alpha V_{LO}) \cos 2\omega_{LO}t + \cdots] - I_{sat} \tag{1.20}$$

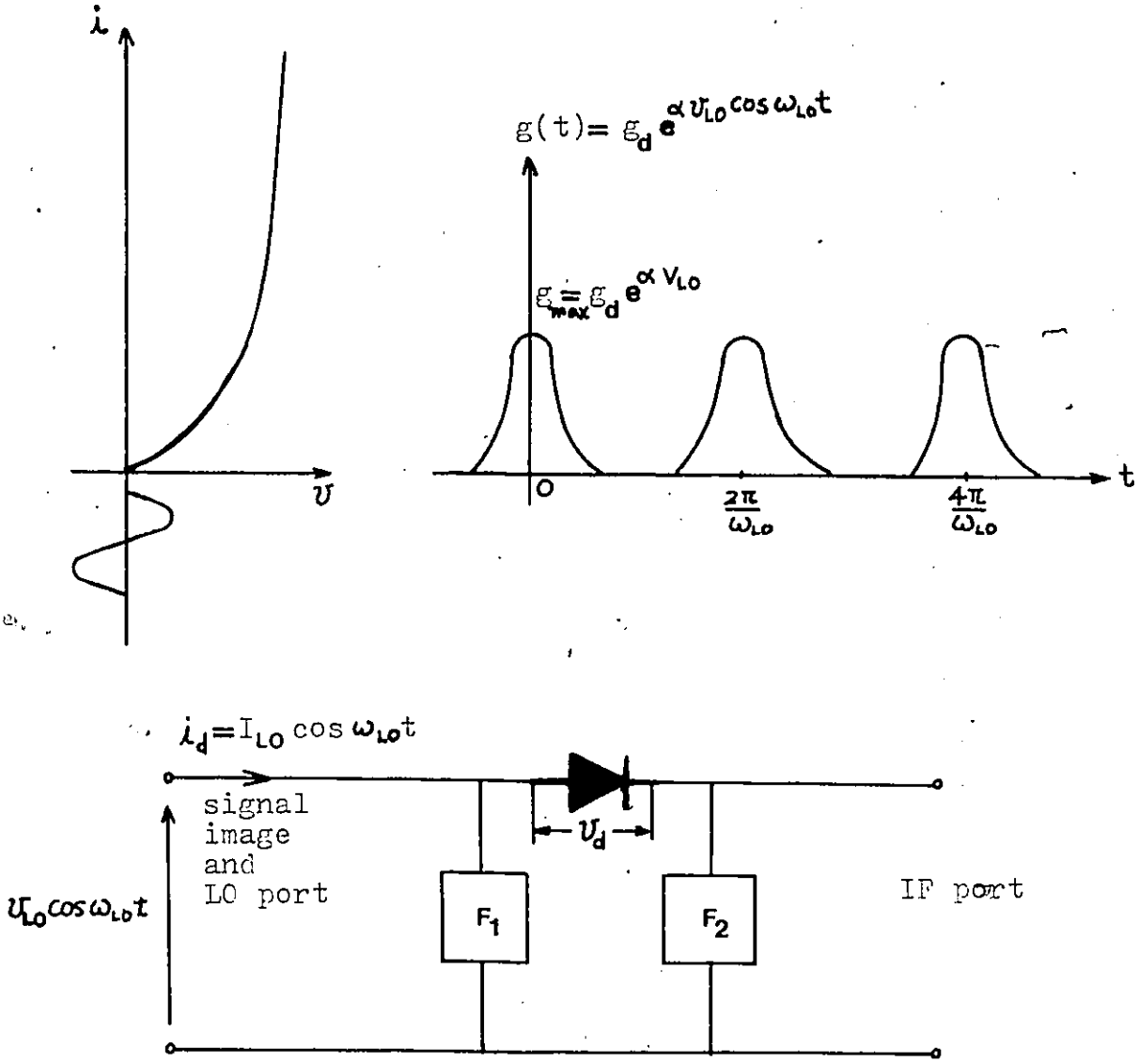

F_n are ideal parallel resonators,

F_1 is for ω_s and ω_{LO}, F_2 for ω_I

Figure 1-4. An exponential diode pumped by a sinusoidal LO voltage g(t).

If the reverse saturation current is neglected, it follows that

$$I_{dc} = I_{sat} e^{\alpha} I_0(\alpha V_{LO}) \cong I_{sat} \frac{e^{\alpha V_{LO}}}{\sqrt{2\pi\alpha V_{LO}}} , \qquad (1.21)$$

if $\alpha V_{LO} >> 1$ or $\gtrsim 20$ [5]

The amplitude of the LO component of the diode current is

$$I_{LO} = 2I_{sat} e^{\alpha} I_1(\alpha V_{LO}) \cong 2I_{dc}, \text{ if } \alpha V_{LO} >> 1 \text{ or } \gtrsim 20 \qquad (1.22)$$

The small signal time-varying conductance waveform can be calculated from (1.16), (1.18) and (1.20) to be

$$g(t) = \alpha I_{sat} e^{\alpha V_{LO} \cos\omega_{LO} t} = g_0 + 2g_1 \cos\omega_{LO} t + 2g_2 \cos\omega_{LO} t + \cdots\cdots \qquad (1.23)$$

where

$$g_0 = \alpha I_{sat} e^{\alpha} I_0'(\alpha V_{LO})$$

$$g_1 = \alpha I_{sat} e^{\alpha} I_1(\alpha V_{LO})$$

$$g_2 = \alpha I_{sat} e^{\alpha} I_2(\alpha V_{LO}) \qquad \text{etc.}$$

Different values of optimum conversion loss L_3 are found, depending on whether the image frequency $\omega_{image} = 2\omega_{LO} - \omega_s$ is short- or open-circuit. Thus, the optimum conversion loss L_3 with an open-circuit at the image frequency [4] is

$$L_3^{opt} = \frac{1 + \sqrt{1 - \varepsilon'}}{1 - \sqrt{1 - \varepsilon'}} \cong 1 + \sqrt{\frac{2}{\alpha V_{LO}}} \quad , \text{ if } \alpha V_{LO} >> 1 \tag{1.24}$$

where

$$\varepsilon' = \frac{\varepsilon}{1 - \varepsilon}\left(\frac{1 - \theta}{1 + \theta}\right)$$

and

$$\varepsilon = \left(\frac{g_1}{g_0}\right)^2 = \left[\frac{I_1(\alpha V_{LO})}{I_0(\alpha V_{LO})}\right]^2 \cong 1 - \frac{1}{2V_{LO}} + 0\left[\frac{1}{(\alpha V_{LO})^3}\right] ,$$

$$\theta = \frac{g_2}{g_0} = \frac{I_2(\alpha V_{LO})}{I_0(\alpha V_{LO})} \cong 1 - \frac{2}{\alpha V_{LO}} + \frac{1}{(\alpha V_{LO})^2} \quad \text{if } \alpha V_{LO} >> 1$$

The above approximate results are taken from the works of Saleh and Barber [4] [6], and the optimum conversion loss L_3 can be represented by Figure 1-5.

The third type of conversion loss in the mixer is

$$L_3 \simeq 1 + \sqrt{2}/\sqrt{\alpha V_{LO}} \qquad \text{(dB)} \tag{1.25}$$

Therefore the overall conversion loss is the sum of the above mentioned three types of the conversion losses as shown in (1.7). For specific diodes, L_1 is fixed and cannot be improved. Consequently, circuit optimization should be concentrated on the reduction of mismatch loss (L_2) and intrinsic junction loss (L_3). But if a perfect matched condition is realized, (1.7) becomes

$$L_c = L_3(1 + 2\omega_s R_s C_B) \tag{1.26}$$

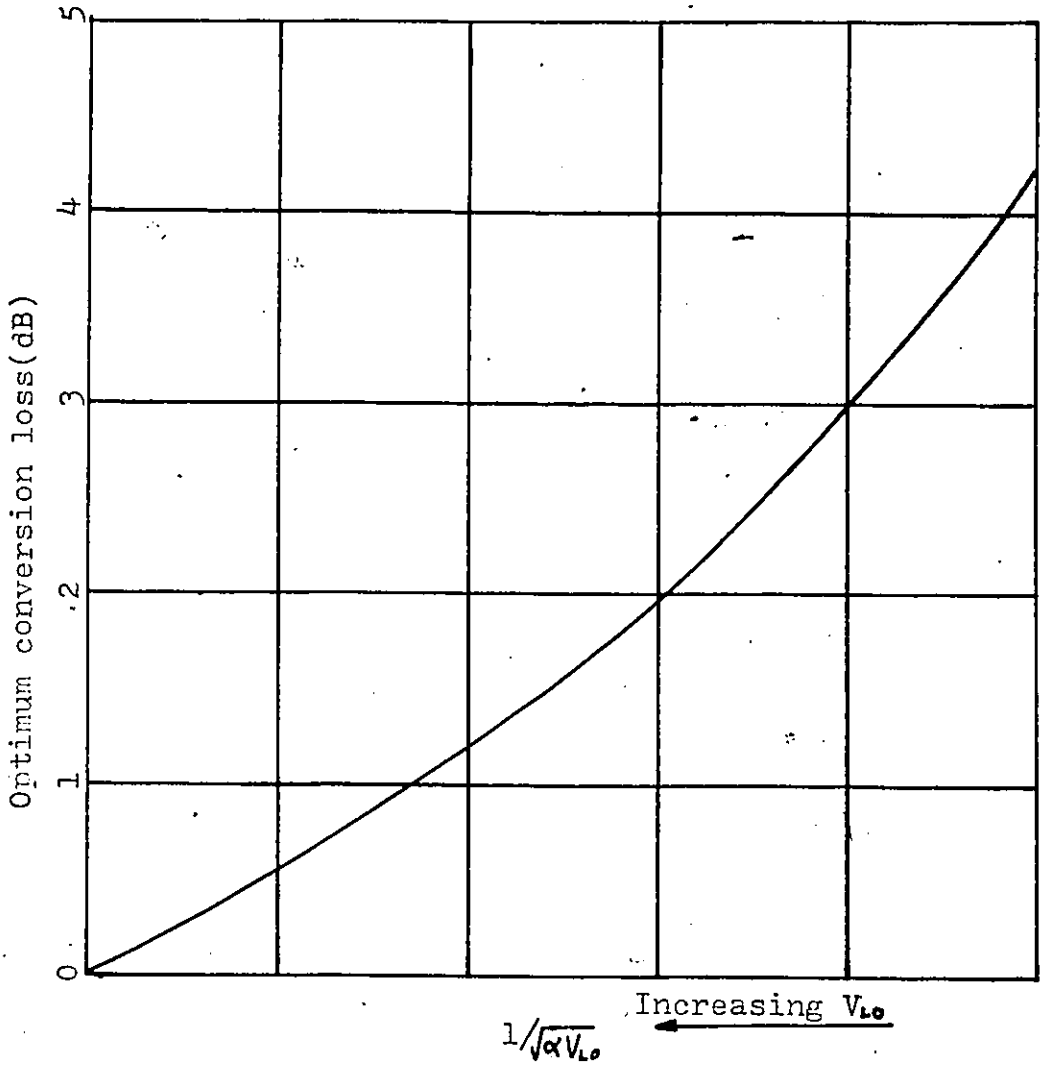

Figure 1-5. The optimum conversion loss for a single exponential diode with open-circuit termination at image frequency [4].

Thus at any frequency at which the barrier capacitance is significant, the product of the parasitics (spreading resistance and barrier capacitance) must be minimized for the optimum conversion loss. The conversion loss can be approximated by

$$L_c \propto C_B R_s \tag{1.27}$$

It should be noted that this is consistent with the cut-off frequency expression of the mixer diode in Chapter 2.

1.4 Mixer Noise Figure

If there were no noise present in the receiver, it would be possible to detect any signal, no matter how small, by providing the receiver with sufficient amplification. This cannot be achieved in practice since noise is always present, and unlimited amplification of weak signals amplifies noise as well.

The use of Schottky barrier diodes for microwave and mm-wave mixers is limited by several types of noises in the diodes, since it is the diode noise characteristic which limits the sensitivity of the mixer receiver. So, the noise figure of a mixer is an important mixer parameter. If the mixer is located right after the receiving antenna the overall receiver noise figure depends mainly on the mixer noise figure. Therefore to obtain low noise figure in a receiver, the noise figure of the mixer should be reduced as much as possible, especially in the mm-wave range where no cost-effective low noise amplifiers for receiver front-end exist. Since reduced noise level

at the front-end allows less transmitter power and receiving antenna gain, there is a high economic return for better receiver noise figure.

Noise at the receiver output is the sum of the noise arising from the input source, noise generated within the mixer diode, and noise from the following IF amplifier. The noise figure F_o is defined as

$$F_o = \frac{S_i/N_i}{S_o/N_o} \qquad (1.28)$$

where S_i = available receiver (mixer + IF amplifier) input signal power

S_o = available receiver (mixer + IF amplifier) output signal power

N_i = available receiver (mixer + IF amplifier) input noise power

N_o = available receiver (mixer + IF amplifier) output noise power

Any practical mixing device will not only attenuate the input noise, but also introduce some additional noise. N_e represents this additional noise at the output, and is referred to as the excess noise. Thus,

$$N_o = N_i/L_c + N_e \qquad (1.29)$$

where L_c is the conyersion loss of the mixer.

Thus (1.28) may be rewritten

$$F_o = \frac{S_i / N_i}{\frac{S_i/L_c}{N_i/L_c + N_e}} \qquad (1.30)$$

This simplifies to

$$F_o = \frac{N_i/L_c + N_e}{N_i/L_c} = \frac{\text{(output noise from input) + (excess noise)}}{\text{(output noise from input)}}$$

$$= \frac{N_o}{N_i/L_c} \qquad (1.31)$$

F_o in (1.31) is dependent upon the input noise level N_i. The input noise is usually defined for the purpose of noise figure measurement by

$$N_i = kT_oB \qquad (1.32)$$

where k is Boltzmann's constant, B is the bandwidth being considered, and T_o is the room temperature (290°K).

The usual requirement for a mixer is that it takes energy at the signal frequency and convert it to IF. There is however, another input frequency at which energy may enter the mixer and, when mixed with the fundermental of the LO, produce energy at the IF. This is referred to as the "image". Noise from the RF source at both signal and image frequencies enters the mixer and is converted to IF. Thus, there are two separate source kT_oB at the input as shown in Figure 1-6.

$$N_o = \frac{2kT_oB}{L_c} + N_e \qquad (1.33)$$

To determine the noise figure of the mixer in Figure 1-7, we consider the signal to noise ratios at input and output.

If RF power S_i enters the mixer at the signal frequency,

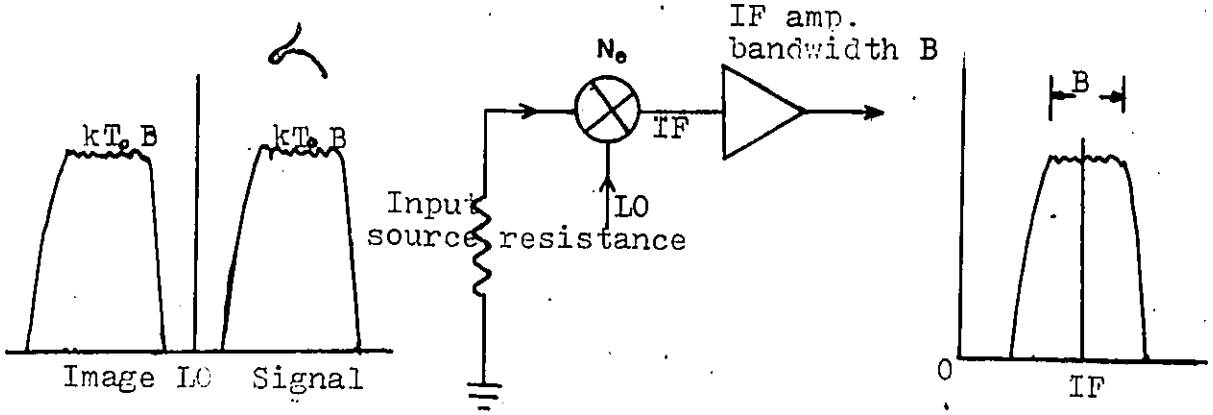

Case (a)

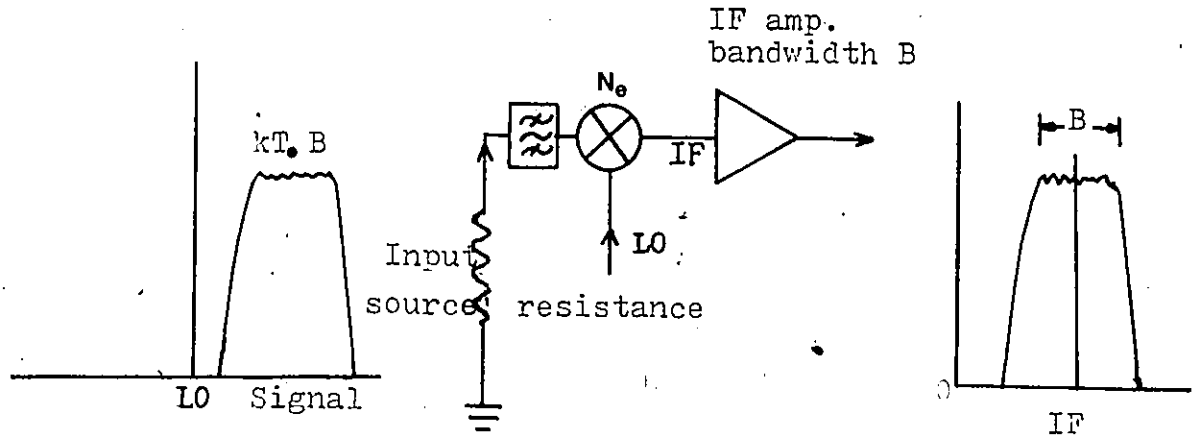

Case (b)

Figure 1-6. The two different cases of mixer input noise.
Case (a) Source noise at both signal and image frequency.
Case (b) Source noise at signal frequency only.

$$\frac{S_i}{N_i} = \frac{S_i}{kT_oB} \tag{1.34}$$

Note that N_i here is the noise in the signal band only. From (1.33),

$$\frac{S_o}{N_o} = \frac{\frac{S_i}{L_c}}{\frac{2kT_oB}{L_c} + N_e} \tag{1.35}$$

Thus from (1.28), (1.34) and (1.35)

$$F_o = \frac{\frac{2kT_oB}{L_c} + N_e}{\frac{kT_oB}{L_c}} \tag{1.36}$$

If the input source is not broadband (Case(b) in Figure 1-6), but instead only presents noise in the signal band (this can be achieved by using a filter, although there are complications in achieving this in practice) a different formula for noise figure results.

The output noise is then reduced and is given by

$$N_o = \frac{kT_oB}{L_c} + N_e \tag{1.37}$$

Thus a second formula for the noise figure can be derived in the same way for the mixer in Figure 1-6 (Case(b)).

$$F_o = \frac{\frac{kT_oB}{L_c} + N_e}{\frac{kT_oB}{L_c}} \tag{1.38}$$

Examining (1.36) and (1.38) it can be seen that for a given conversion loss L_c and excess noise N_e, (1.38) describes the noise figure better than (1.36).

Thus a factor affecting the mixer noise figure has been found, while exists, whether or not the image source noise is suppressed. This factor is manifest in the parameter mixer noise ratio N_r.

The noise ratio is defined as the ratio of output noise to input noise

$$N_r = \frac{N_o}{kT_oB} \tag{1.39}$$

It can be shown that (See (1.31)),

$$F_o = L_c N_r \tag{1.40}$$

The noise ratio for the two mixers, Figure 1-6 Case(a) and (b), is derived from (1.33), (1.37) and (1.39)

i) image noise NOT suppressed

$$N_r = \frac{\frac{2kT_oB}{L_c} + N_e}{kT_oB} \tag{1.41}$$

ii) image noise suppressed

$$N_r = \frac{\frac{kT_oB}{L_c} + N_e}{kT_oB} \tag{1.42}$$

Thus for a mixer followed by an IF amplifier as shown in Figure 1-7, i.e., for the overall noise figure of the receiver front-end, several subsystem can be cascaded.

The general formula for the noise figure of a cascade as shown in Figure 1-7 is

$$F = F_1 + \frac{(F_2 - 1)}{G_1} + \frac{(F_3 - 1)}{G_1 G_2} + \cdots\cdots\cdots\cdots$$

$$= F_1 + (F_2 - 1)L_1 + (F_3 - 1)L_1 L_2 + \cdots\cdots\cdots\cdots \qquad (1.43)$$

Thus the total noise figure F_T of the receiver front-end is

$$F_T = L_R + (F_o - 1)L_R + (F_{IF} - 1)L_R L_c \qquad (1.44)$$

By substituting (1.40) into (1.44),

$$F_T = L_R + (L_c N_f - 1)L_R + (F_{IF} - 1)L_R L_c \qquad (1.45)$$

Usually in calculating the noise figure of a receiver front-end (whether a mixer or an amplifier is in the first stage) the noise figure of the first stage becomes a major factor contributing to the total noise figure. Actually the noise figure of the RF circuit due to loss between antenna and the first stage (mixer in this study) is negligible because the length of the transmission line between them is usually made as short as possible. Then (1.44) becomes

$$F_T = F_{(\text{mixer + IF amp})} = F_o + (F_{IF} - 1)L_c \qquad (1.46)$$

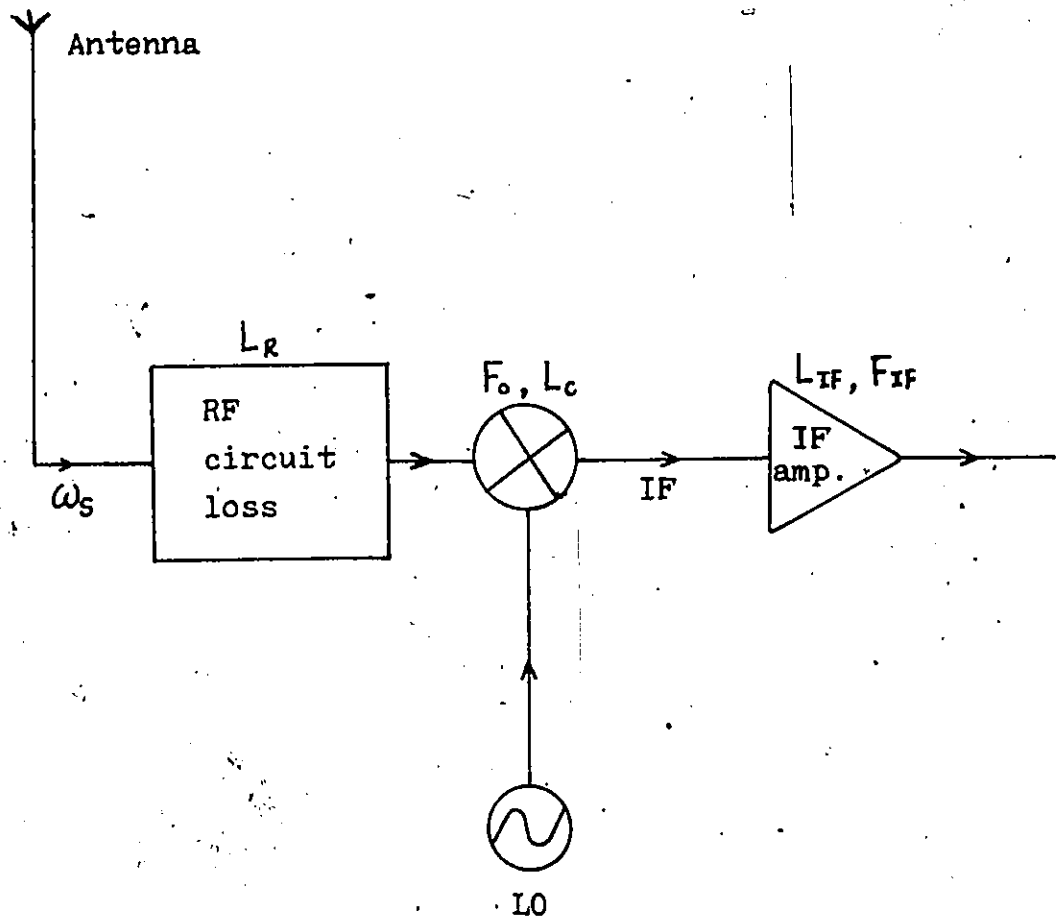

Figure 1-7. The receiver front-end configuration.

Substituting (1.40) into (1.46) yields;

$$F_T = (N_r + F_{IF} - 1)L_c \tag{1.47}$$

Eqn.(1.47) can be simplified as follows: since for IF frequencies greater than 1 MHz, the 1/f noise has decreased to the level of the white noise, we can set the noise ratio of the diode practically equal to unity:

$$N_r \cong 1 \tag{1.48}$$

and the noise figure of a mixer receiver front-end as shown in Figure 1-7 is given approximately by;

$$F_T = L_c \cdot F_{IF} \tag{1.49}$$

Therefore, since the noise figure determines the low-level sensitivity of the mixer, mixers are usually optimized for lowest conversion loss. The importance of the conversion loss L_c and the diode noise ratio parameters for the overall noise figure performance F_T are illustrated in Figure 1-8. As a result of the reductions in the barrier resistance R_B with LO drive level, the shunting effect of the barrier capacitance C_B is reduced so that L_c reduces with drive level. At very high levels, however, L_c will increase as the available power at R_B will be dissipated in R_s.

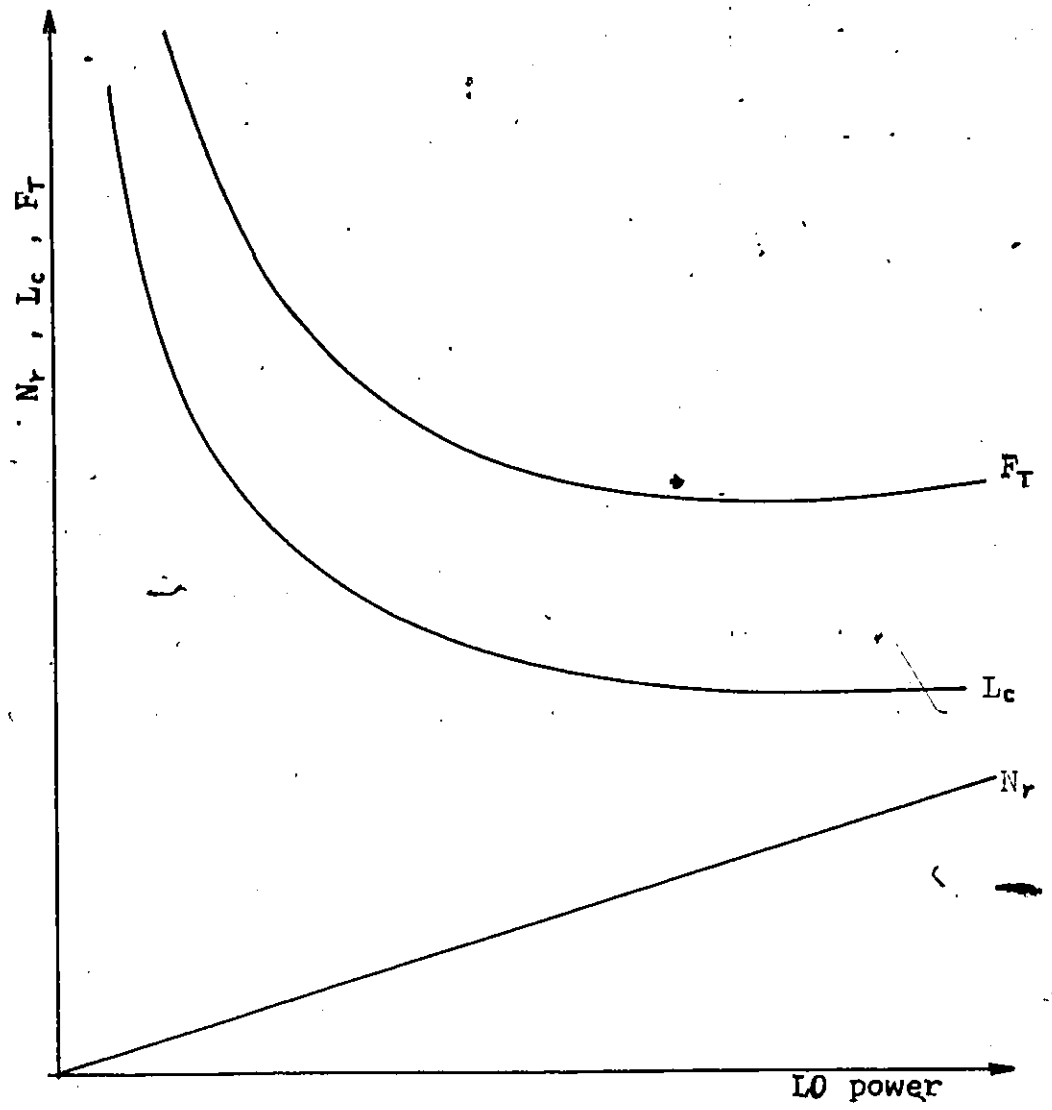

Figure 1-8. L_c, N_r and F_T as a function of LO power [3].

1.5 Intermodulation

The most troublesome spurious responses in a super-heterodyne receiver are usually caused by intermodulation. Spurious intermodulation response is commonly caused by the mixing of harmonics from an interfering signal with those from the local oscillator to produce the IF.

To predict a receiver's susceptibility to a particular RF environment, the usual procedure is first to calculate the intermodulation frequencies and then to determine if they coincide with those of signals present in the environment. If any do, the receiver sensitivity to such responses is measured or calculated [7] to determine if they are above "threshold", where threshold is the minimum usable signal level of the receiver.

Intermodulation distortion resulting from simultaneous reception of the desired signal and multiple in-band undesired signals (external interference) are mostly encountered in mixers and comprise the most difficult interference to suppress. External interference differs from internal interference (caused by harmonic spurious responses) in that once the desired and interfering signals reach the resistive mixer input, no form of filtering, balancing, or cancelling can eliminate or reduce the distortion [8].

The theory developed in Reference [8] relates the relative intermodulation distortion in resistive mixers to the diode parameters and the mixer's operating conditions, and predicts the relative intermodulation distortion caused by diode nonlinearity. The theory also

shows that the intermodulation ratio can be reduced by increasing the LO power.

Interference in a mixer can generally be divided into two classes. The first is that due to spurious responses at the reception of two undesired signals separated by IF frequency or the mixing of an undesired signal with a harmonic of the LO. These types of interferences can generally be eliminated by preselection.

The second type of interference falls into three subgroups, intermodulation distortion, cross-modulation distortion and harmonic distortion. These types of interference cannot be reduced by preselection. In this thesis only intermodulation will be treated explicitly, but the results apply equally to cross-modulation distortion.

If two sinusoidal signals and a LO signal are applied to a nonlinear mixing element, the output, i.e., the result of (1.1), is

$$\begin{aligned} B_{out} = K_0 &+ K_1(S_1 \cos\omega_1 t + S_2 \cos\omega_2 + S_{LO} \cos\omega_{LO} t) \\ &+ K_2(S_1 \cos\omega_1 t + S_2 \cos\omega_2 + S_{LO} \cos\omega_{LO} t)^2 \\ &+ K_3(S_1 \cos\omega_1 t + S_2 \cos\omega_2 + S_{LO} \cos\omega_{LO} t)^3 \\ &+ K_4(S_1 \cos\omega_1 t + S_2 \cos\omega_2 + S_{LO} \cos\omega_{LO} t)^4 \end{aligned}$$

If the above equation is multiplied out to the 4th power, a multitude of outputs at different frequencies are obtained. Among the terms of interest are the IF terms and distortion terms. The IF terms are

$$B_{IF} = 2K_2S_1S_{LO} \cos(\omega_1 - \omega_{LO})t + 2K_2S_2S_{LO} \cos(\omega_2 - \omega_{LO})t + \cdots\cdots\cdots \quad (1.51)$$

Outputs called intermodulation terms are produced,

$$B_{IM} = 3K_4S_1^2S_2S_{LO}\cos(-2\omega_1 + \omega_2 + \omega_{LO})t + 3K_4S_1S_2^2S_{LO}\cos(-2\omega_2 + \omega_1 + \omega_{LO})t \quad (1.52)$$

These outputs are shown in Figure 1-9.

Also cross modulation terms are produced in the output.

$$B_{CM} = 3K_4S_1^2S_2S_{LO}\cos(\omega_2 - \omega_{LO})t + 3K_4S_1S_2^2S_{LO}\cos(\omega_1 - \omega_{LO})t \quad (1.53)$$

These outputs occur at the IF frequencies of each signal but contain the information of the other signal.

Comparing the intermodulation distortion terms and the cross modulation term with S_1 equal to S_2 it is seen that the magnitudes of these terms are identical and therefore the percent of distortion due to intermodulation is equal to the percent of distortion due to cross modulation. When a multitude of signals is applied to the mixer, the voltage across the diode may be expressed as:

$$V = S_1\cos\omega_1t + S_2\cos\omega_2t + S_{LO}\cos\omega_{LO}t \quad (1.54)$$

where S_1 is the peak voltage at angular frequency ω_1, S_2 the voltage at ω_2, and S_{LO} the LO voltage at LO frequency (ω_{LO}). Substituting (1.54) into (1.2), (1.55) yields:

$$i = \sum_{n=1}^{\infty}K_n(S_1\cos\omega_1t + S_2\cos\omega_2t + S_{LO}\cos\omega_{LO}t)^n \quad (1.55)$$

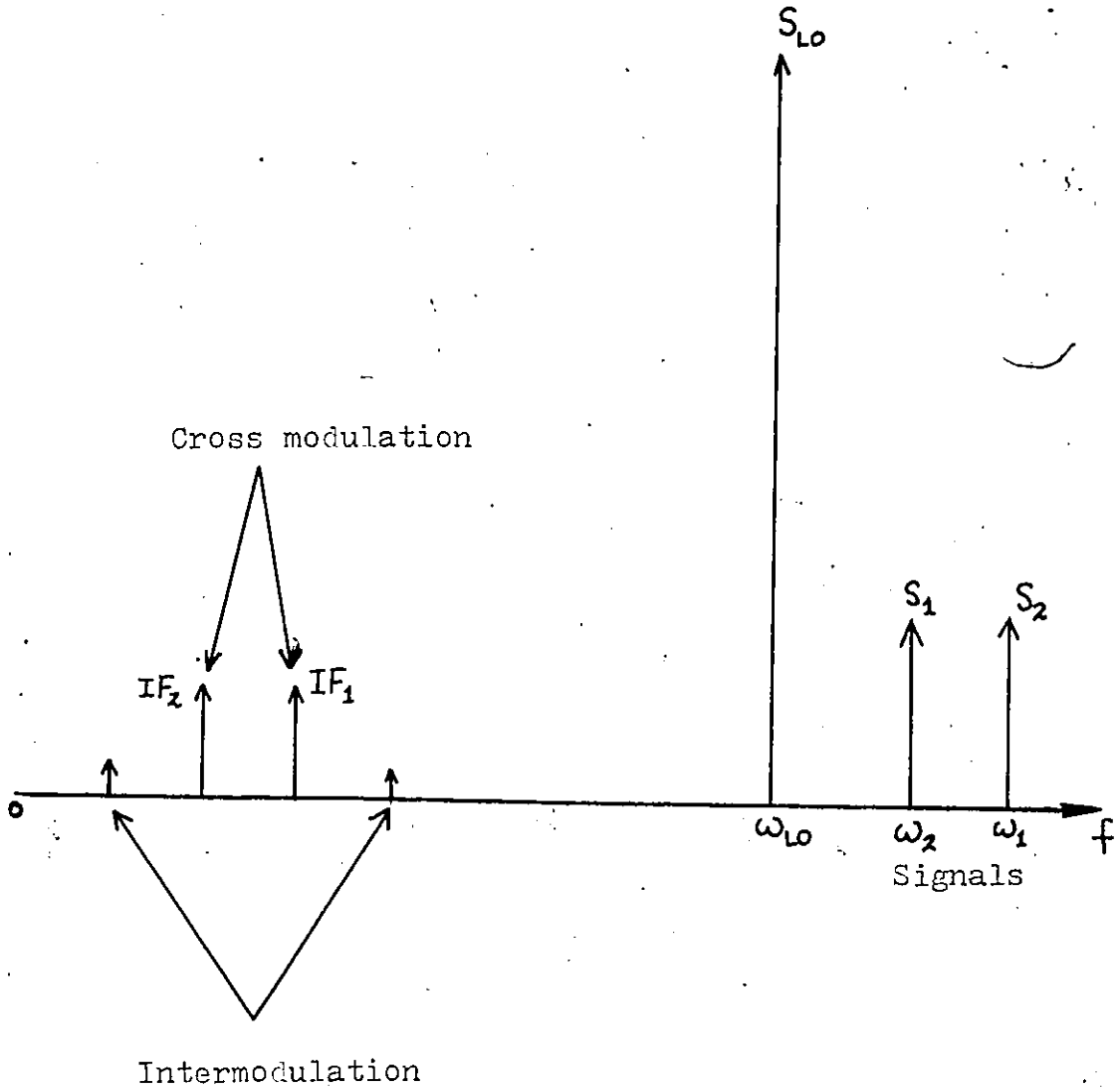

Figure 1-9. Intermodulation products.

(1.55) is an expression of the various currents flowing at the different frequencies in the nonlinear element. All possible combinations of the three frequencies are included in this equation.

The desired down-converted output frequency is

$$\omega_{IF1} = \omega_{s1} - \omega_{LO} \quad \text{or} \quad \omega_{IF2} = \omega_{s2} - \omega_{LO} \tag{1.56}$$

The intermodulation distortion appears at frequencies

$$\omega_{IM1} = 2\omega_{s1} - \omega_{s2} - \omega_{LO} \quad \text{or} \quad \omega_{IM2} = 2\omega_{s2} - \omega_{s1} - \omega_{LO} \tag{1.57}$$

The distortion present due to the intermodulation is best expressed as the ratio of the currents flowing at the intermodulation frequency to the current at the IF output frequency.

$$\% \text{ intermod distortion} = \frac{i_{IM1}}{i_{IF1}} \quad \text{or} \quad = \frac{i_{IM2}}{i_{IF2}}$$

To find which terms in (1.55) yield currents at the frequencies in (1.56) and (1.57), and to find the ratio of these currents, an approximate solution may be obtained by truncating the series (since (1.55) is an infinite series).

As an approximation the series is stopped at n=4. Then the current at frequencies in (1.56) is

$$i_{IF1} = 2K_2S_1S_{LO} + 3K_4S_1^3S_{LO} + 3K_4S_1S_{LO}^3 + 3K_4S_1S_2^2S_{LO} \tag{1.58a}$$

Also, in (1.57)

$$i_{IM1} = 3K_4S_1^2S_2S_{LO} \tag{1.58b}$$

Thus

$$\frac{i_{IM1}}{i_{IF1}} = \frac{1}{\frac{2}{3}\frac{K_2}{K_4}\frac{1}{S_1 S_2} + \frac{S_1^2 + S_2^2 + S_{LO}^2}{S_1 S_2}} \tag{1.58c}$$

If $S_1 = S_2$, then $S_1 = S_2 = S$, and

$$\frac{i_{IM1}}{i_{IF1}} = \frac{1}{\frac{2}{3}\frac{K_2}{K_4}\frac{1}{S^2} + 2 + \frac{S_{LO}^2}{S^2}} \tag{1.58d}$$

If a large LO voltage is applied to the diode and the signal voltages are small, then (1.58d) becomes approximately

$$\frac{i_{IM1}}{i_{IF1}} \cong \frac{S^2}{S_{LO}^2} \tag{1.59}$$

The ratio of intermodulation power to IF output power is S^4/S_{LO}^4. From this it can be shown that a one dB increase in LO power would yield a two dB decrease in percent intermodulation distortion for the same signal input power. Also a one dB increase in signal power increases the percent intermodulation distortion by two dB.

Mixing products like $n\omega_{LO} \pm m\omega_s$ shown in Section 1.2 are called "single tone (harmonic intermodulation)" IM products because they appear with only one RF input present. When two simultaneous input RF signals mix with the LO as shown in the above analysis to produce $f_{IM} = \pm f_{s1} \pm f_{s2} \pm f_{LO}$, these are called "two tone" IM products.

1.6 Dynamic Range

The dynamic range of any mixer is usually defined as the power range between the minimum detectable signal and the maximum input signal that can be accepted before compression or undesirable intermodulation effects take place. In the case of a superheterodyne receiver, the minimum detectable signal is determined by the overall noise figure and the maximum input signal is normally taken to be the point where a specified compression (normally 1 dB compression) occurs in the RF to IF overall gain response and the mixer transfer characteristic (will be shown in Chapter 4) as shown in Figure 1-10. Assuming that the IF amplifier does not limit the system, this implies compression in the mixer conversion loss response.

If the minimum detectable signal (MDS) sensitivity of a receiver is expressed as the signal power which is 3 dB greater than the system noise power, then

$$MDS = 2kT_oBF_T \tag{1.60}$$

where k is Boltzmann's Constant, T_o the absolute temperature in °K, B the receiver bandwidth, and F_T the overall receiver noise figure. The input signal level which produces receiver compression is related to the overall RF to IF gain (G) of the receiver, and the dynamic range DR is the difference between the two input levels P_{comp} and P_{MDS} in dB, such that

$$DR = \frac{P_{comp}}{G} - P_{MDS} \quad (dB) \tag{1.61}$$

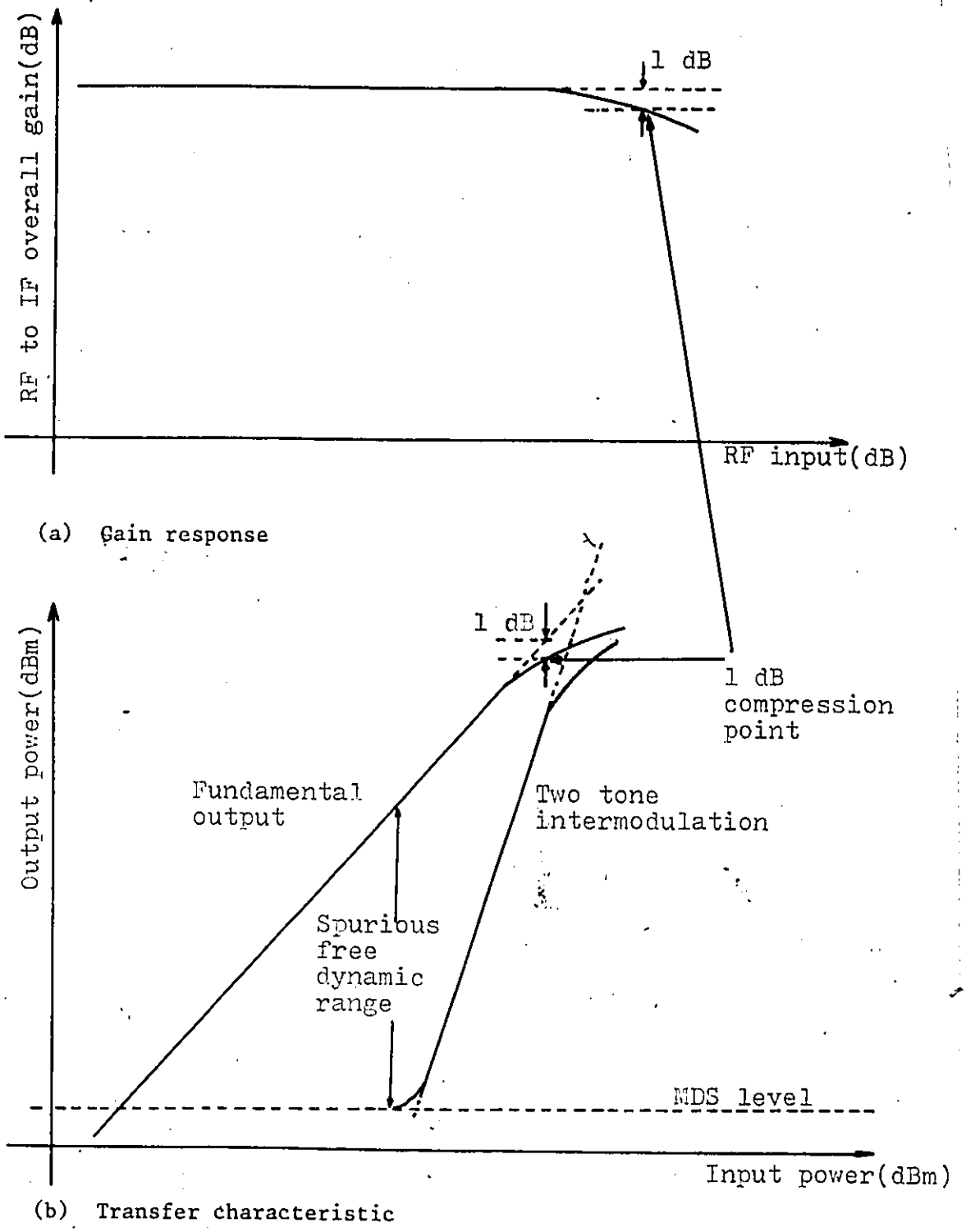

Figure 1-10. Dynamic range compressions in (a) gain response and (b) transfer characteristic.

With reference to compression in the mixer conversion loss response(= mixer transfer characteristic), the input power for 1 dB compression (assuming that the IF amplifier does not limit the receiver response again), will be given by

$$P_{\text{mixer compression}} = P_{\text{receiver compression}} - G_{amp} \quad \text{(dB)} \quad (1.62)$$

where

$$G_{amp} = G_{\text{receiver}} - L_c \quad \text{(dB)}$$

In practice (neglecting the IF amplifier contribution), for high dynamic range the mixer diode should be operated in its linear region and the input signal level should be maintained below the applied LO power.

1.7 Bias

DC bias is sometimes made use of for specific applications. This is shown in Figure 1-11.

The main advantage of forward DC bias is that it enables operation with reduced LO drive, or operation at reduced impedance levels (RF and IF). A possible disadvantage for the low LO drive is reduced dynamic range. DC forward current will, however, increase the diode noise (temperature) ratio and this will provide a limit for this DC component.

The advantage of reverse DC bias, providing the reverse i(v) characteristic has low current leakage over the range of interest,

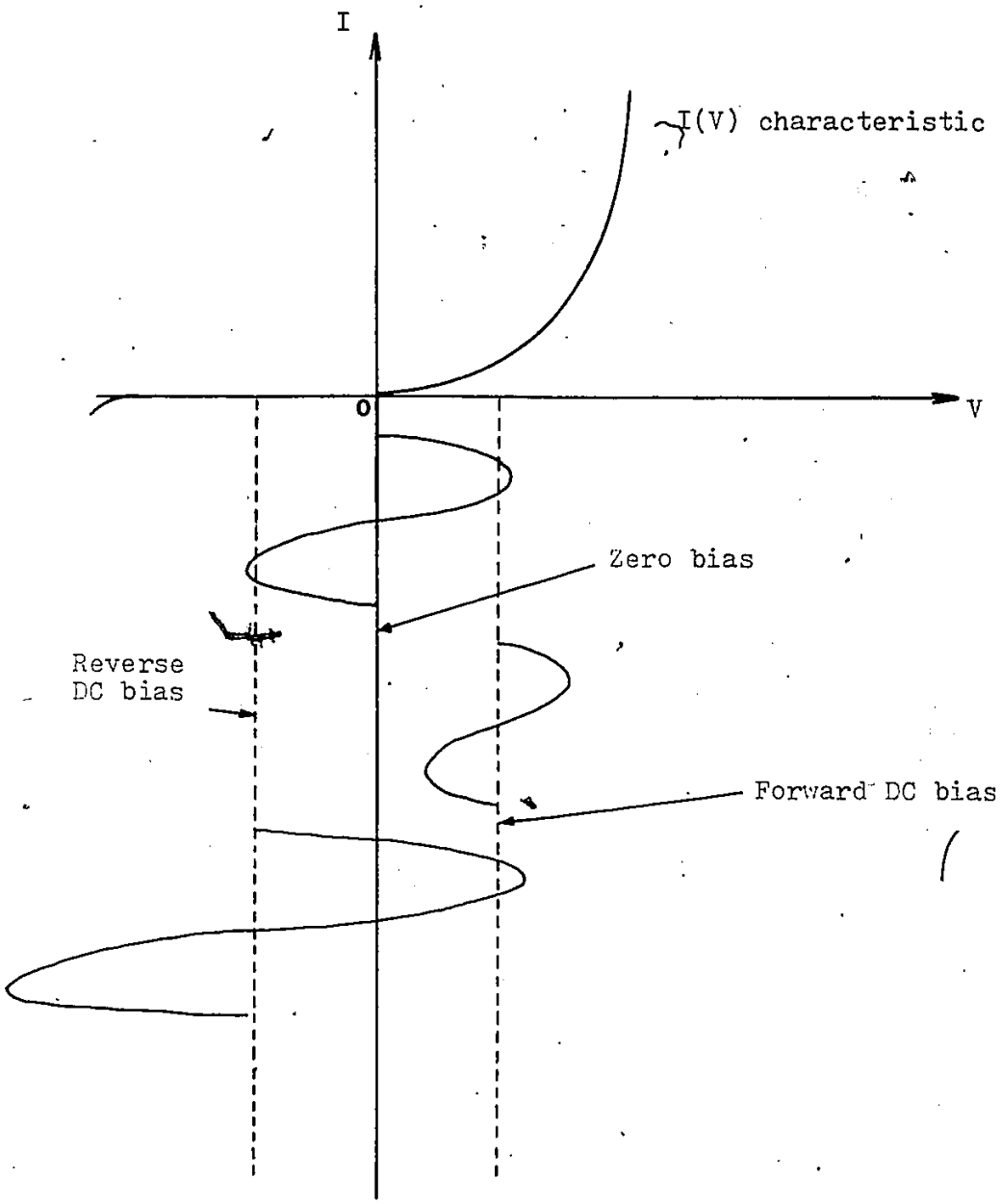

Figure I-11. The application of DC bias.

is high LO power operation, with the possibility of increased dynamic range.

If the application of forward bias requiring a voltage supply had been used, then different polarity lines had been required in this study, i.e., for a single balanced mixer. If the bias is derived from a low source impedance, then this value can be optimized so that the negative voltage developed by the diode rectified current will compensate for the applied positive DC bias, resulting in a variable bias with LO drive and consequent performance fairly independent of LO drive. This makes the circuit more complex.

In order to obtain low noise characteristics and simplicity of design for the mixer as a first stage in a receiver, zero bias has been used for this study.

1.8 Burnout

Burnout is a term given to the overload effect which results in significant deterioration in diode performance. At least two important factors affect the burnout resistance of Schottky barrier mixer diodes. The first is RF impedance matching. High burnout Schottky barrier diodes have a self-protecting behavior at high-power levels by appearing as mismatch and reflecting most of the incident power back toward the RF source. This behavior could be due to variation of the barrier capacitance [9]. Generally, low barrier Schottky diodes are better matched, and therefore, absorb more incident RF energy.

A second burnout factor involves resistance to nano-second pulses. Schottky barrier diodes tend to avalanche in localized areas

around the junction periphery due to high electric fields and fail catastrophically due to a localized alloyed site through the metal-semiconductor junction. The first degradation occurs in 1/f noise due to excessive leakage current and then is followed by an overall degradation in noise figure due to loss of nonlinear characteristics. Use of high eutectic temperature barrier metal systems generally results in higher burnout resistance Schottky barrier diodes. This is also true to some extent for CW and microsecond RF pulses. However, in the long pulse duration condition, diodes fail in the center of the junction indicating a thermal dissipation phenomenon.

The old resistive mixer diodes use a point contact type of construction that limits maximum permissible pump power. The small breakdown voltage of this type of diode restricts the maximum permissible pump power that can be applied without causing excessive noise figure due to breakdown. If large pump power is applied to a point contact diode, the noise figure becomes intolerable, and the probability of diode burnout becomes prohibitively large.

One technique that will permit the use of high power is the use of circuits that incorporate several diodes. Since each diode receives a smaller signal than in a single diode circuit, the intermodulation is lowered. But the large number of diodes required to obtain a significant reduction of intermodulation distortion results in complicated circuitry at microwave and mm-wave frequencies. An alternative technique requires the design of diodes that can withstand large pump powers. Therefore, high barrier GaAs Schottky barrier diodes are preferred for eliminating intermodulation distortion.

1.9 Local Oscillator Requirements

All superheterodyne type receivers use one or more local oscillators to convert an input frequency to an intermediate frequency before the signal is demodulated.

To be suitable for use in a superheterodyne receiver, an oscillator must possess the following qualities. It must have adequate power output. Lo power applied to a mixer obviously determines the dynamic range and the amount of distortion caused by intermodulation as discussed in Section 1.5. But there is an objection to increasing the LO power applied to a mixer. To reduce harmonic responses, especially images, it is desirable to reduce the LO amplitude as far as possible without affecting sensitivity or low-voltage operation [10]. When in-band intermodulation responses are considered, it is desirable to increase the LO power as much as practical considerations will permit.

It must possess adequate frequency stability. If AFC (Automatic Frequency Control) is to be used with the reciever, this requirement can be relaxed considerably.

It must have reasonable power supply requirements; that is, it should not take an unreasonably high voltage or require an unreasonably high power input.

1.10 Single Balanced Mixer Using 180° Hybrid

Single balanced mixers in receivers have one advantage over single ended mixers: the concellation of the LO AM noise and of the DC component at the IF port. Balanced mixers using hybrid junctions

have additional advantages:

a. Local oscillator and signal input are isolated.

b. The isolation is independent of frequency.

A single balanced mixer containing a hybrid junction is shown in Figure 1-12. For many years, before the advent of microwave integrated circuits, hybrid junctions were realized with a waveguide magic-Tee [11]. In planar technology such a junction can be built by combining two orthogonal mode transmission media as realized in Section 3.3.

A hybrid junction is basically a 4-port device, as shown in Figure 1-12, so constructed that power, incident at one port, divides equally into two of the other ports, and does not pass directly to the fourth or conjugate port. The inverse relationship of two equal inputs producing full output from one port and zero from another also will be obtained, and is in fact a special case of the property that two coherent inputs produce their vector sum and difference at the other two ports. One other property of a hybrid junction is of interest; it is the only branching junction capable of appearing matched looking into any port when the other ports are terminated in their characteristic impedances.

We assume that the ports, 1 and 2, in Figure 1-13 are terminated by matched diodes operating in the square law region. The RF signal coming from the antenna at port 3 and the LO signal at port 4 can be represented as shown in Figure 1-13.

Two diodes are mounted at equal distance from the center of the junction. At one of the diodes, LO signal and RF signal are in phase; at the other, they are 180° out of phase. The IF signal from

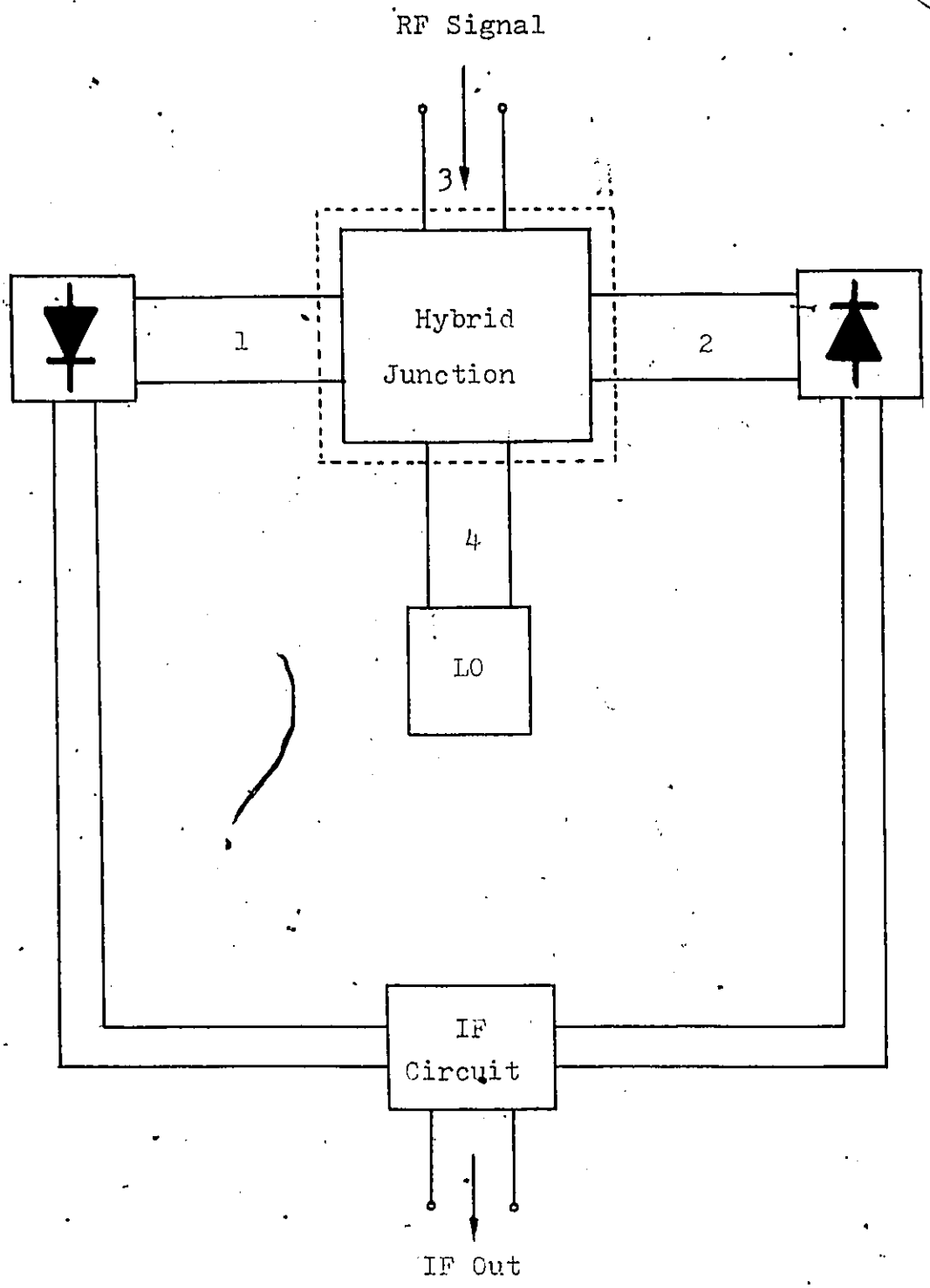

Figure 1-12. Schematic diagram of a single balanced mixer (receiver frone-end).

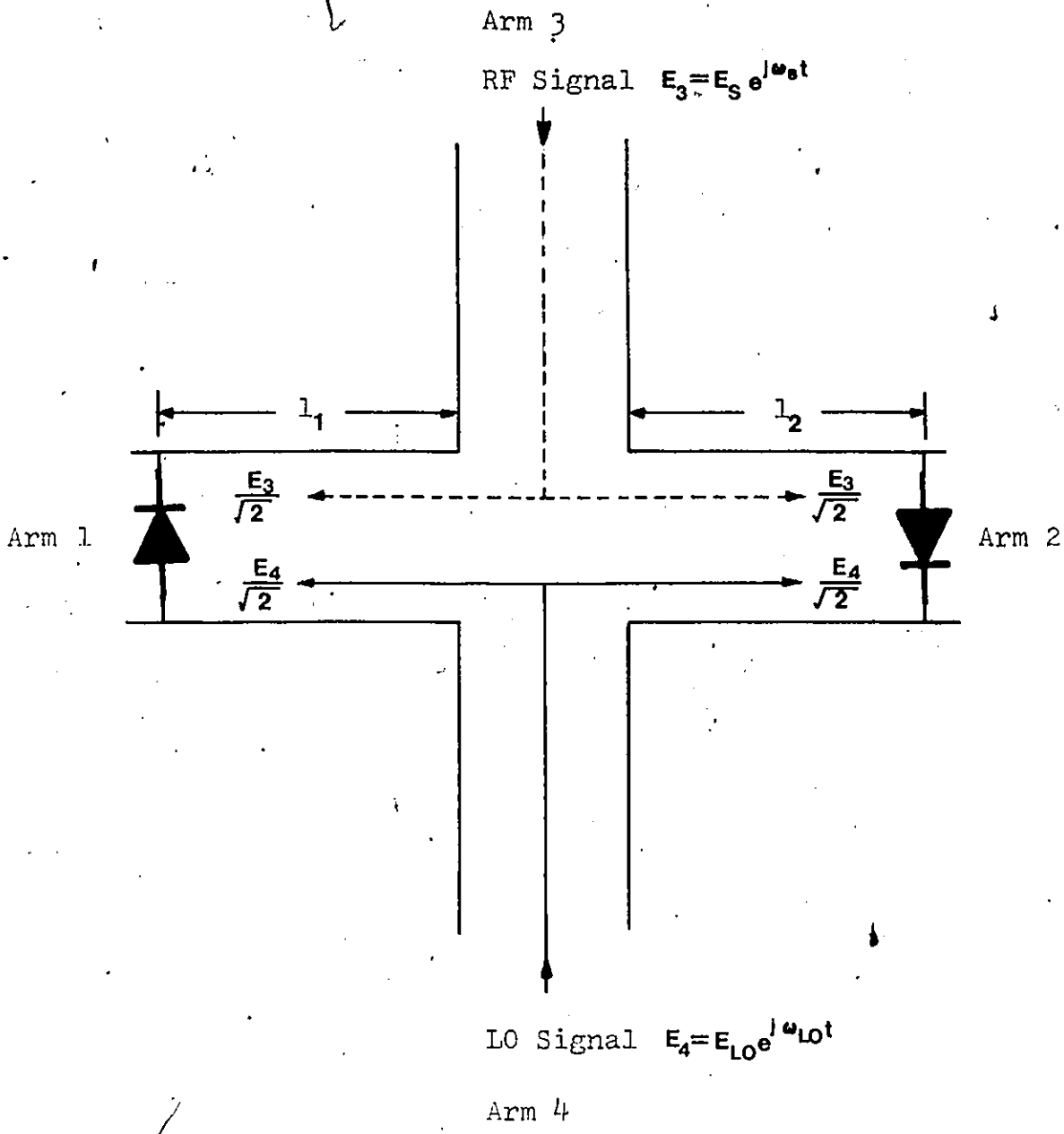

Figure 1-13. Equivalent circuit of balanced mixer using 180° hybrid.

one diode will also be 180° out of phase compared with the IF signal from the other diode. The IF signal is recovered by substracting the the outputs of the two diodes.

Therefore by substracting the two voltage outputs, V_1 and V_2, in the square law region of the diodes, we obtain a IF signal at the output of a single balanced mixer

$$V_1 - V_2 \cong 4E_{LO}E_s \cos(\omega_s - \omega_{LO})t \tag{1.63}$$

where we have assumed equal, well matched diodes (no reflections) and equal power splits with opposite polarities.

1.11 The Suppression of LO AM Noise [12]

Let the signal be

$$e_s = \sqrt{2}E_s[(1 + S)\sin\omega_s t] \tag{1.64}$$

where S may be any complicated function of t, with a spectrum extending out to f_c. Let the LO voltage be;

$$e_{LO} = \sqrt{2}E_{LO}\left\{[1 + V_n(p,t)]\ \sin\omega_{LO}t\right\} \tag{1.65}$$

where the open-circuit rms noise voltage,

$$V_n(p,t)_{(rms)} = [\int_{f_1}^{f_2}(N_{oa})_{fm}\ df_m]^{\frac{1}{2}} \tag{1.66}$$

and f_1 and f_2 are the limits of the relevant frequency range, N_{oa} (f) is the single sideband amplitude noise power density per Hz of RF

bandwidth corresponding to the offset frequency f, argument p is the offset frequency, f_m is the frequency offset from the carrier, and N_{oa} is the AM noise power density. With the exception only of very poor oscillators

$$V_n(p,t) \ll 1 \tag{1.67}$$

over any limited offset frequency range.

The two signals are combined in a hybrid junction in such a way that half the power from e_s and e_{LO} goes to each mixer diode. Either e_s or e_{LO} is out of phase in the two diodes. We shall consider only the case where the phase of e_s is the same in both diodes and the phase of e_{LO} differs by π radians at the two diodes. This is the case shown in Figure 1-13. We will now study the situation at the two diodes of the balanced mixer.

a) At one diode the sum of the two signals is

$$E_1 = e_s/\sqrt{2} + e_{LO}/\sqrt{2} \tag{1.68}$$

$$= E_{LO}\,[1 + V_n(p,t)]\,\sin\omega_{LO}t \;+ E_s[(1 + S)\,\sin\omega_s t]$$

Assume the signal frequency to be above the LO frequency. Let the angular IF frequency be ω_{IF}. Then;

$$\omega_s - \omega_{LO} = \omega_{IF}$$

and

$$E_1 = E_{LO}[1 + V_n(p,t)]\,\sin[(\omega_s - \omega_{IF})t] + E_s[(1 + S)\,\sin\omega_s t]$$

$$= E_{LO}[1 + V_n(p,t)][\cos\omega_{IF}t \sin\omega_s t - \sin\omega_{IF}t \cos\omega_s t]$$

$$+ E_s[(1 + S) \sin\omega_s t]$$

$$= E_{LO}[1 + V_n(p,t)] \cos\omega_{IF}t \sin\omega_s t + E_s(1 + S) \sin\omega_s t$$

$$- E_{LO}[1 + V_n(p,t)] \sin\omega_{IF}t \cos\omega_s t$$

$$= \left\{E_{LO}[1 + V_n(p,t)] \cos\omega_{IF}t + E_s(1 + S)\right\} \sin\omega_s t$$

$$- \left\{E_{LO}[1 + V_n(p,t)] \sin\omega_{IF}t\right\} \cos\omega_s t,$$

The square of the amplitude $(A_1)^2$ is given by the sum of the squares of the $(\sin\omega_s t)$ and $(\cos\omega_s t)$ terms.

Thus;

$$(A_1)^2 = E_{LO}^2[1 + V_n(p,t)]^2 \cos^2\omega_{IF}t + E_s^2(1 + S)^2$$

$$- 2E_{LO}E_s[1 + V_n(p,t)](1 + S) \cos\omega_{IF}t$$

$$+ E_{LO}^2[1 + V_n(p,t)]^2 \sin^2\omega_{IF}t \qquad (1.69)$$

But

$$E_{LO}^2[1 + V_n(p,t)]^2 = E_{LO}^2[1 + V_n(p,t)]^2[\cos^2\omega_{IF}t + \sin^2\omega_{IF}t]$$

Thus;

$$(A_1)^2 = E_{LO}^2[1 + V_n(p,t)]^2 + E_s^2(1 + S)^2$$

$$- 2E_{LO}E_s[1 + V_n(p,t)](1 + S) \cos\omega_{IF}t \qquad (1.70)$$

Superficially it might seem that the only term to be passed by a following IF amplifier with an angular center frequency ω_{IF}, would be the last term and that both the first and second terms of (1.70), being at baseband frequencies, would be rejected.

However, in practice $E_{LO}^2 V_n^2(p,t)$ will have components at an angular frequency ω_{IF}, and E_{LO}^2 being very much larger than $2E_{LO}E_s$, they may be of significant power relative to the wanted signal component.

Such terms will be the result of LO AM noise sidebands at an offset frequency approximately equal to the IF.

Thus after dropping terms which will be rejected by the IF amplifier:

$$(A_1)^2 = E_{LO}^2[1 + V_n(p,t)]^2$$

$$- 2E_{LO}E_s[1 + V_n(p,t)](1 + S)\cos\omega_{IF}t \qquad (1.71)$$

b) At the other diode, the signal phase is the same as that at diode 1 and the LO phase is shifted by 180° relative to its phase at diode 1.

An analysis similar to that carried out for diode 1 will give an equation similar to (1.71) except that the sign of the second term will be changed. The equation is:

$$(A_2)^2 = E_{LO}^2[1 + V_n(p,t)]^2$$

$$+ 2E_{LO}E_s[1 + V_n(p,t)](1 + S)\cos\omega_{IF}t \qquad (1.72)$$

From (1.71) and (1.72)

$$(A_1^2 - A_2^2) = 4E_{LO}E_s[1 + V_n(p,t)](1 + S)\cos\omega_{IF}t$$

where

$$(A_1^2 - A_2^2) = (A_1 - A_2)(A_1 + A_2)$$

Thus

$$(A_1 - A_2) = \frac{4E_{LO}E_s[1 + V_n(p,t)](1 + S)\cos\omega_{IF}t}{(A_1 + A_2)} \qquad (1.73)$$

Now

$$E_{LO}^2 >> E_{LO} \cdot E_s$$

where the normal condition in practice is:

$$E_s << E_{LO}$$

(1.71) and (1.72) may be approximated by:

$$A_1^2 = E_{LO}^2[1 + V_n(p,t)]^2$$

$$A_1 \cong E_{LO}[1 + V_n(p,t)] \qquad (1.74)$$

and

$$A_2 \cong E_{LO}[1 + V_n(p,t)] \tag{1.75}$$

so,

$$A_1 + A_2 \cong 2E_{LO}[1 + V_n(p,t)] \tag{1.76}$$

and

$$(A_1 - A_2) = \frac{4E_{LO}E_s[1 + V_n(p,t)](1 + S)\ \cos\omega_{IF}t}{2E_{LO}[1 + V_n(p,t)]}$$

Therefore

$$(A_1 - A_2) = 2E_s(1 + S)\ \cos\omega_{IF}t \tag{1.77}$$

It will be noted that $(A_1 - A_2)$ is the result of connecting the outputs of the two mixer diodes in opposition and that, in doing so, the LO noise component is cancelled. In practice the mixer balance will not be perfect as we had assumed in theory, but 20 dB to 30 dB rejection of LO AM noise may readily be achieved. Nevertheless, one of the main advantages of a single balanced mixer has been demonstrated.

1.12 Conclusion

The basic resistive diode mixer principles and practical parameters for design have been studied in this chapter with the assumption of a square law device.

It has been shown that a 1 dB increase in LO power results in a 2 dB decrease in the intermodulation distortion. Therefore the use

of large LO power will result in a mixer that is relatively immune to distortion caused by interference.

A single balanced mixer using 180° hybrid was also shown to have the advantages of preventing the LO signal from radiating into the RF port and suppressing the LO AM noise at the IF port.

CHAPTER 2

PLANAR MIXER TECHNOLOGY

Brief descriptions of the planar device technology including device selection criteria, and of the planar microwave and mm-wave transmission media, fin line and shielded microstrip line, adopted in our mixer design, are given in this chapter.

2.1 Introduction

For many years waveguides provided the basic transmission medium for all types of microwave and mm-wave circuit applications. The advent of the planar transmission media for that frequency range has set up a cost effective way of microwave and mm-wave circuit production. Also planar active device technology compatible with such transmission media has stimulated developments of the microwave and mm-wave components in planar form. Those techniques are obviously advantageous for low cost microwave and mm-wave applications.

We shall discuss the planar device technology and planar microwave and mm-wave transmission media for our mixer design in this chapter.

2.2 Mixer Diodes for Planar Circuits

Point contact and Schottky barrier diodes are used as mixers from UHF to EHF. The nonlinear rectifying characteristic of these diodes resides in a metal-semiconductor contact (junction). The first published paper on the subject appeared in 1874 when Braun reported the asymmetrical nature of conduction between metal points and crystals. Until 1965 point contact diodes were fabricated by contacting a semiconductor surface with a metal whisker. The contact pressure in the point contact diode, however, can damage the junction, depending on the amount of pressure exerted. The Schottky barrier diode provides better mechanical and environmental reliability, and more repeatable fabrication than an equivalent point contact diode. As a result of

advanced planar technology, this diode has been produced in beam lead configuration suitable for microwave and mm-wave frequency applications.

2.2.1 Physical Configurations

For diodes operating at microwave and mm-wave frequencies, beam lead packaging as shown in Figure 2-1 was developed in an effort to overcome the inherent large inductance of the pill package. Beam lead packages are very compatible with microwave and mm-wave integrated circuits. Two coplanar beams are formed, one contacting the rectifying junction and the other providing an ohmic contact as shown in Figure 2-1(a). The junction contacting beam gives rise to an unaviodable overlay capacitance of 0.02 to 0.05 pF. In an effort to reduce this capacitance, diode manufacturers have endeavored to make the area of the beam lead contact smaller and smaller. But this has accentuated mounting problems since the fragile leads may easily break off while a diode is being bonded into a circuit. Figures 2-1(b) and (c) show four different beam lead packaging styles for single and double balanced mixers. Each Schottky barrier beam lead diode consists of two and four closely matched diodes respectively, formed monolithically to assure close matching of electrical characteristics such as capacitance, forward voltage and series resistance. Various styles of packagings other than beam lead packagings are available commercially.

(a) Beam lead configuration for a single ended mixer. (NEC 5558-00)

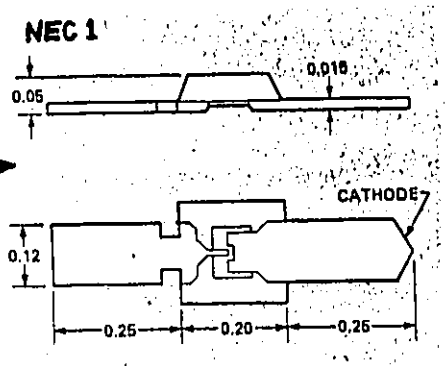

(b) Beam lead configuration for a single balanced mixer. (ALPHA)

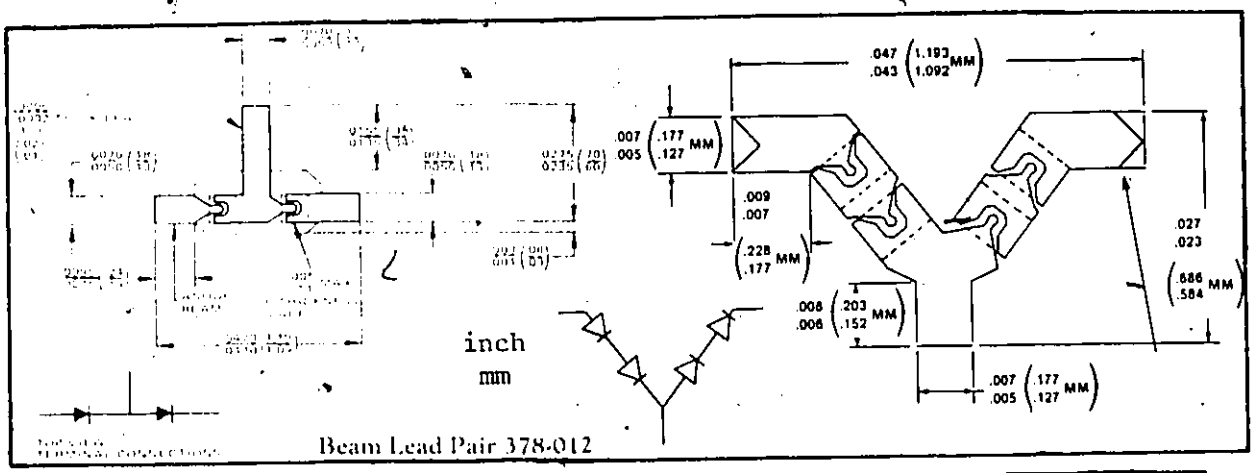

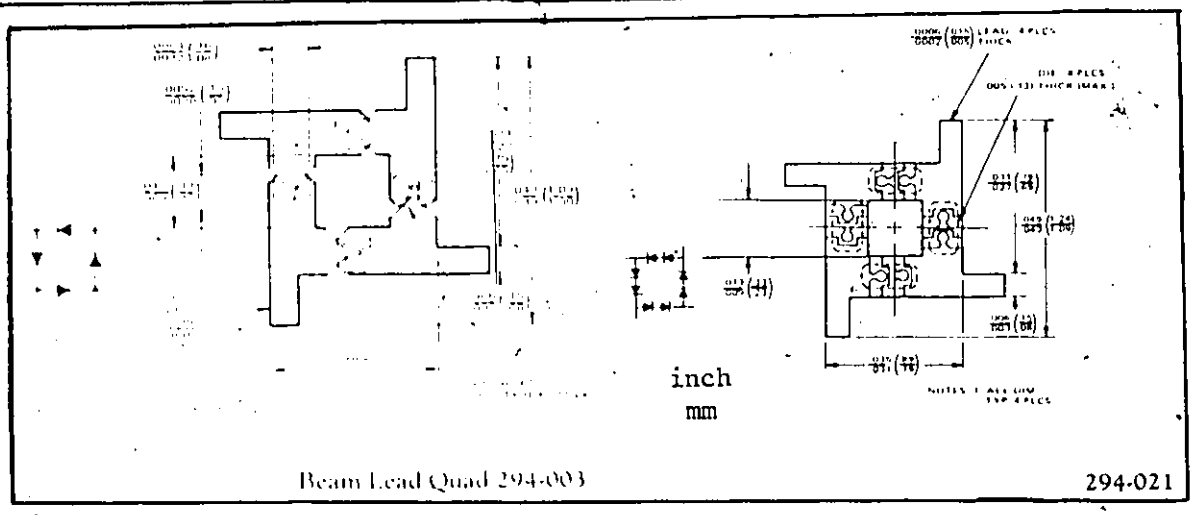

(c) Beam lead configuration for a double balanced mixer. (ALPHA)

Figure 2-1. Some beam lead packaging configurations for various mixers.

2.2.2 Electrical Characteristics and Selection Criteria

For efficient conversion, a high reverse resistance and a low forward resistance together with a sharp curvature of the i(v) characteristic at the origin are obvious desirable features. However, good static characteristics are not a sufficient condition for good microwave and mm-wave performance. At sufficiently high frequencies the shunting effect of the junction capacitance becomes important. Also, in microwave and mm-wave applications, other factors such as noise and dynamic impedance are significant.

Unlike p-n junction diodes, the Schottky barrier diode has rectifying characteristics based on majority carrier conduction, and in normal operation exhibits virtually no storage of minority carriers. This results in more efficient rectification at high frequencies. The fast response and low inherent noise make the Schottky diode particularly useful in mixer as well as in detector applications.

To select the best diode for a given mixer design, DC parameters such as spreading resistance (R_s), zero bias capacitance (C_0) and quality factor (η) can be investigated [13]. η is a dimensionless parameter which appears in the exponent of the expression for the i(v) characteristic (1.15)

$$\alpha = \frac{q}{\eta kt} \tag{2.1}$$

This quality factor, which is equal to or greater than unity, was originally introduced to describe deviations from the ideal

characteristics.

When different diodes are placed in the same mixer circuit, variations in conversion loss depend principally on the value of R_s and C_0, while η determines to a very large extent the noise performance of the diode. For minimum conversion loss, the cutoff frequency f_c of a mixer diode should be as high as possible. The cutoff frequency is defined as follows;

$$f_c = [2\pi R_s C_0]^{-1} \tag{2.2}$$

In practice, most diodes have a sufficiently high cutoff frequency, except for EHF applications. High turn on GaAs Schottky barrier diodes with lower series resistance and total capacitance have also raised the compression point of components. The small size of low capacitance millimeterwave diodes complicates the task of obtaining a metal semiconductor interface completely free of any contaminating layer. Thus in many cases, η will be much larger than unity, which is the ideal value.

The importance of η in determining the noise performance of a diode can be seen when we consider that the main sources of noise in a Schottky diode are shot noise from current flowing across the depletion region and thermal noise from the spreading resistance R_s. For a diode at room temperature, the shot noise contribution is by far the greater [13]. It is possible to model this shot noise by assuming that the diode junction conductance is at an equivalent temperature T_{eq} such that the resulting thermal noise has the same

magnitude as the shot noise. The equivalent noise temperature of a Schottky barrier diode is given by

$$T_{eq} = \eta \frac{T}{2} \qquad (2.3)$$

where T is the ambient temperature. Eqn.(2.3) shows the physical significance of η in determining the sensitivity of a diode. Thus, the quality factor is an important diode parameter and its value should be specified by a manufacturer. In general, its value should be as close to unity as possible; however, as mentioned above, this is difficult to achieve as the diode diameter gets smaller. For diodes operating at mm-wavelengths, the following values are typical;

diameter $\leq$ 5 μm
value of η $\leq$ 1.18 at room temperature.

Diode packaging parasitics are also important parameters in the design of mixers, since they usually set a lower limit for the zero bias capacitance of the diode, thus effectively limiting its cutoff frequency.

2.3 Planar Transmission Media

2.3.1 Introduction

Microstrip lines and fin lines belong to the general group of waveguiding structures composed of planar thin conductors, supported by dielectric substrates and are frequently shielded by grounded con-

ducting planes. Since all microwave and mm-wave circuits require metallic shielding to control higher order modes, reduce radiation losses, and eliminate external electromagnetic interference, the mixer must be shielded. In addition to shielding, low value dielectric constant materials are required to keep specially mm-wave integrated circuit dimensions as large as possible. Because of their potential for circuit integration, fin line and the shielded microstrip have been paving the way for improved mm-wave integrated circuit development.

Conventional forms of mm-wave integrated circuits generally utilize fused quartz dielectric substrates. This material has an extremely smooth surface (very desirable for reducing conductive loss), low dielectric loss, and can be made thin enough for use up to 100 GHz. The most undesirable features of fused quartz include high cost, ease of breakage, nondrillability, and high required precision in the dimensioning of shielding enclosures.

Glass fibre-enforced teflon (trade name-- RT/duroid 5880, $\varepsilon_r = 2.22$) was chosen as a suitable substrate for mm-wave integrated circuits after some experimentation [14]-[16].

Table 2-1 compares some features of fused quartz and RT/duroid. Note in particular, the 40:1 cost advantage of RT/duroid which becomes significant for large size substrates.

True TEM propagation is impossible on a line surrounded by two different media. Generally there will be longitudinal field components. The boundary conditions for two similar dielectrics (air $\varepsilon_r = 1.0$, RT/duroid $\varepsilon_r = 2.22$) are not as stringent as when one of the

materials has a much higher dielectric constant than the other, e.g. air vs alumina.

The propagation characteristics in inhomogeneous waveguides with small substrate permitivities are therefore very similar to those in homogeneous structures. This means that a microstrip line on RT/duroid behaves practically like a TEM line, and a fin line on RT/duroid has essentially the properties of a homogeneous ridged waveguide. Insertion losses for fin lines on several low dielectric constant substrates are shown in Table 2-2.

In this thesis, fin line and the shielded microstrip line are used to construct a integrated single balanced mixer. Specially fin line is chosen as a suitable transition medium from waveguide to the diodes and the microstrip line. The shielded microstrip line is used for constructing a band pass filter and a low pass filter to diplex the LO and IF signals in the mixer.

2.3.2 Shielded Microstrip Line

Microstrip is a very attractive transmission line for microwave integrated circuit applications involving a large number of identical units and requiring a high density of packaging. For low microwave frequencies the quasi-TEM theory can be employed to obtain the characteristics of microstrip lines and, using this approximation, extensive design data have been calculated for both single and coupled lines [22], [23]. When the wavelength in a microstrip line becomes comparable to the transverse dimensions of the line, i.e., above 20 GHz, the deviation from

	ε_r	Dielectric Loss Tan.	Minimum Thickness (in)	Minimum Metal Clad (in)	Loss/λ (dB)	Cost ($/in²)
RT/duroid	2.22	0.001	0.004	0.0007	0.15	0.10
Fused Quartz	3.78	0.0001	0.002	0.0001	0.05	4.00

Table 2-1

substrate	ε_r	Thickness (μm)	Loss(dB/cm) at 27 GHz	Loss(dB/cm) at 40 GHz
RT/duroid 5880	2.22	127	0.01	0.02
Mylar	3	100	0.03	0.03
Kapton	3	125	0.06	0.09

Table 2-2

quasi-TEM behavior becomes significant. Thus this planar transmission medium becomes too lossy and too small in size (difficult tolerances). Furthermore, multimoding becomes a problem in microstrip circuits at higher frequencies.

Figure 2-2 shows the cross section of a shielded microstrip line. The transmission line consists of a perfectly conducting strip of zero thickness, and finite width, W, residing on top of a dielectric substrate of thickness, H, which, in turn, is enclosed inside a perfectly conducting box. In addition, the dielectric material and the metal shielding are assumed to be lossless.

Since the analysis and synthesis formulas of shielded microstrip line have been extensively reported in the literature [17]-[19], [34]-[36], these will not be presented here. Figure 2-3 shows the electric field configuration in single and coupled microstrip lines.

In order to design couplers and filters, the characteristics of coupled transmission lines must be known, i.e., the desired values of Z_{oe} (even mode characteristic impedance) and Z_{oo} (odd mode characteristic impedance) [18], [19] have been used to calculate the circuit dimensions of W/H and S/H as shown in Figure 2-2. The first step to obtain W/H and S/H is to find the two single line shape ratios $(W/H)_{se}$ and $(W/H)_{so}$ corresponding to the impedances $Z_{oe}/2$ and $Z_{oo}/2$, respectively.

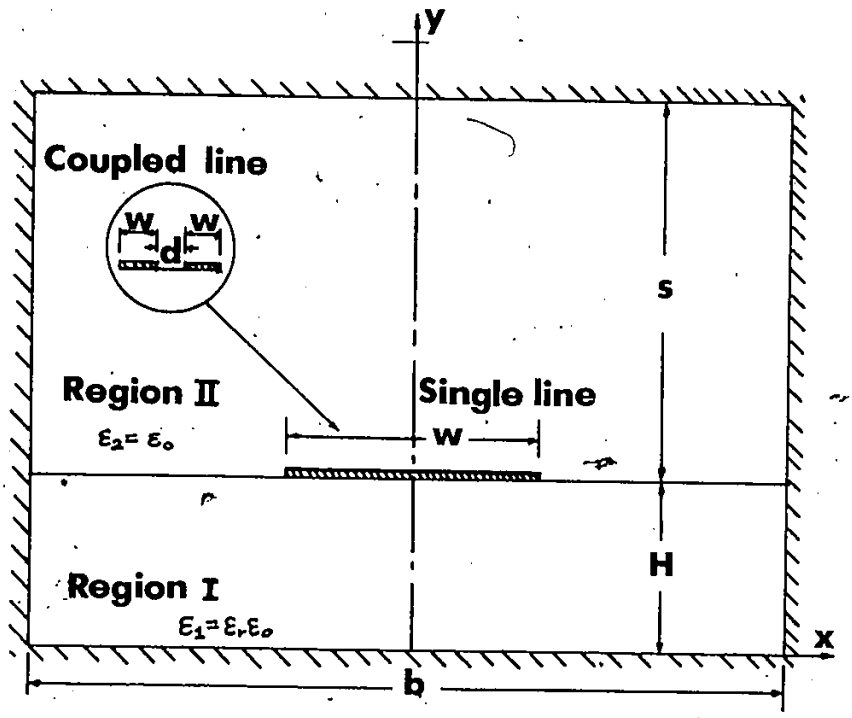

Figure 2-2. Cross sectional geometry of the shielded microstrip.

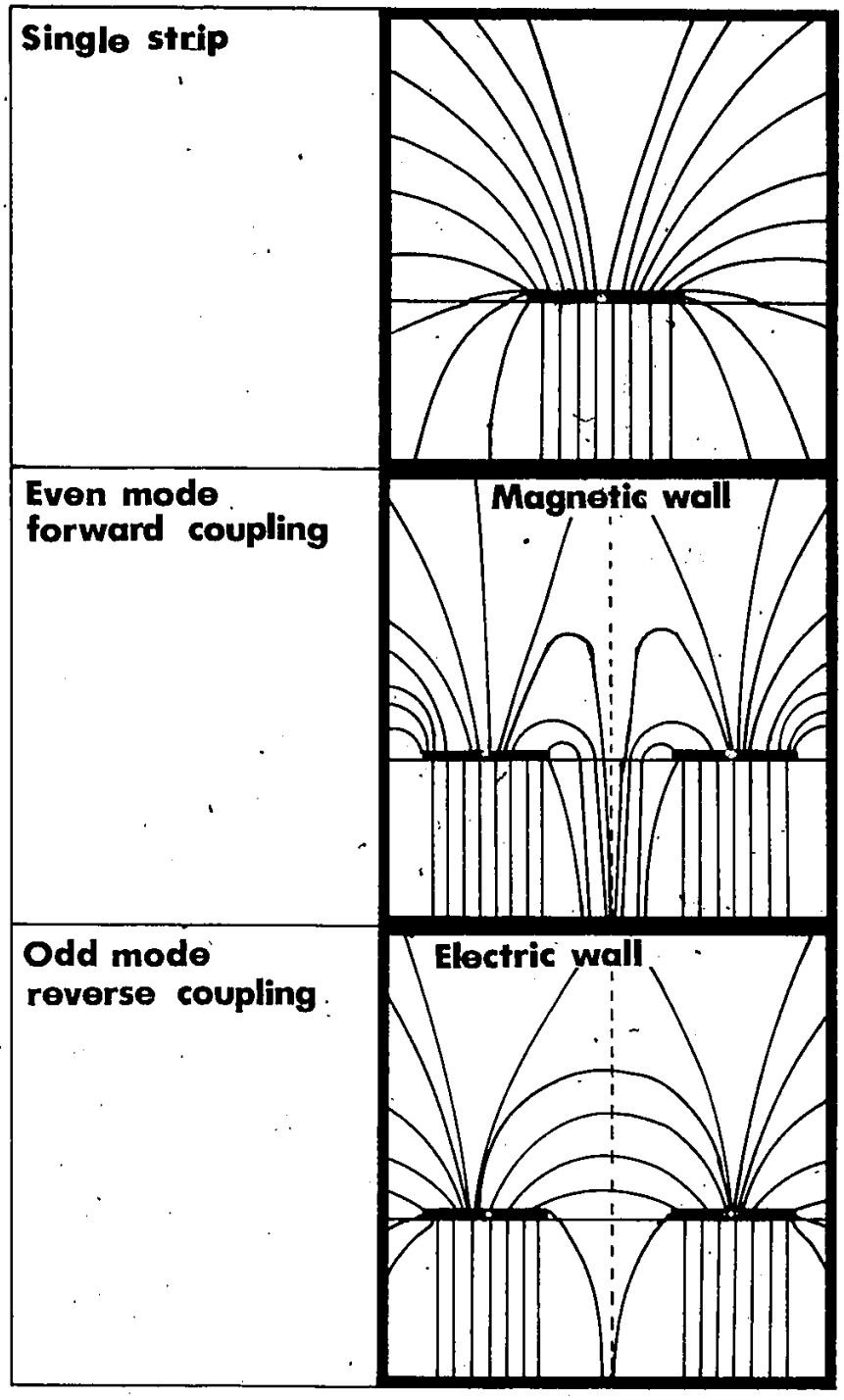

Figure 2-3. Electric field configurations of single and coupled microstrip lines.

2.3.3. Fin Lines

Fin lines are waveguides carrying a planar circuit in the E-plane, i.e., in the plane bridging the broad sides of the waveguide. Figure 2-4 shows the cross section of four possible fin line configurations.

Even though fin lines are basically loaded waveguides, their propagation properties are essentially determined by the geometry of the fins rather than the dimensions of the waveguide enclosure. This alleviates the stringent tolerance requirements for the waveguide dimensions and therefore reduces the cost of fabrication.

Figure 2-4 also suggests that fin lines are realized by inserting a planar metallization pattern on a dielectric substrate between the two identical halves of a split housing. Circuit elements such as impedance steps, inductive or capacitive discontinuities or short circuits are realized by simply changing the distance between the fins. There is no need to modify the dimensions of the enclosure. Thus, the fin lines combine the advantages of planar photolithographic realization and the high electrical quality of shielded waveguides.

Figure 2-5 shows the electric field lines of the dominant mode in unilateral fin line. The thickness of the substrate is exaggerated for the purpose of easier presentation. It can be seen that in the fundamental mode the energy is concentrated in the slot, thus providing a good impedance match between the line and devices connected across the slot. It is also obvious that the planar circuit capacitively loads the waveguide, thus lowering the cutoff frequency

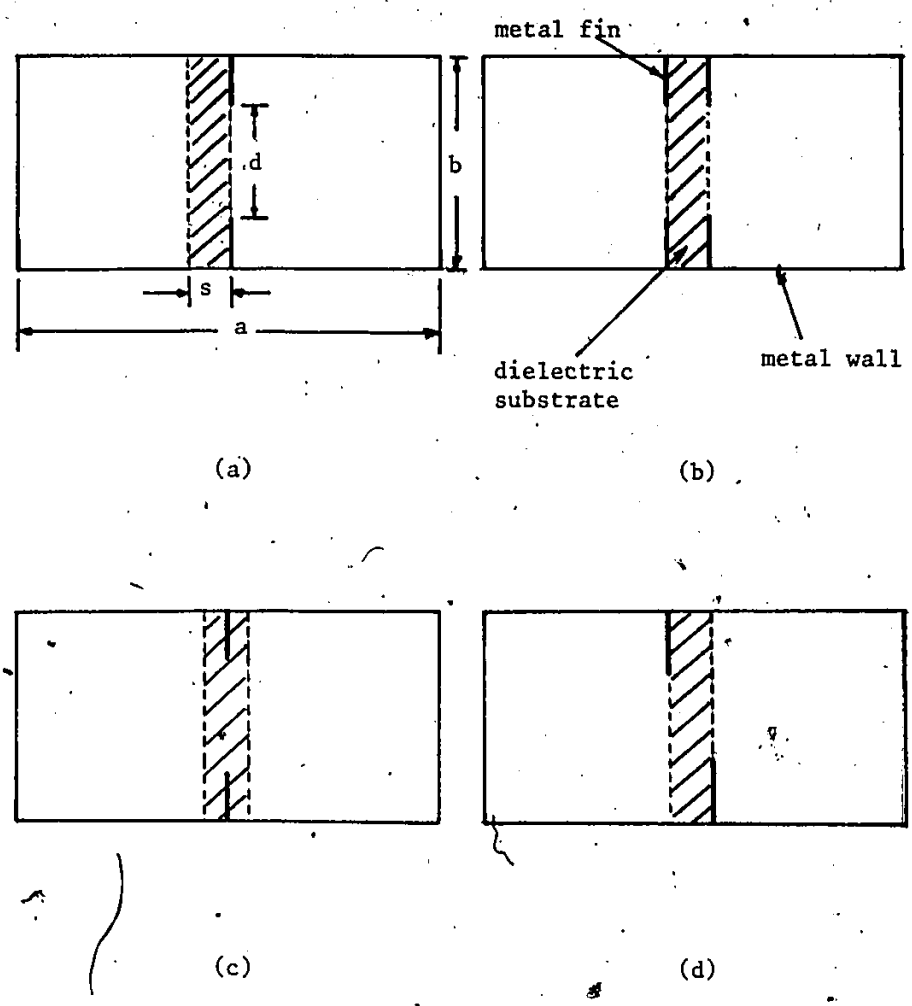

Figure 2-4. Cross sections of (a) unilateral, (b) bilateral, (c) insulated and (d) antipodal fin lines.

Aspect Ratio $b/a = 0.5$
Normalized Gap Width $d/b = 0.5$
Normalized Substrate Thickness $s/b = 0.25$
Dielectric Constant $\epsilon_r = 2.22$
Normalized Cutoff Frequency $b/\lambda_c = 0.1882$

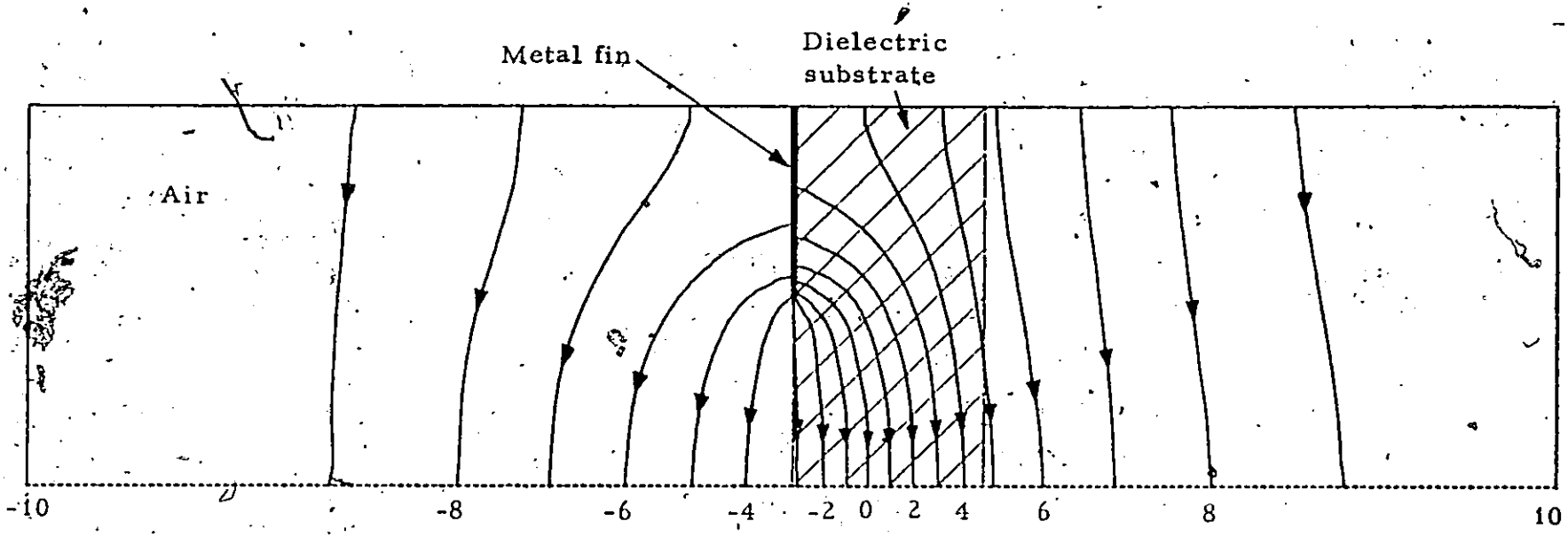

Figure 2-5. The transverse E field lines of the fundamental mode in a unilateral fin line.

of the dominant mode. The next higher mode, however, is hardly affected by the planar circuit, and its cutoff frequency is thus almost the same as in the empty waveguide. This means that the single mode bandwidth of fin lines is larger than that of commensurate waveguides and can effectively exceed one octave.

Since fin lines cannot sustain a static field, they have a non-zero cutoff frequency and exhibit linear distortion due to dispersion of the phase velocity. This results in a frequency dependence of the effective dielectric constant and the characteristic impedance as shown in Figure 2-6.

The effective dielectric constant, ε_{eff}, is conveniently defined as the square of the ratio of free-space wavelength and guided wavelength

$$\varepsilon_{eff} = (\lambda/\lambda_g)^2 \qquad (2.4)$$

The characteristic impedance of a fin line cannot be defined in an unambiguous way. Nevertheless, some specific definitions are useful in the treatment of non-TEM transmission lines as long as they are appropriate for a given application. Two different definitions of the characteristic impedance are presented. One definition for the characteristic impedance is given by

$$Z_o = V^2/2P$$

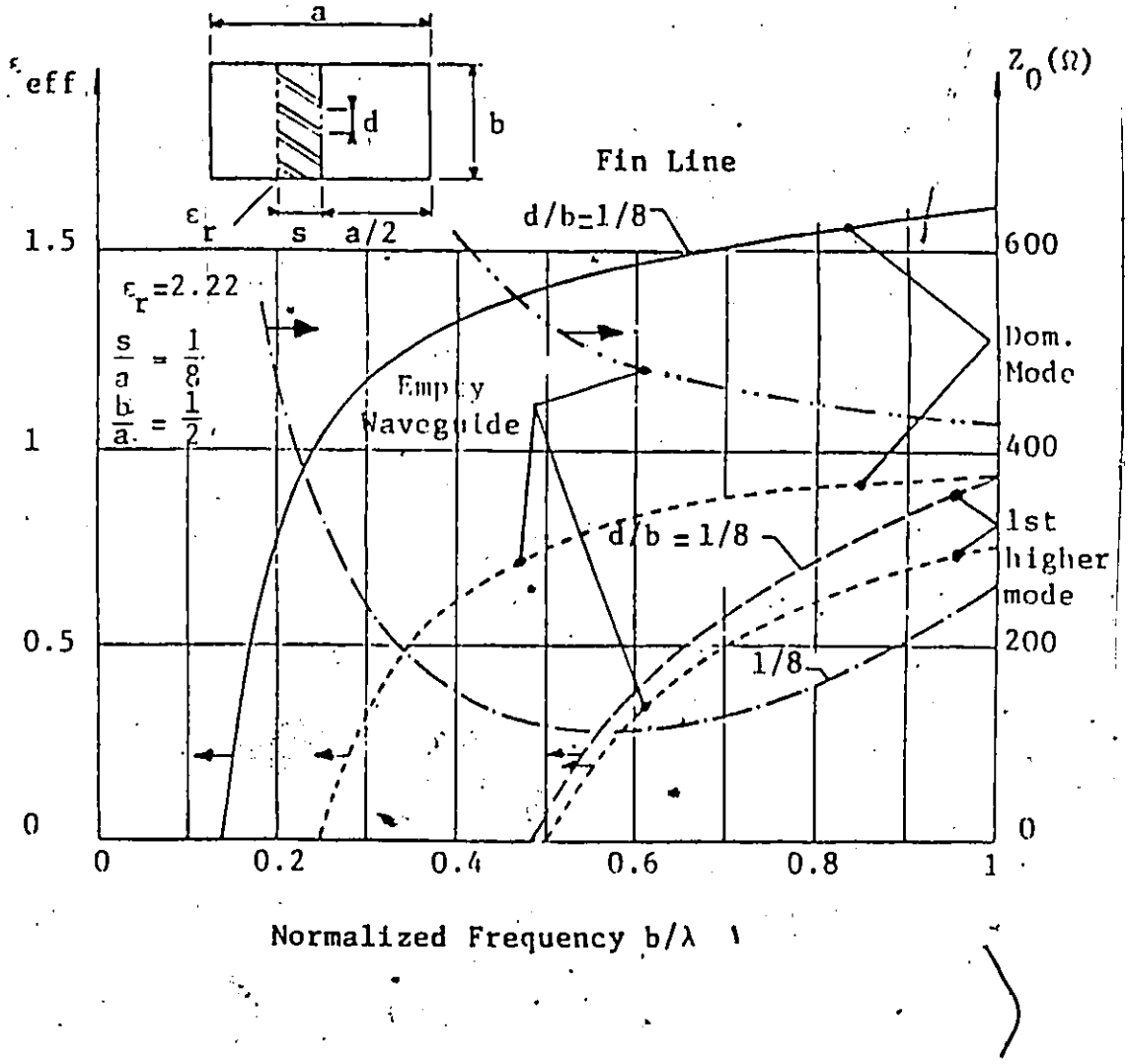

Figure 2-6. Effective dielectric constant and characteristic impedance in fin line & commensurate waveguide.

where V is the voltage measured across the slot between the fins along the dielectric, and P is the average power carried by the line. But it is noted that there is a difference between the value of the characteristic impedance obtained from this definition and that of the characteristic impedance in the definition

$$Z_o = V/I$$

as shown in Figure 2-7.

At cutoff, ϵ_{eff} becomes zero since λ_g tends toward infinity, and Z_o is infinite because the transmitted power is zero. As frequency increases, ϵ_{eff} tends asymptotically toward ϵ_r of the substrate. This is due to the fact that with increasing frequency the RF power is concentrated more and more in the dielectric. This concentration also causes the voltage across the gap to increase with frequency, thus Z_o increases as well.

A comparison of these characteristics with those of the commensurate empty waveguide (dotted lines in Figure 2-7) show clearly the following features of fin lines:

i) The dominant cutoff frequency is considerably lowered. The cutoff frequency of the first higher mode is practically the same. Hence, the operating bandwidth of the fin line is larger than that of the waveguide.

ii) Within the original waveguide band, the fin line is less dispersive than the waveguide. (Its ϵ_{eff} changes less

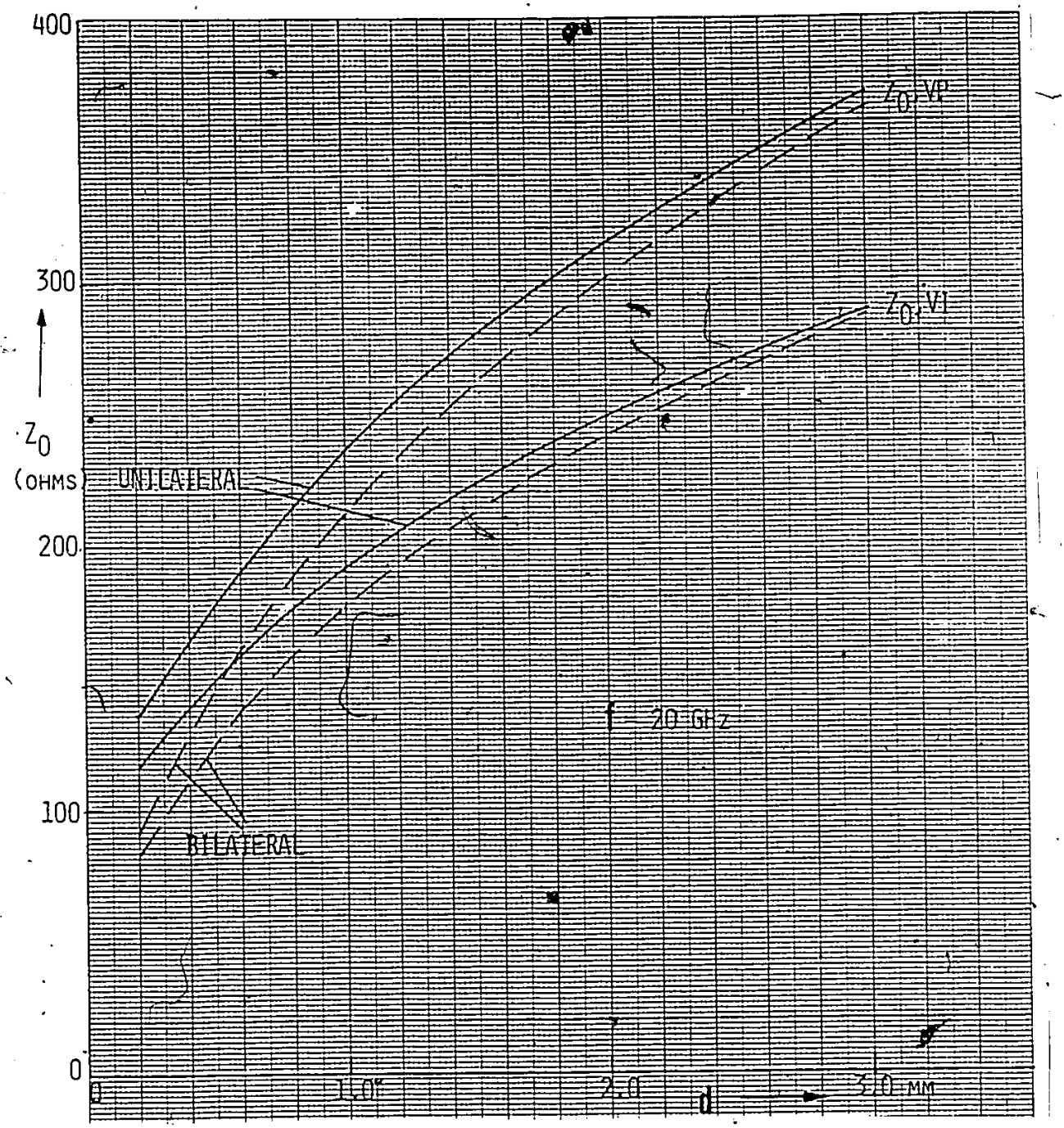

Figure 2-7. Fin line characteristic impedances obtained from two different definitions at 20 GHz (RT/duroid 5880 (ε_r=2.22), thickness: .254 mm (.01 in), WR 42 waveguide enclosure).

with frequency.) Hence, it has less linear distortion than the waveguide.

iii) Within the operating bandwidth, the fin line has lower characteristic impedance than the waveguide, which is advantageous when introducing semiconductor devices into the line.

The lowest characteristic impedance (less than 10 Ω) can be obtained with antipodal fin lines by overlapping the fins. However, the insertion of devices is more difficult in such lines since they must be placed across the dielectric substrate.

Losses are about one order of magnitude higher in fin lines than in commensurate waveguides. This is due to the fact that fields are concentrated in the vicinity of fin edges, thus the current is distributed over a much smaller area causing higher conductor losses. Furthermore, dielectric losses occur in the substrate. Since for fin lines with narrow slots the attenuation constant increases linearly with frequency, it is convenient to express fin line losses in dB/wavelength.

For typical fin lines, the attenuation constant at millimeter wavelengths is approximately 0.1 dB/wavelength. This is about three times as low as that of a comparable microstrip line and corresponds to an unloaded Q of about 260.

Fin line circuits are usually realized with enclosures of standard waveguide size. This ensures compatibility with instrumentation and waveguide components. Transitions are realized by tapering

The length of the fins from zero to the final value over a distance of one to three wavelengths.

The only role of the substrate is to mechanically support the delicate metallic fins and the devices connected to them. In order to reduce its electrical influence on the line, it is made as thin as mechanical considerations permit, and its permittivity as well as its loss tangent should be as small as possible. The two most frequently used substrates are RT/duroid 5880 ($\varepsilon_r = 2.22$, $\tan\delta = 10^{-3}$) and fused quartz ($\varepsilon_r = 3.75$, $\tan\delta = 10^{-4}$). The metallic pattern are produced on one or both sides of the substrate using conventional thin film photolithographic techniques. Devices in beam lead or chip form can easily be mounted in the fin line pattern.

The closed form expressions for fin line synthesis are also reported in the Appendix for easy reference.

2.4 Conclusion

At mm-wave frequencies, the attenuation constant of microstrip line is about three times as high as that of a comparable fin line as mentioned in the previous section. Also higher order modes and fabrication tolerances become considerable problems in the higher millimeter band.

At 17 GHz, the combination of the microstrip line and fin line for our mixer design permits one to take best possible advantage of the properties of these transmission media.

CHAPTER 3

DESIGN AND REALIZATION OF A PLANAR SINGLE BALANCED MIXER FOR 17 GHz

The design and the realization of a planar single balanced mixer at 17 GHz are illustrated in this chapter. The descriptions of two fin line transitions, two microstrip filters, the planar 180° hybrid junction, matching networks, and enclosure designs are included.

3.1 Introduction

The development of a Ku-band single balanced mixer using a 180° hybrid in quasi-planar technique is described in this chapter. Considerable design information for this type of mixer is available in the literature [20]-[24].

The mixer pumped by a 16.1 GHz local oscillator converts a RF signal at 17 GHz down to an IF of 900 MHz with a bandwidth of 1 GHz.

The elements which are designed and realized include unilateral and antipodal fin line transitions, two microstrip low pass and band pass filters, a 180° hybrid junction combining fin line and microstrip line, and a matching (tuning) network. These components are integrated on 0.03 in. thick RT/duroid 5880 substrate ($\varepsilon_r = 2.22$) which is suspended in the E-plane of the waveguide (WR 62) channel using 0.5 mm deep slots.

3.2 Overall Configuration of the Mixer

The mixer receiver front end design in this thesis covers the signal path from the output of the receiving antenna to the input of the IF amplifier but does not include the local oscillator design.

Figure 3-1 is a photograph of the completed mixer showing the elements mentioned in the previous section and Figure 3-2 shows a low frequency equivalent circuit with the most important features of the mixer.

COLOURED PICTURES
Images en couleur

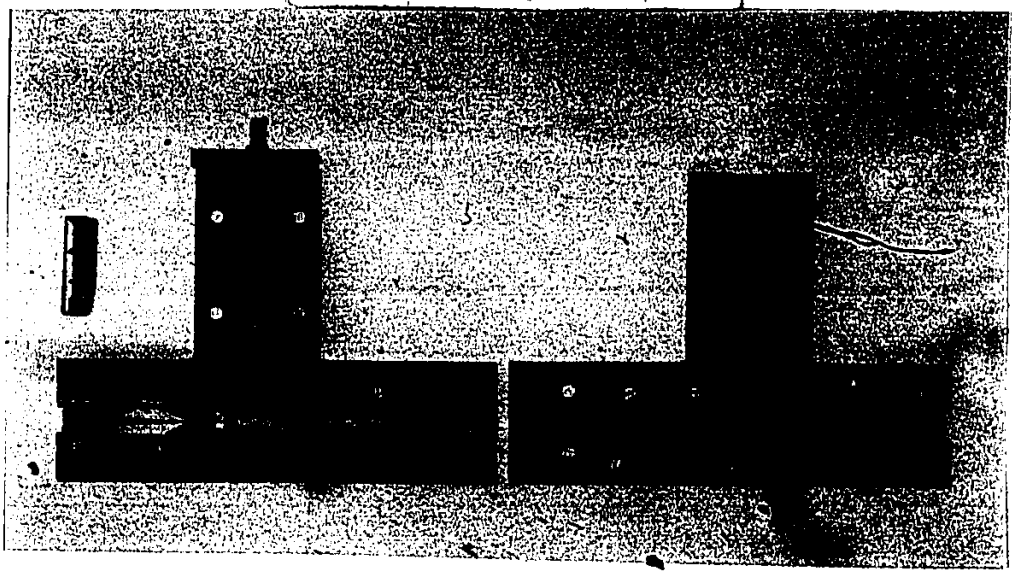

Figure 3-1. A photograph showing the complete circuit of the mixer.

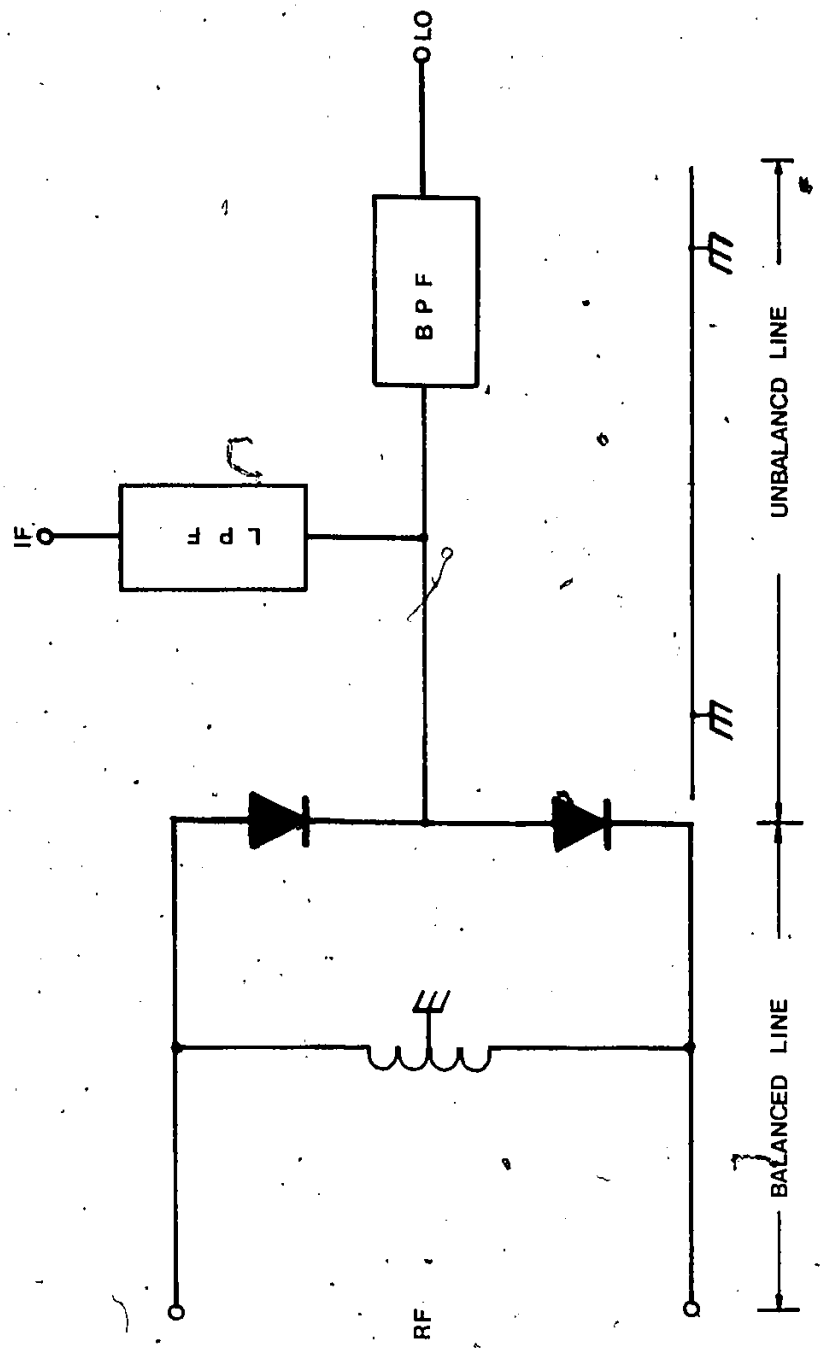

Figure 3-2. Schematic diagram of single balanced mixer using 180° hybrid

The main feature of the mixer design is in the junction (180° hybrid) formed by a balanced transmission line (fin line) and an unbalanced transmission line (microstrip line). In the particular design chosen, the RF signal is incident on the balanced line and the LO signal on the unbalanced line. Basically the unbalanced signal from the microstrip line cannot propagate past the junction, while the balanced signal from the fin line can pass the junction. The junction ensures symmetrical excitation by the LO signal and antisymmetrical excitation by the RF signal.

With the nonlinear mixing elements (two beam lead GaAs Schottky barrier diodes) connected across the interface between two transmission media as shown in Figure 3-2, when RF and LO signals are applied to the diodes, the signals are radiatively coupled to the diodes and heterodyned in them. The IF signal appears on the unbalanced line side: therefore a diplexer is required to seperate the LO from the IF signal. Figure 3-2 shows a diplexer consisting of the parallel connection of a low pass filter and a band pass filter.

Since the mixer is a three port device, three transitions to external circuits as explained in Section 3.4 are required in the mixer design.

3.3 Realization of the Hybrid Junction

The most important part of the single balanced circuit is the 180° hybrid junction realized in planar technology.

To obtain a 3 dB 180° hybrid characteristic in planar circuit form, two orthogonal mode transmission lines, namely fin line and

microstrip line have been used. The electric field configurations of the two quasi-planar transmission media are shown in Figure 3-3. The planar 180° hybrid junction is formed by combining two orthogonal mode planar transmission media as shown in Figure 3-4. This planar hybrid has the same characteristics as a conventional waveguide magic Tee.

The E-fields on the unbalanced microstrip line which carries the LO signal are divided symmetrically at the junction. Areas 1 and 2 shown in Figure 3-4 provide in-phase excitation of the LO signal. The fin line carrying the RF signal provides antisymmetric and hence, out-of-phase excitation in areas 1 and 2. The balance of the above mentioned characteristic depends on the symmetry of the junction geometry.

The fact that the unbalanced signal from the LO port cannot pass the junction effectively isolates the RF port from the LO port and prevents the radiation of the LO signal through the receiving antenna. ω_{LO}-to-ω_s isolation is usually greater than 20 dB. But this property also causes the VSWR for both ω_s and ω_{LO} ports to depend on the match between the respective transmission lines and the diode in the same way as in single ended mixers.

Both the LO and IF signals exist on the unbalanced microstrip line. Thus, a low pass filter for separating both signal is necessary.

The mixer has been designed by connecting two GaAs Schottky barrier diodes across the junction. It is important to match the diodes to the RF and IF ports for a low conversion loss. LO match

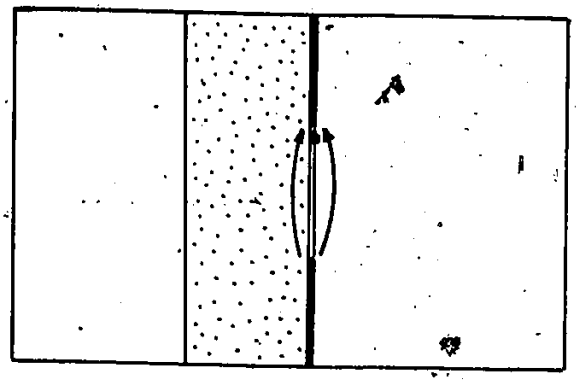

fin line

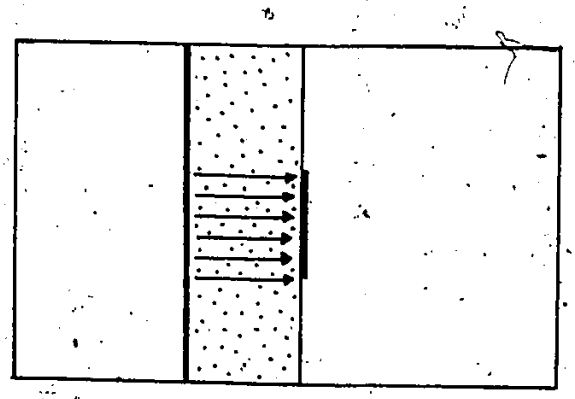

microstrip

Figure 3-3. E-field configurations of two orthogonal transmission media.

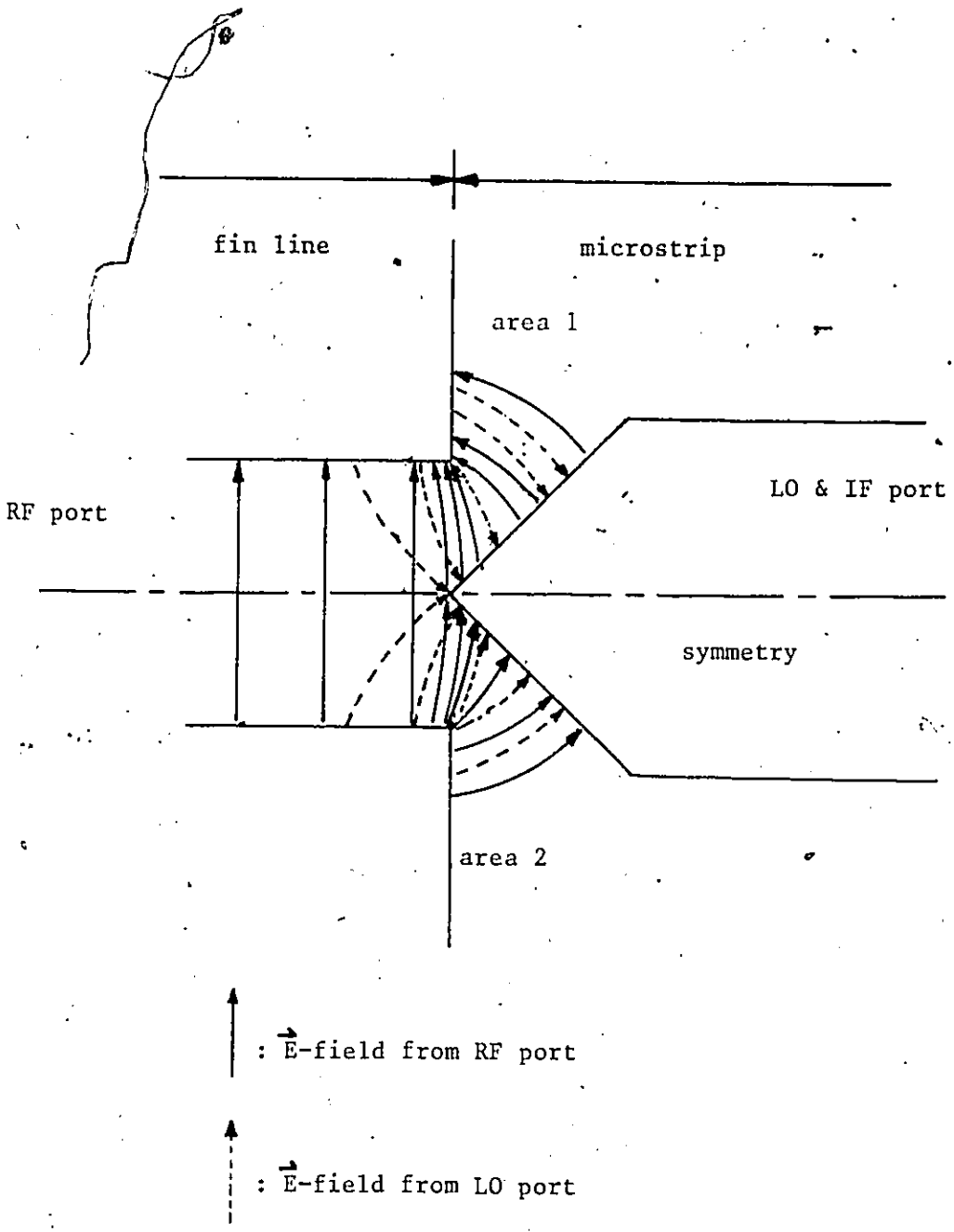

Figure 3-4. E-field configuration across the junction.

can be degraded at the expense of increased LO power. But the matching networks for the RF and LO sides are related, because the diode parasitics are common to both. At 17 GHz, the diode parasitics are strong functions of the mounting structure, particularly the series inductance L_s and the mounting capacitance C_m as shown in Figure 3-5. Although the diode impedance should be characterized in an environment similar to that of the final application, it is almost impossible to characterize the diode in the same fin line-microstrip junction. Therefore, in designing this mixer two types of tunable diode matching circuits have been included in order to optimize diode match empirically. Figure 3-5 shows the equivalent circuits of the input matching networks of the RF and LO signals as seen by one individual diode.

The Beam leads of GaAs Schottky barrier diodes have inductive components rather than capacitive ones. This is so because manufacturers keep the capacitance as small as possible to avoid RF shunting effects. To compensate the inductive component of the diode beam lead, an open stub was introduced with a length

$$\ell_{stub} < \lambda_{gRF}/4 \qquad (3.1)$$

The impedance of the open stub can be expressed as $Z = -jZ_o \cot\beta\ell$. A special method described below has been used to tune the diode reactance since it is very difficult to measure the exact impedance of such diodes mounted on the junction. Figure 3-6 shows the realization of the input matching network. It consists of the symmetrical microstrip

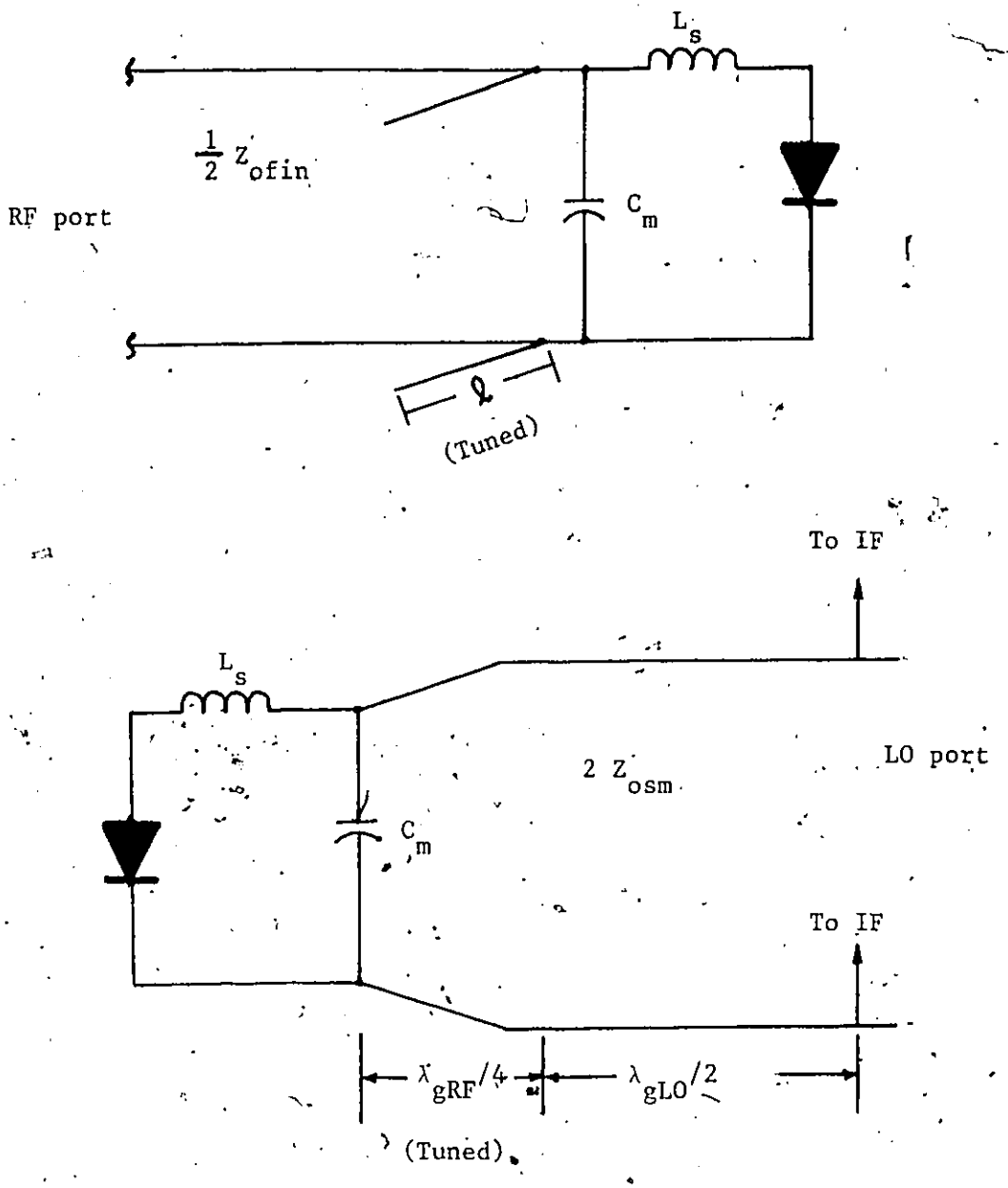

Figure 3-5. The equivalent diode matching networks for the RF and LO ports.

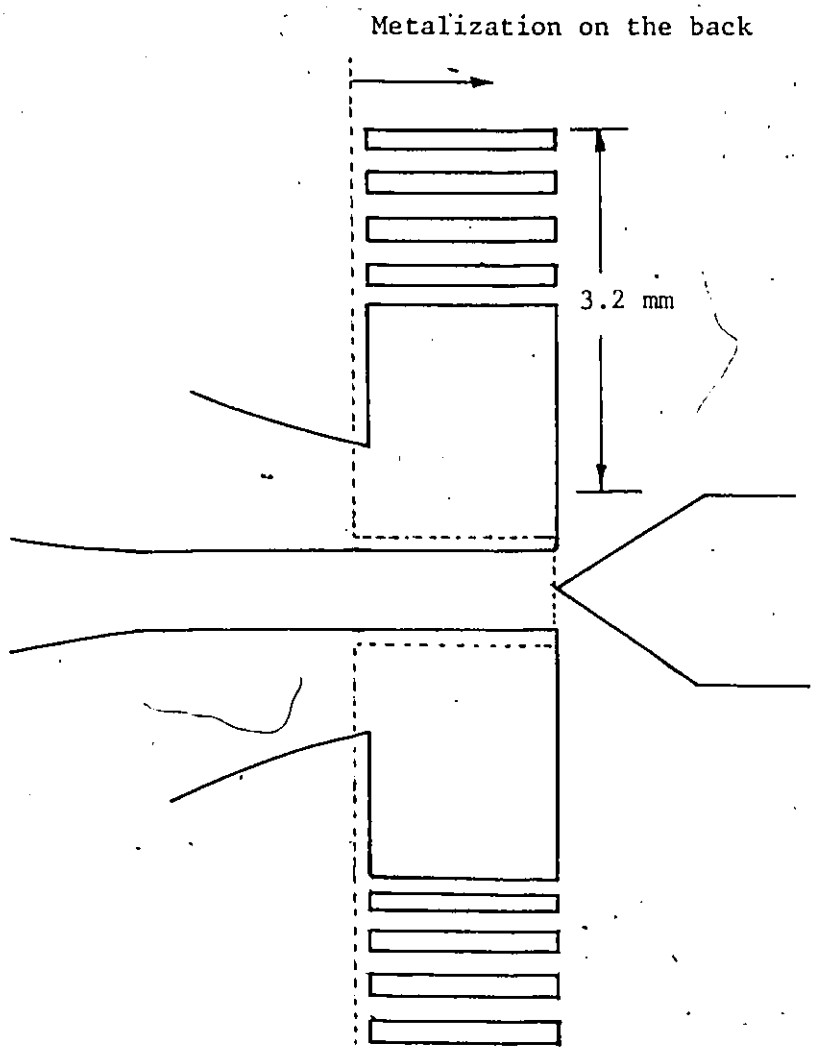

Figure 3-6. The experimental tuning circuit for compensating the reactance components of the diodes.

stubs with a number of metallic segments. The electrical length of the stubs can be increased in steps by covering the gaps with solder.

The $\lambda_{gLO}/2$ section in Figure 3-5 was chosen for resonance at the LO frequency, and $\lambda_{gRF}/4$ was also chosen to return the RF reflection passing the junction to the diodes again for more mixing in the diodes. The IF signal can be extracted through the LPF and the IF port right after the $\lambda_{gLO}/2$ section.

A photomicrograph of the junction is shown in Figure 3-7. The two beam lead GaAs Schottky barrier diodes have been connected across the junction between fin line and microstrip line by means of the epoxy soldering technique [25]. Epoxy soldering-- a low temperature soldering-- requires a temperature 125° for about 1 hour. ABLEBOND 36-2 (trade name) which contains silver as a lead has been used as a soldering material. The typical properties of the epoxy (ABLEBOND 36-2) are shown in Table 3-1. When connecting the diodes across the junction, very careful attention is required, and because of the tiny dimensions of the diodes, toothpicks have been used to handle and to position the diodes.

3.4 Design of Transitions

Three types of transitions are used in this mixer.

- a tapered transition from waveguide to unilateral fin line.
- a tapered transition from waveguide to microstrip line via an antipodal fin line.
- a short transition from microstrip line to coaxial line.

Table 3-1. Typical properties of ABLEBOND36-2.

Consistency	Very soft, very smooth paste	
Filler	pure silver	
Specific Gravity	2.4 grams/ml	
Suggested Cure schedules (MIN)	1 hour @ 125°C or 1/2 hour @ 150°C	
Hardness (Shore D)	82	
Volume Resistivity	Cured one hour @ 125°C	0.0001 ohm-cm
	Cured 1/2 hour @ 150°C	0.0001 ohm-cm
	Cured 5 minutes @ 200°C	0.0001 ohm-cm
	Cured 3 minutes @ 250°C	0.00006 ohm-cm
Volume Resistivity After 250 hours @ 85°C and 95% RH		0.0001 ohm-cm
Volume Resistivity After 1000 hours @ 150°C		0.0001 ohm-cm
Volume Resistivity @ 150°C		0.0001 ohm-cm
@ 200°C		0.0001 ohm-cm
@ 300°C		0.0001 ohm-cm
@ 400°C		0.0001 ohm-cm
Return to 25°C		0.00004 ohm-cm

Temperature increased 55°C each 15 minutes

Lap Shear Strength To Gold	1800 PSI	
Aluminum	1200 PSI	
Lap Shear Strength To Gold after 250 hours @ 200°C	1000 PSI	
Thermal Conductivity @121°C	1.0 $\frac{BTU/ft}{ft^2 hr/°F}$	

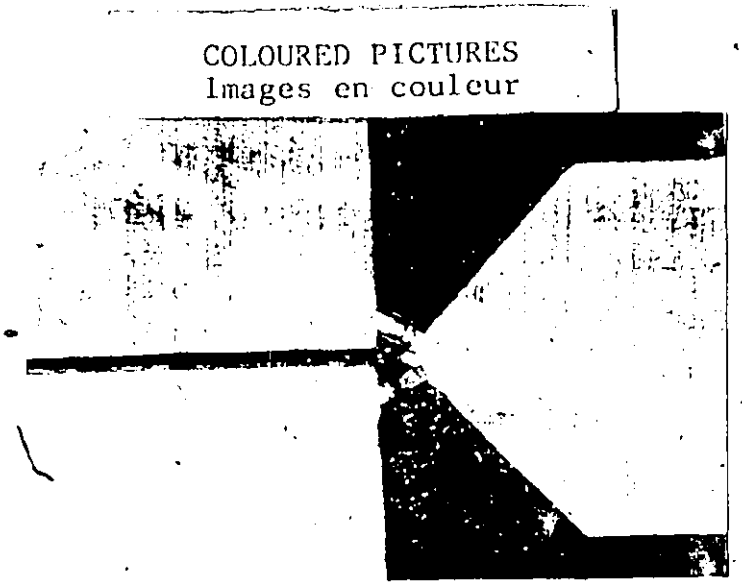

Figure 3-7. A photomicrograph showing the two beam lead diodes connected across the junction.

First we will consider the input impedance transformer to match the diode pair to the signal input via a unilateral fin line taper. The equivalent circuit between the output of the receiving antenna and the diode pair is shown in Figure 3-8(a). The waveguide impedance [26] at the fundamental mode, Z_{in}, is given by

$$Z_{in} = 668 \frac{b}{a} \frac{\lambda_g}{\lambda_o} \qquad (3.2)$$

where a and b are the waveguide inside dimensions. λ_g and λ_o are the guided wavelength in waveguide and the free space wavelength respectively.

The resistive mixing diode impedance was assumed to be 100 Ω, the value suggested by the manufacturer. But the matched diode pair is connected in series at the RF port and in parallel at the LO port respectively. Therefore the slot width of the fin line right before the diode pair was designed to be 200 Ω. Two capacitive open stubs described earlier were added. The tuning network right after the diode pair must block the RF signal passing across the junction. It consists of a $\lambda_{gRF}/4$ section of microstrip line. Since the matched diode pair is connected in parallel at the LO port, a 50 Ω microstrip line was placed after the matched diode pair.

The fin line taper was designed as follows: since at the diode pair, the fin line impedance had to be equal to 200 Ω, the corresponding slot width for a RT/duroid 5880 substrate (ε_r = 2.22, thickness 0.03 in) has been calculated with a computer program [27] to be 0.46 mm. The fin line taper transition layout was then obtained

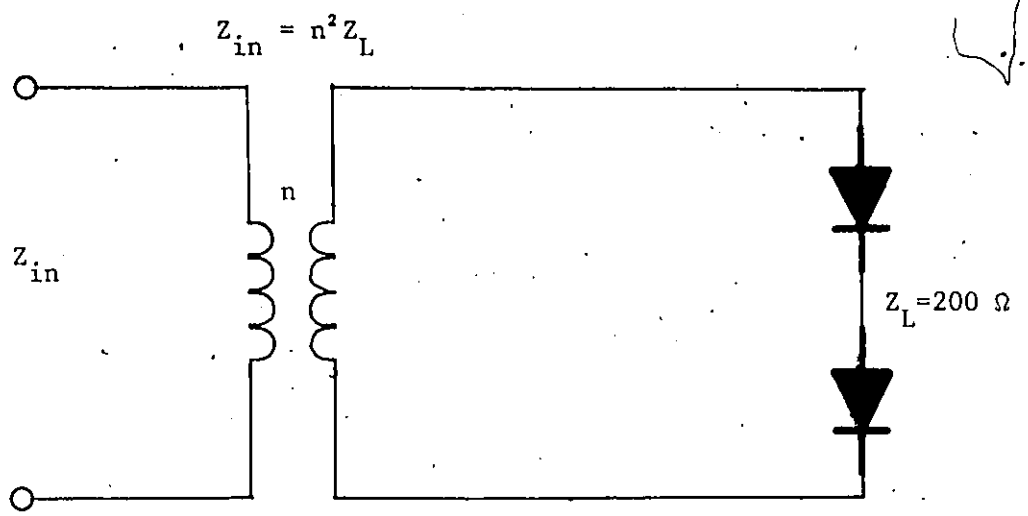

(a) equivalent circuit looking from the RF port

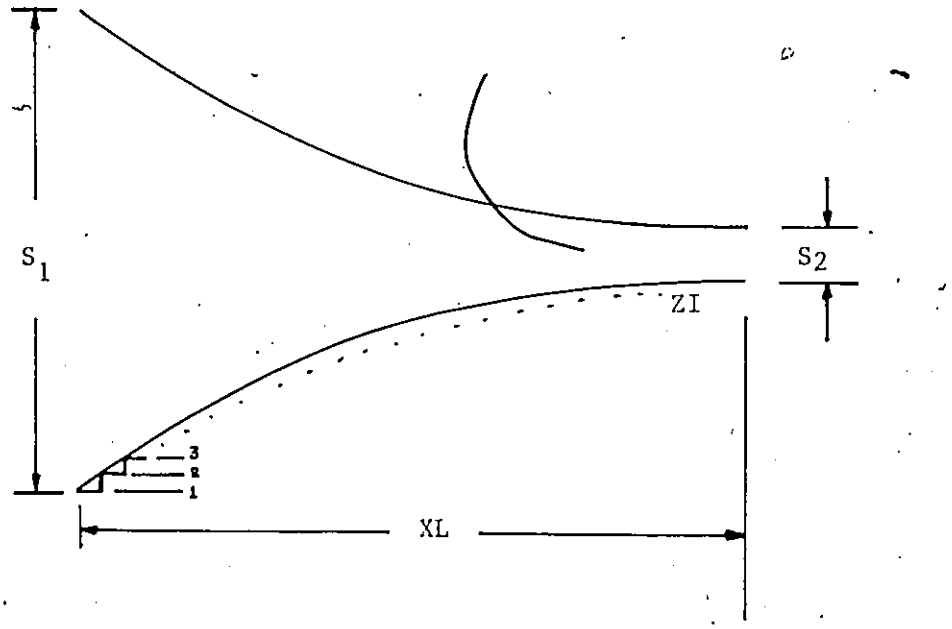

(b) configuration of the taper transition synthesis

Figure 3-8. Design and realization examples of the RF port unilateral fin line taper transition.

with (3.3) using a CALCOM plotter as shown in Figure 3-8(b).

The equation of the profile is given by (3.3)

$$S = S1 - (S1 - S2)\left(1 - \frac{ZI \cdot \Delta\ell}{XL}\right)^3 \qquad (3.3)$$

where S : the width between two taper lines shown in Figure 3-8(b).

ZI: the increment number for a given taper length. ZI_{max}=400 was chosen for this thesis.

S1: largest slot width (7.8 mm).

S2: smallest slot width (0.46 mm).

XL: length of the taper transition (40 mm = $2\lambda_{gRF}$).

$\Delta\ell$: incremental length (XL/ZI_{max}).

The unilateral fin line taper transition for the RF port to the matched diode pair was realized as shown in Figure 3-8. The antipodal fin line taper transition from the LO port to the 50 Ω microstrip section has been designed and the taper layout has also been obtained with the same method as the unilateral taper shown in Figure 3-9. The VSWR of the shielded microstrip line to SMA coaxial line transition at IF port can be neglected because of the low frequency (900 MHz). The resulting VSWR at the IF port is shown in Figure 4-9.

3.5 Design of Microstrip Filters

As we mentioned earlier, a diplexer is required to obtain the IF signal since the two signals, the LO and IF signals, appear at the output of the diode pair. To realize such a diplexer, we have designed a low pass filter for the IF signal and a band pass filter for the LO

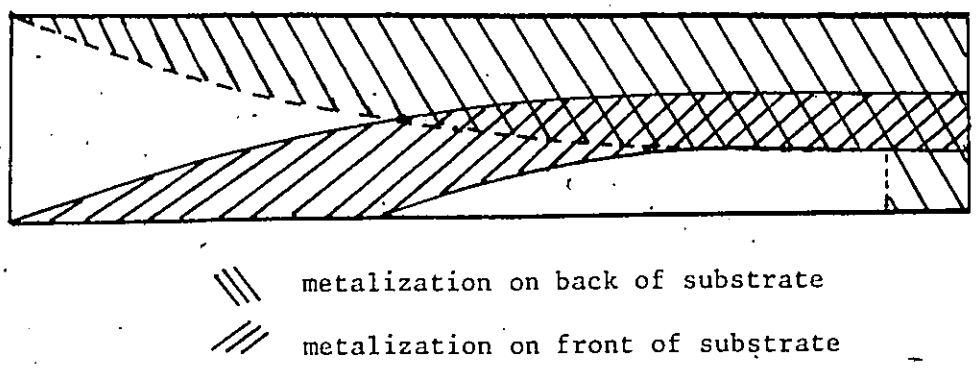

Figure 3-9. Antipodal fin line taper transition for the LO port.

signal. In this section the design details of the filters will be explained in sequence.

3.5.1 Microstrip Low Pass Filter

A symmetrical Tchebyscheff low pass prototype filter with 0.01 dB ripple at the IF (900 MHz, Δf = 1 GHz) and 30 dB attenuation at 2 GHz, have been designed with a LC cascaded network [28] as shown in Figure 3-10. 5 sections were chosen to meet the filter specification.

From the symmetrical property of the LC network in Figure 3-10,

$g_1 = g_3 = g_5$: inductance

$g_2 = g_4$: capacitance

g_0 = generator internal impedance (50 Ω)

g_6 = load impedance (50 Ω)

The normalized generator impedance and the normalized radian frequency of the pass band edge respectively.

$g_0 = 1$

$\omega_1' = 1$

Since the LPF has a symmetrical configuration, we need the calculation of 3 section components.

$n = 3$

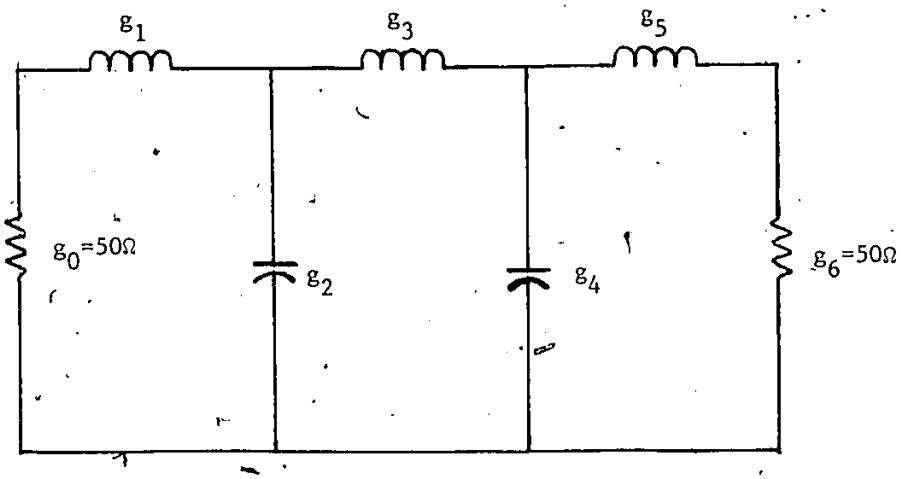

(a) lumped circuit form

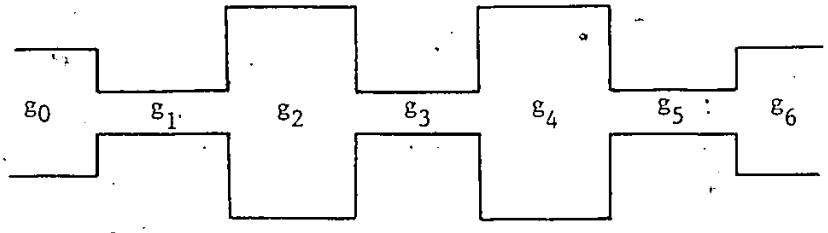

(b) microstrip form

Figure 3-10. LPF realization from the lumped circuit form to microstrip form.

The normalized values of the components can be obtained from Table 4-2 in the Reference [28].

Thus

$$G_0' = G_6' = g_0 = g_6 = 1 \text{ [Mho]}$$

$$L_1' = L_5' = g_1 = g_5 = 0.7563 \text{ [H]}$$

$$C_2' = C_4' = g_2 = g_4 = 1.3049 \text{ [F]}$$

$$L_3' = g_3' = 1.5773 \text{ [H]}$$

The real values of the components can be obtained by the following transformation formulas [28]. For resistances or conductances,

$$R = \left(\frac{R_0}{R_0'}\right) R' \quad \text{or} \quad G = \left(\frac{G_0}{G_0'}\right) G' \tag{3.4}$$

For inductances,

$$L = \left(\frac{R_0}{R_0'}\right)\left(\frac{\omega_1'}{\omega_1}\right) L' = \left(\frac{G_0'}{G_0}\right)\left(\frac{\omega_1'}{\omega_1}\right) L' \tag{3.5}$$

And for capacitances,

$$C = \left(\frac{R_0'}{R_0}\right)\left(\frac{\omega_1'}{\omega_1}\right) C' = \left(\frac{G_0}{G_0'}\right)\left(\frac{\omega_1'}{\omega_1}\right) C' \tag{3.6}$$

where $G_0 = 0.02$, $f_1 = 1.4$ GHz, $\omega_1 = 2\pi f_1$

$$\frac{\omega_1'}{\omega_1} = 0.1137 \times 10^{-9}$$

$$\frac{G_0'}{G_0} = 50, \quad \frac{G_0}{G_0'} = 0.02$$

Therefore, we obtain

$$L_1 = L_5 = 4.3 \text{ nH}, \; L_3 = 8.97 \text{ nH}$$

$$C_2 = C_4 = 2.97 \text{ pF}$$

where the effect of the dispersion at the IF frequency (less than 1.4 GHz) is neglected.

The next step is the realization of a microstrip LPF with the above mentioned components. In general, the distributed lumped model impedance of a transmission line can be assumed

$$Z_{oC} \text{ (capacitance)} < Z_o \text{ (50 } \Omega) << Z_{oL} \text{ (inductance)} \qquad (3.7)$$

To ensure that no LO signal reached the IF port, two $\lambda_{gLO}/4$ sections were used to realize g_1 and g_5, and the impedances of the two $\lambda_{gLO}/4$ sections were selected in accordance with their length. Reasonable starting values for the inductive and capacitive section impedances have been assumed in accordance with (3.7). For the capacitive line:

$$Z_{oC} = 25 \ \Omega.$$

For the inductive line:

$$Z_{oL} = 130 \ \Omega.$$

It was further assumed that losses were negligible.

The lengths for the mainly inductive elements (short line ($< \lambda_g/4$)) are given by

$$X_L = Z_o \sin (2\pi\ell/\lambda_g)$$

$$\ell = (\lambda_g/2\pi) \sin^{-1}(\omega L/Z_o) \tag{3.8}$$

By using a small angle approximation ($2\pi\ell/\lambda_g << \pi/4$), (3.8) is simplified to

$$\ell \cong \frac{f\lambda_g L}{Z_o} \tag{3.9}$$

Lengths of mainly capacitive elements can be realized by

$$B_C = \frac{1}{Z_o} \sin (2\pi\ell/\lambda_g)$$

$$\ell = \frac{\lambda_g}{2\pi} \sin^{-1}(\omega C Z_o) \tag{3.10}$$

As in the previous inductance case,

$$\ell \cong f\lambda_g Z_o C \tag{3.11}$$

The combination of low impedance (wide microstrip line) and high impedance (narrow microstrip line) results in a significant step discon-

tinuity. But the stray series inductance due to the discontinuity can be neglected. The expression for the step capacitance for short length is approximately given by [29]

$$C_L \cong \frac{1}{2fZ_o\lambda_g} \qquad (3.12)$$

The capacitance actually calculated for the capacitive length of line must in fact be less than the required total lumped value C because the inductive sections of line and the steps in width already contribute their capacitances, C_L and C_s respectively.

Therefore, for the capacitive line

$$C_{line} = C_T - C_{L1} - C_{L2} - C_{s1} - C_{s2} \qquad (3.13)$$

where C_{L1} and C_{L2} are obtained from (3.12), applied to each adjacent inductive line, and C_{s1} and C_{s2} are determined using the expression given in Reference [30]. $C_2' = C_4' = 2.45$ pF was obtained for this LPF. The overall 1.4 GHz microstrip low pass prototype filter has been realized as shown in Figure 3-11.

3.5.2. Parallel Coupled Resonator Band Pass Filter

The microstrip band pass filter was designed by cascading half wave resonators / each quarter-wave parallel coupled to its neighbor. This type of filter has a narrow-to-moderate (10~15%) bandwidth characteristic. The advantage of parallel or side coupling over the end coupling is that the filter length is reduced by approxi-

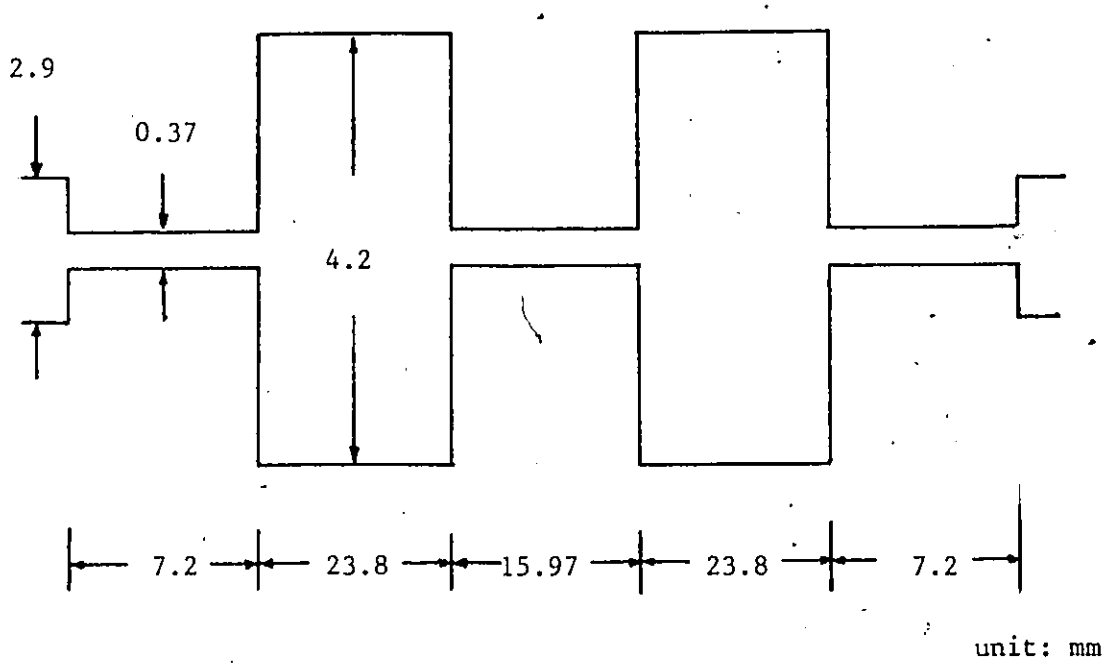

Figure 3-11. Actual 1.4 GHz microstrip low pass prototype filter.

mately half. The mixer unit becomes more compact in size than when direct (end) coupled structures are used. Also the parallel arrangement provides relatively large coupling for a given spacing between resonators.

The actual structure of the microstrip parallel coupled BPF using half-wavelength resonators, positioned so that adjacent resonators parallel each other along half of their length is shown in Figure 3-12.

The Tchebyscheff BPF for the LO signal in the mixer has been designed with the following characteristics: 0.1 dB insertion loss at pass band and 30 dB or more attenuation (isolation) at 14 and 18.2 GHz. To meet this specification, n=4 is required.

Figures 3-14(a) and (b) show a typical low pass prototype design and a corresponding BPF design, which can be obtained directly from the prototype as explained in the previous section by a low pass to band pass transformation [28].

In the equations for the band pass filter element values, the g_j are the prototype filter element values, ω' and ω_1' correspond to the prototype filter response as shown in Figure 3-14(a) for a typical Tchebyscheff case, and ω, ω_0, ω_1, and ω_2 apply to the corresponding band pass filter response as shown in Figure 3-13(b).

The filter structure in Figure 3-14(b) consists of series resonators alternating with shunt resonators, an arrangement which is difficult to achieve in a practical microwave or mm-wave structure. In micriwave and mm-wavw filters, it is much more practical to use a structure which approximates the circuit in Figure 3-14(c), or its

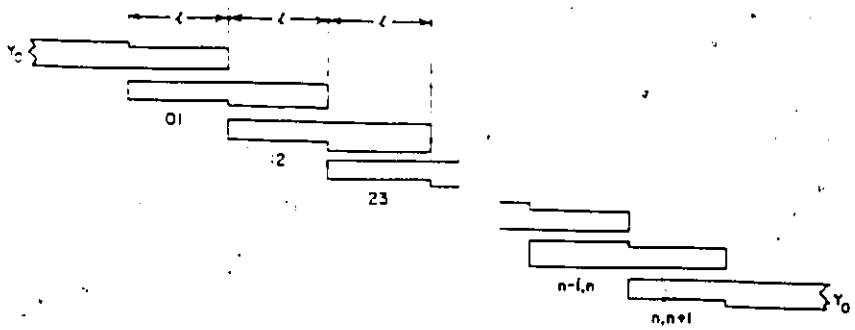

Figure 3-12. The shape of microstrip parallel coupled BPF.

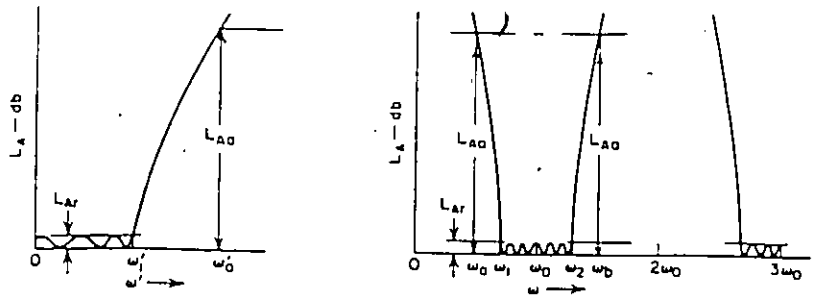

(a) (b)

Figure 3-13. Low pass prototype response and corresponding band pass filter response.

dual. In this structure all of the resonators are of the same type, and an effect like alternating series and shunt resonators is achieved by the introduction of "impedance inverters" [28].

An idealized admittance inverter operates like a quarter-wavelength line of characteristic admittance J at all frequencies. Thus if an admittance Y_b is attached at one end as shown in Figure 3-15, the admittance Y_a seen looking in at the other end is

$$Y_a = \frac{J^2}{Y_b} \tag{3.14}$$

As explained in Figure 3-15 [28], an inverter may have an image phase shift of either ±90 degrees or an odd multiple thereof.

Because of the inverting action indicated by (3.14), a series inductance with an inverter on each side looks like a shunt capacitance from its exterior terminals. Likewise, a shunt capacitance with an inverter on both sides looks like a series inductance from its external terminals. Making use of this property, the prototype circuits in Figure 3-14(a) can be converted to the equivalent form in Figure 3-14(c) which has identical transmission characteristics to the prototype in Figure 3-14(a). From (3.14), the inverter has the ability to shift admittance levels depending on the choice of the J parameters. For this reason in Figure 3-14(c), the sizes of G_A, G_B, and the capacitances C_{an} may be chosen arbitrarily and the response will be identical to that of the original prototype as in Figure 3-14(a). Provided that the inverter parameters $J_{n,\ n+1}$ are specified as indicated by the following equations:

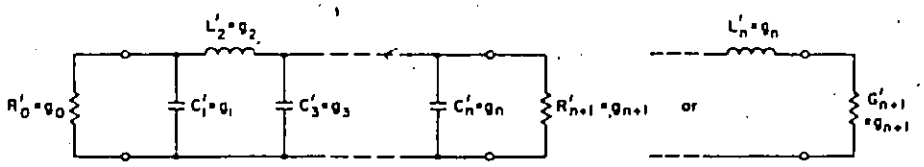

Figure 3-14(a). A low pass prototype filter.

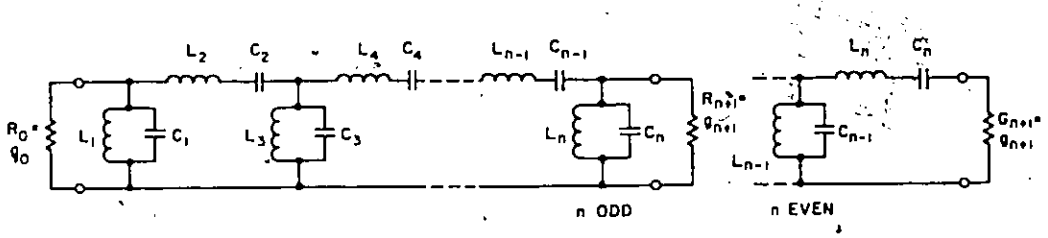

FOR SHUNT RESONATORS:

$$b_j = \omega_0 C_j = \frac{1}{\omega_0 L_j} = \frac{\omega'_1 g_j}{w} = \text{susceptance slope parameter} \qquad (1)$$

FOR SERIES RESONATORS:

$$x_k = \omega_0 L_k = \frac{1}{\omega_0 C_k} = \frac{\omega'_1 g_k}{w} = \text{reactance slope parameter} \qquad (2)$$

$$w = \frac{\omega_2 - \omega_1}{\omega_0}$$

$$\omega_0 = \sqrt{\omega_1 \omega_2}$$

Figure 3-14(b). Band pass filters and their relation to low pass prototypes. Frequencies ω'_1, ω_1, and ω_2 are defined in Figure 3-12 and $g_0, g_1, \cdots, g_{n+1}$ are defined in Figure 3-14(a).

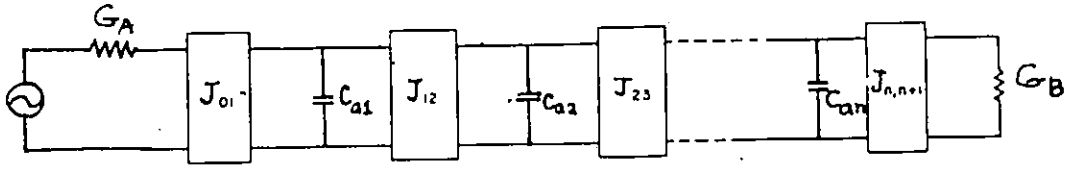

NOTE: Adapted from Final Report, Contract DA-36-039 SC-64625, SRI; reprinted in *Proc. IRE* (see Ref. 1 by S. B. Cohn).

Figure 3-14(c). The band pass filter in Figure 3-14(b) converted to use only series resonators and impedance inverters.

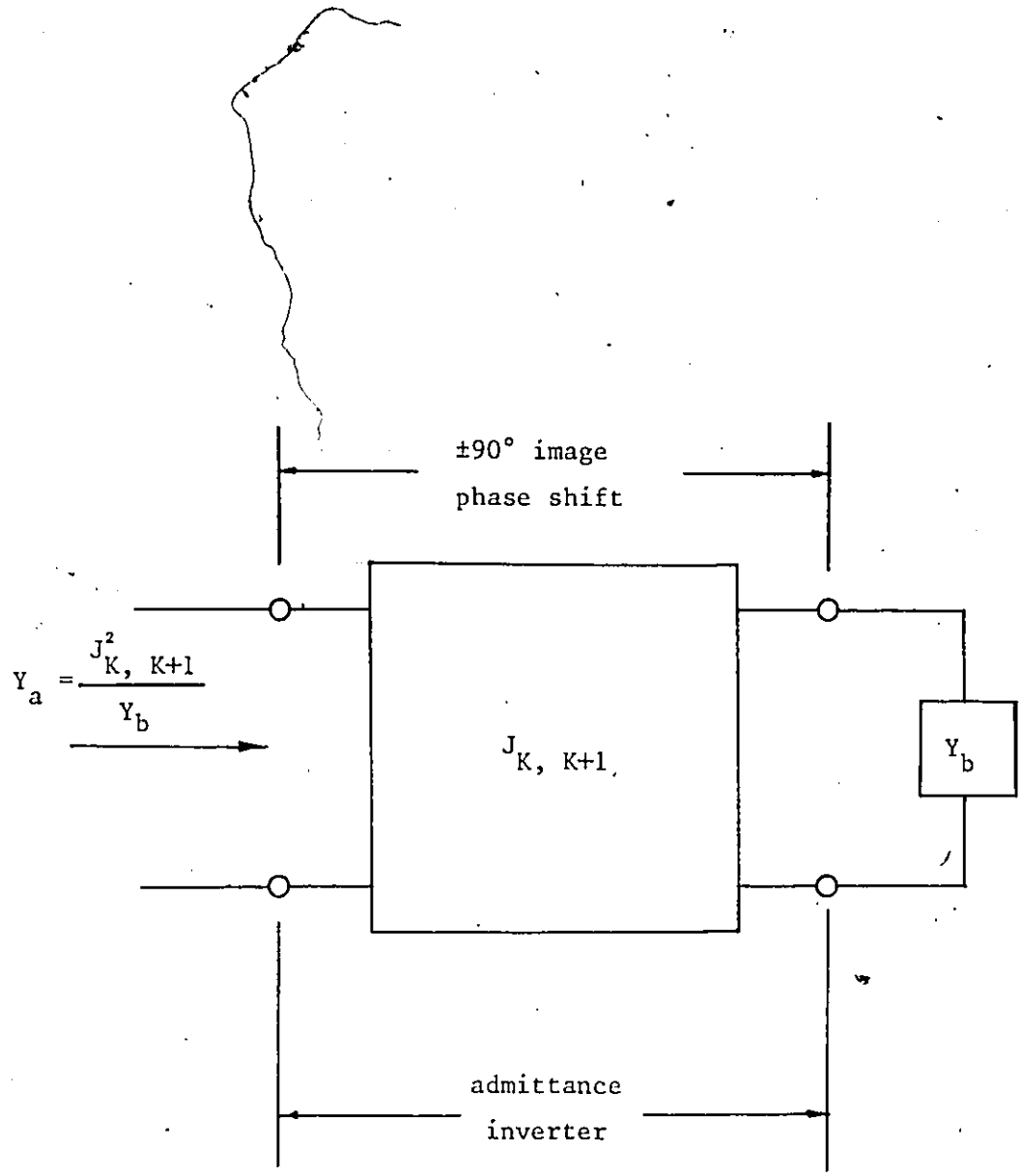

Figure 3-15. Definition of admittance inverter.

$$J_{o1} = \sqrt{\frac{G_A C_{a1}}{g_0 g_1}}$$

$$J_{K,\,K+1}\Big|_{K=1 \text{ to } (n-1)} = \sqrt{\frac{C_{aK} C_{a(K+1)}}{g_K g_{K+1}}} \qquad (3.15)$$

$$J_{n,\,n+1} = \sqrt{\frac{C_{an} G_B}{g_n g_{n+1}}}$$

A way to derive the equations for $J_{n,\,n+1}$ has been found in Reference [28]. Therefore,

for the first coupling structure

$$\frac{J_{o1}}{Y_o} = \sqrt{\frac{\pi\delta}{2g_o g_1}} \qquad (3.16)$$

for the intermediate coupling structures

$$\frac{J_{K,\,K+1}}{Y_o}\Bigg|_{K=1 \text{ to } (n-2)} = \frac{\pi\delta}{2\omega_c' \sqrt{g_K g_{K+1}}} \qquad (3.17)$$

and for the final coupling structure

$$\frac{J_{n,\,n+1}}{Y_o} = \sqrt{\frac{\pi\delta}{2g_n g_{n+1}}} \qquad (3.18)$$

where δ is the fractional bandwidth

$$\delta = \frac{f_2 - f_1}{f_o} = 0.062 \qquad (3.19)$$

The frequency transformation from the low pass prototype filter to the band pass filter is then

$$\frac{\omega_i'}{\omega_c} = \frac{2}{\delta} \frac{f_i - f_o}{f_o} = 2.2 \qquad (3.20)$$

To obtain the coupling structure in microstrip form, the odd- and even-mode coupled line impedances Z_{oo} and Z_{oe} are only required [18], [19]. These are given by

$$(Z_{oe})_{K,\ K+1} = Z_o(1 + aZ_o + a^2Z_o^2) \qquad (3.21)$$

$$(Z_{oo})_{K,\ K+1} = Z_o(1 - aZ_o + a^2Z_o^2) \qquad (3.22)$$

where

$$a = J_{K,\ K+1}$$

To meet our specification, 0.1 dB insertion loss (ripple) at pass band, the graph has been referred [28]. To use the graph, the parameter required is given by

$$\left[\left|\frac{\omega'}{\omega_c}\right| - 1\right] = 1.2$$

30 dB insertion loss or more at 14 and 18.2 GHz (band edges) is realized with the condition n=4. Thus the values of the parameters are shown in Table 3-2.

K	$J_{K,K+1} / Y_o$	$(Z_{oe})_{K,K+1}$ (Ω)	$(Z_{oo})_{K,K+1}$ (Ω)
0	0.296	69.2	33.6
1	0.08	54.3	46.3
2	0.0692	53.7	46.8

Table 3-2

K = 0,1,2 are for the half part of the BPF which has symmetry property.

By computer program with optimization, the equivalent single line synthesis yields:

$$(W/H)_{se} = 8.80056$$

$$(W/H)_{so} = 14.78594$$

Thus for K = 0,

$$S/H = 0.19, \quad S = 0.15 \text{ (where H = 0.762 mm)}$$

$$W/H = 4.4, \quad W = 3.35 \text{ (where H = 0.762 mm)}$$

The length of the half wave resonator becomes

$$\frac{\lambda_g}{2} = 6.74 - 0.734 = 6.006 \text{ mm}$$

And similarly for K = 1,

$$S/H = 0.8352, \quad S = 0.64 \text{ mm}$$
$$W/H = 5.\overline{6}, \quad W = 4.27 \text{ mm}$$

for K = 2, S = 0.7 mm

W = 3.96 mm

The structure of the actual microstrip parallel coupled BPF is shown in Figure 3-16.

3.6 Generation of Circuit Layout

The complete planar mixer has been integrated by combining the planar components designed in the previous sections. The original size planar mixer layouts on the front and back sides of the substrate are shown in Figure 3-17(a) and (b). Those circuit layouts have been obtained by CALCOM plotter. Since this plotter was not compatible with the computer calculating the circuit parameters, the mixer layout has been realized by using the circuit dimensions obtained from the circuit parameters.

For better resolution of the actual circuit, the layouts were enlarged five times by CALCOM plotter and reduced photographically to the original size. Finally the metalization pattern of the circuit board has beeb obtained from that mask by means of photolithographic technique.

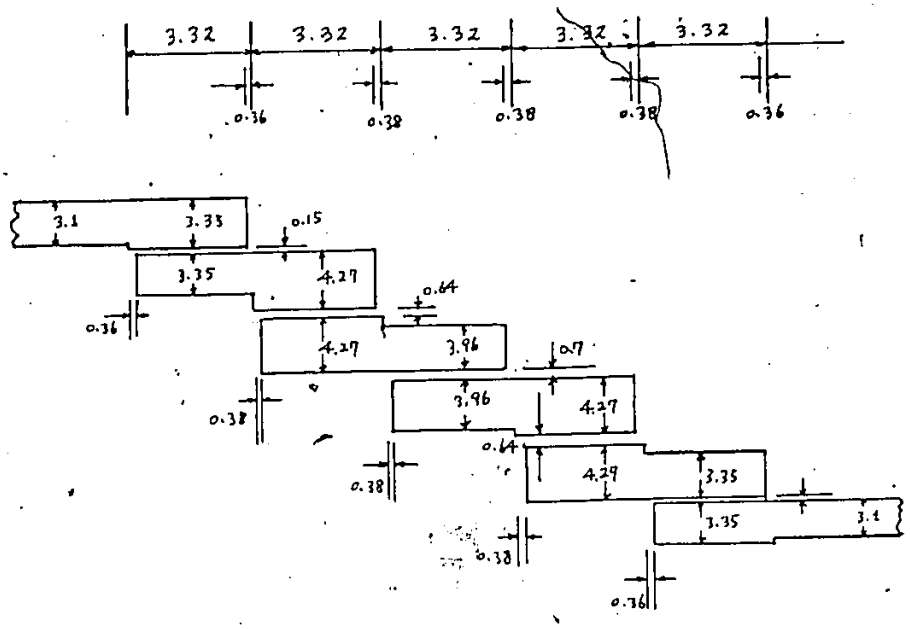

Figure 3-16. The configuration of the microstrip band pass filter for LO.

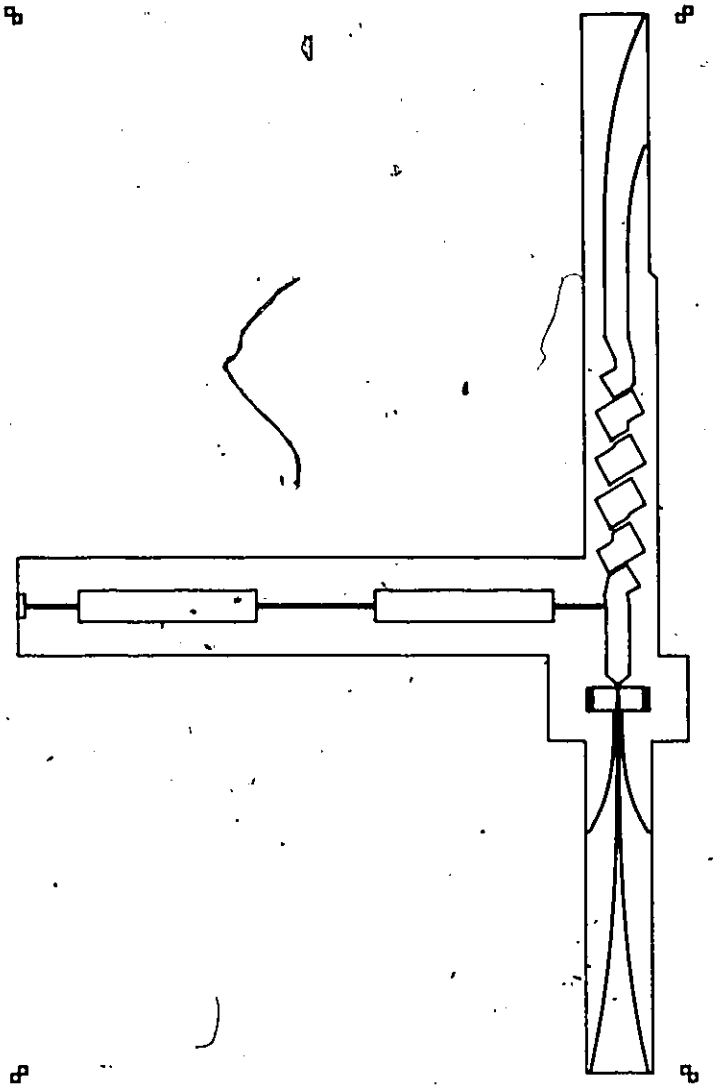

Figure 3-17(a). Front side of the mixer layout. (original size)

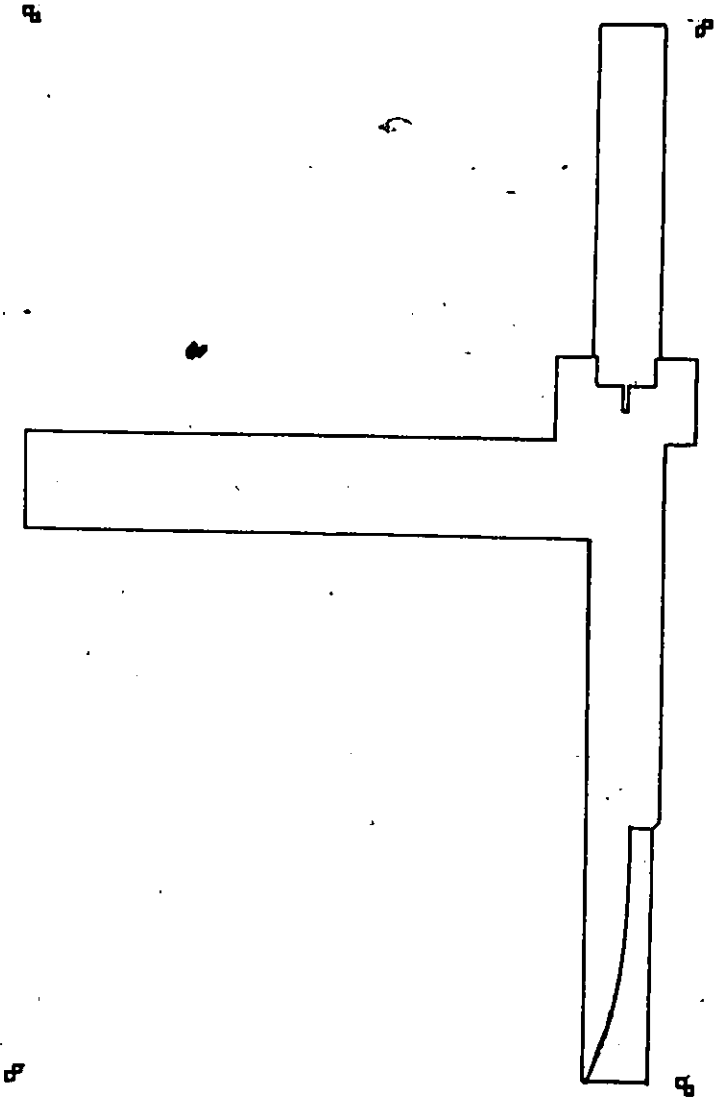

Figure 3-17(b). Back side of the mixer layout. (original size)

3.7 Design of Housing

The housing, an enclosure protecting the planar circuit against radiation loss and external electromagnetic interference was designed and constructed in the physics shop at the University of Ottawa as shown in Figure 3-18 (photograph of the complete housing). The effectiveness of the housing will be documented in Section 4.2, describing a 13 dB improvement of the radiation loss of the LPF.

Figure 3-19 shows the various units of the mixer housing. The waveguide ports for the RF and LO ports have the standard dimensions of WR (62). The space below the ground plane of the microstrip section in WR (62) was of no practical significance. Also, the housing has been designed such that the cover of the mixer could be opened for easy tuning.

3.8 Conclusion

A planar single balanced mixer using 180° hybrid has been designed and realized to convert a 17GHz signal down to an IF of 900 MHz.

The condition that minimizes the conversion loss does not necessarily minimize the mixer noise performance [31]. However, in this thesis the length of the signal path has been shortened as far as possible to reduce the conversion loss due to the circuitry.

Microstrip has been chosen for realizing the LPF and BPF. The mixer circuit has been integrated on a single substrate, RT/duroid 5880 ($\varepsilon_r = 2.22$).

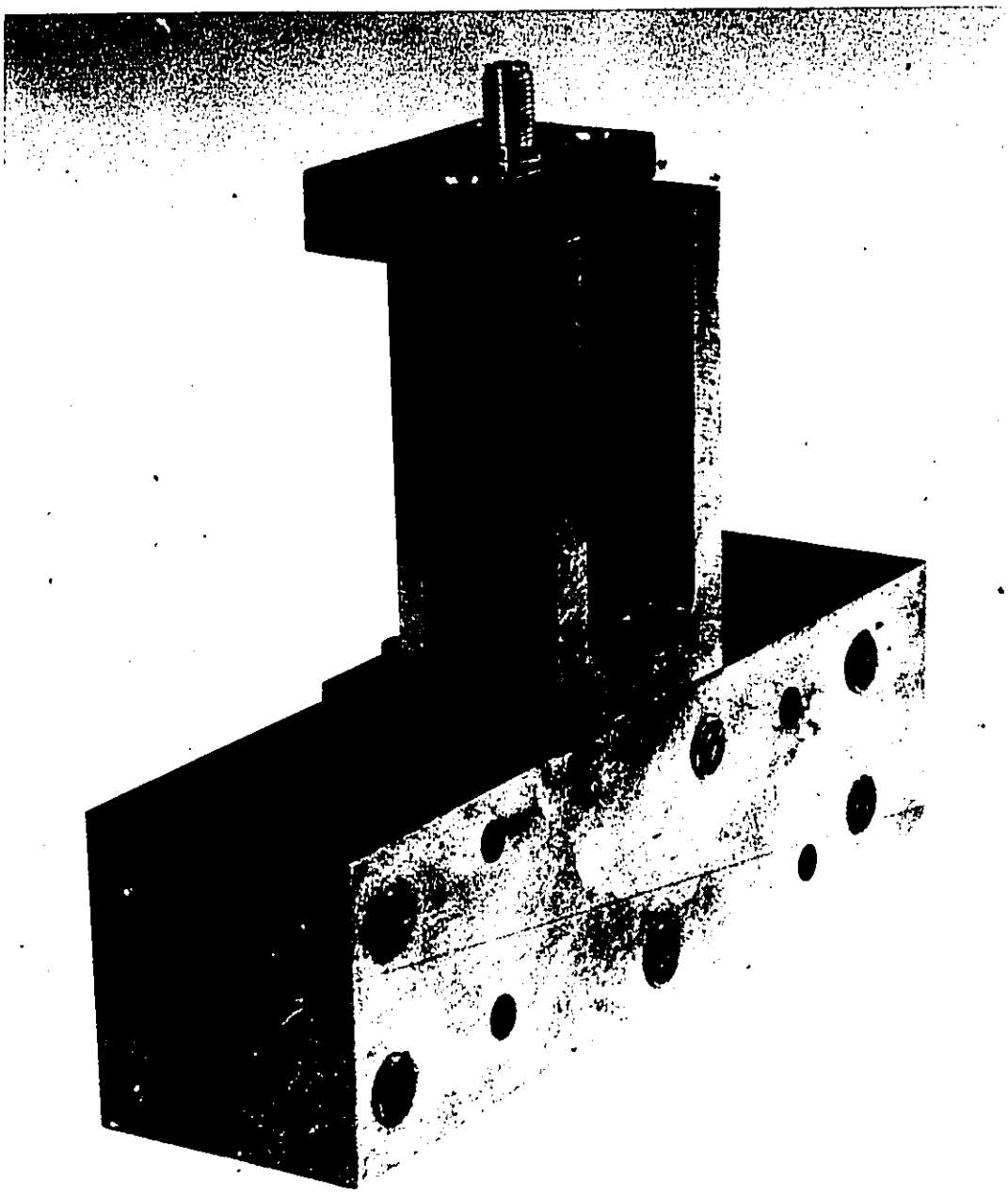

Figure 3-18. Photograph of the complete mixer housing.

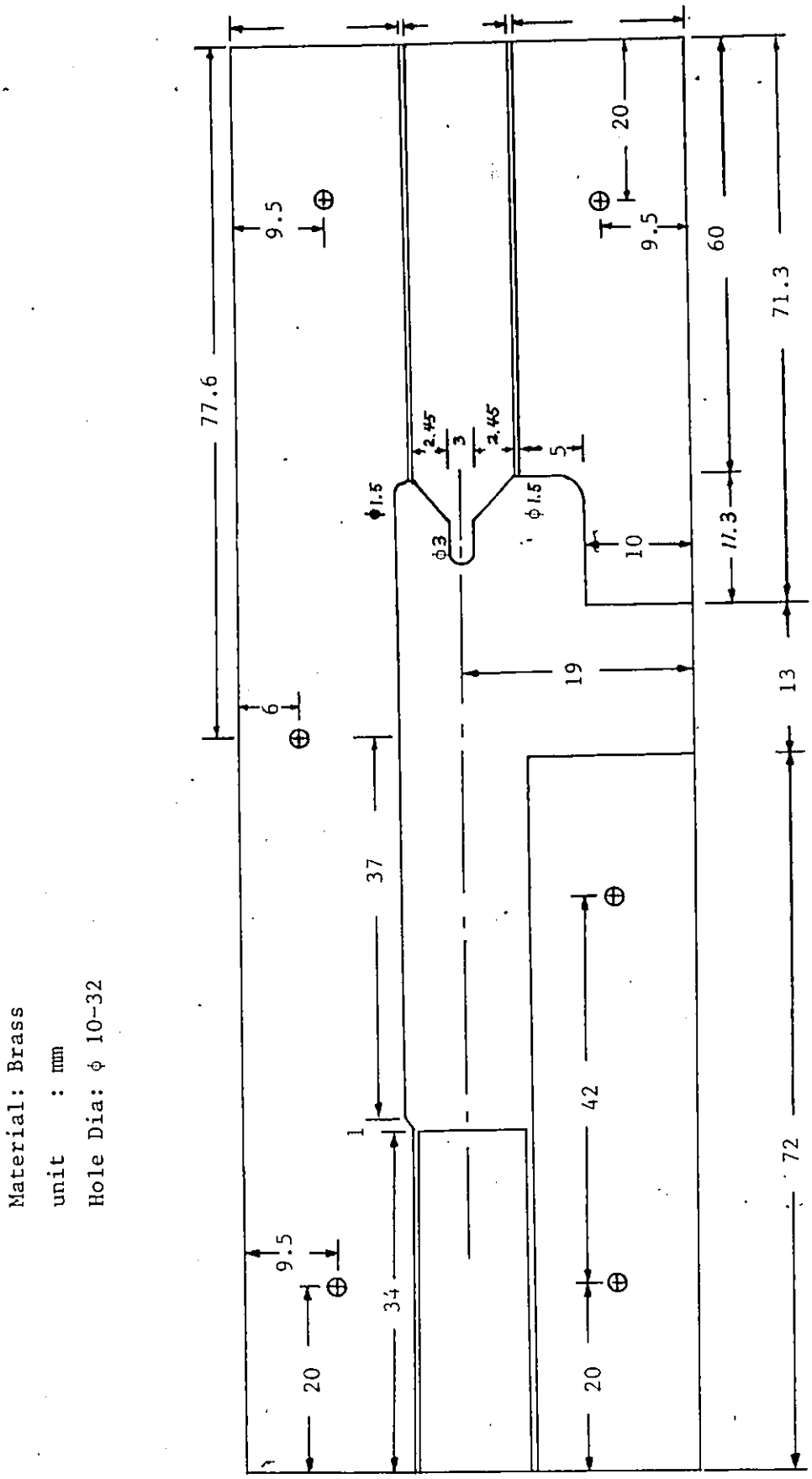

Figure 3-19(a). Mixer enclosure #1.

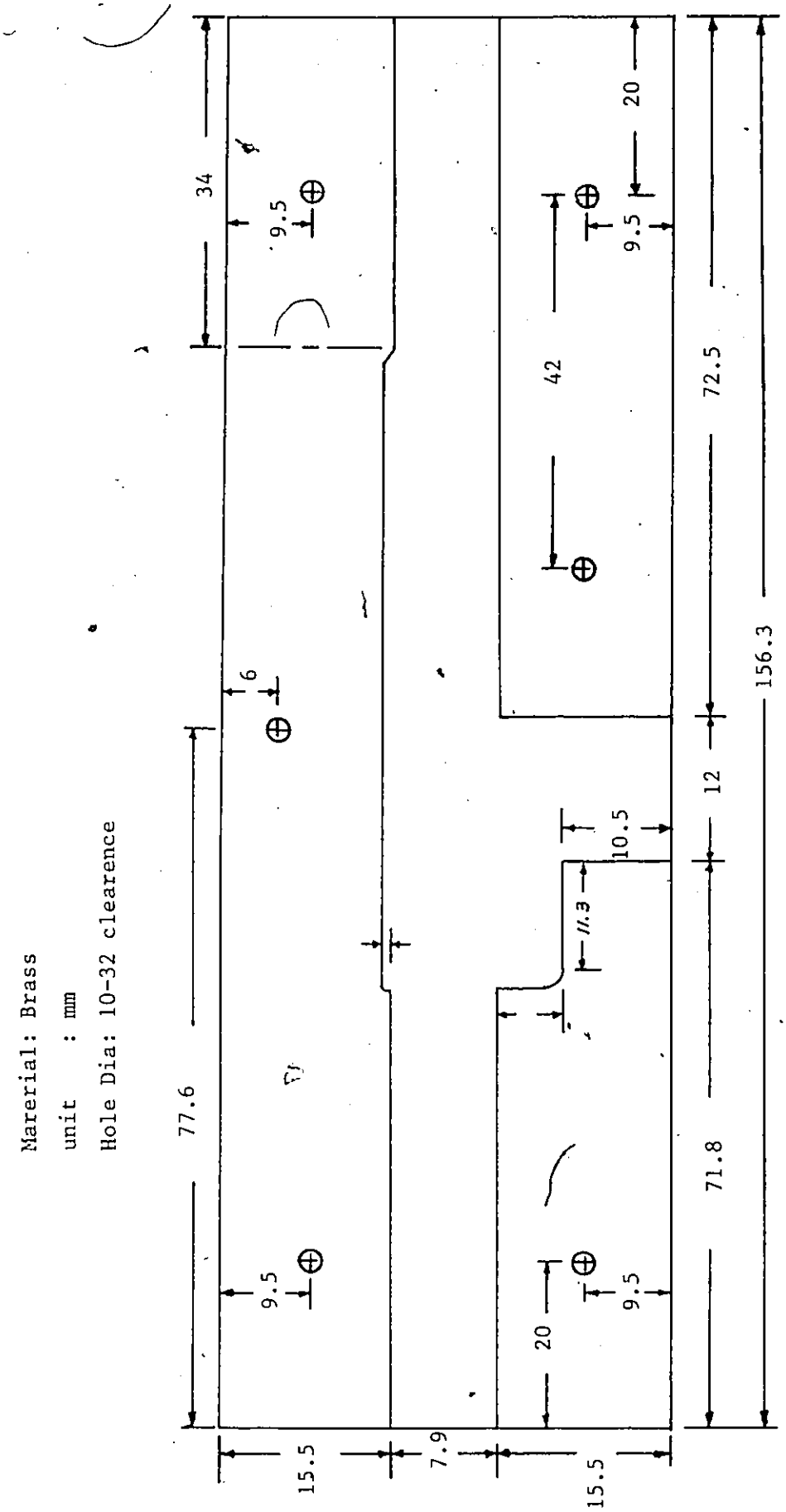

Figure 3-19(b). Mixer enclosure #2.

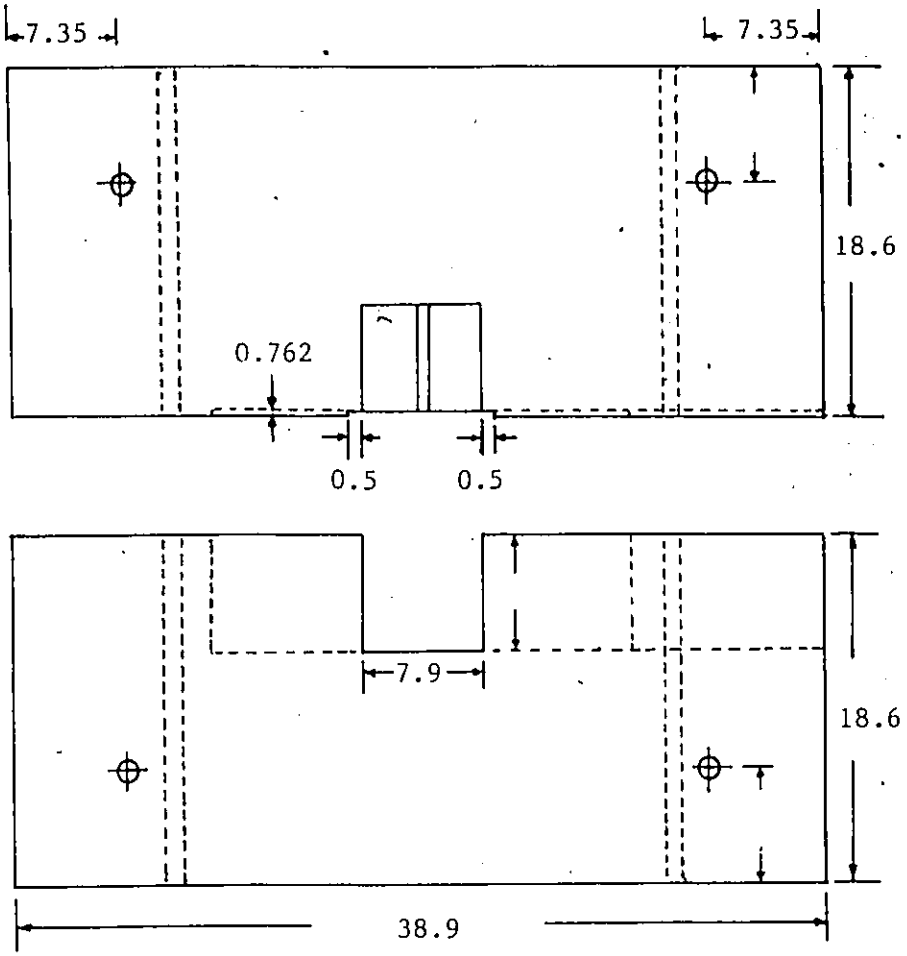

Material: Brass
unit : mm
Hole Dia: 10-36

Figure 3-19(c). Mixer enclosure #3.

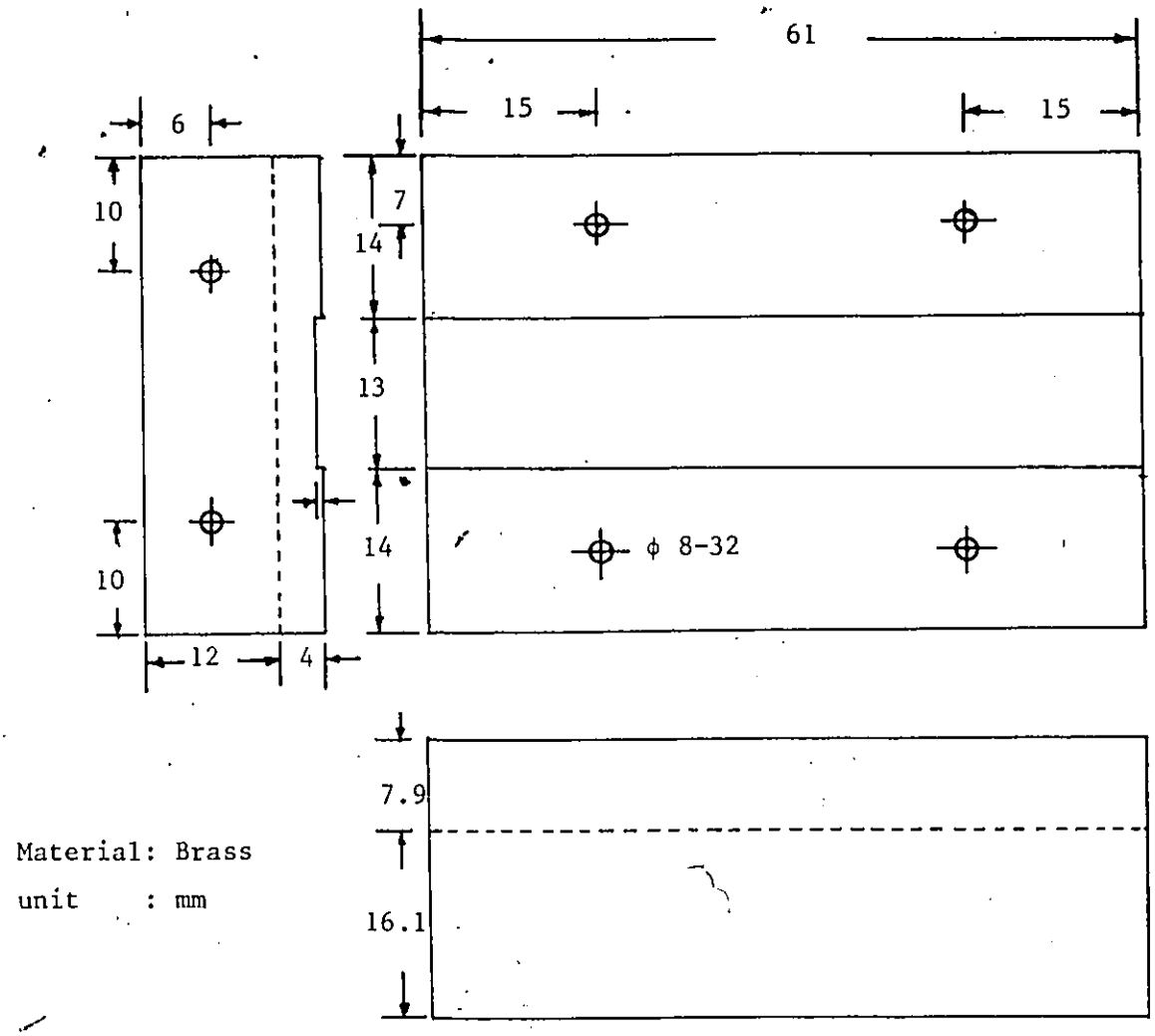

Material: Brass
unit : mm

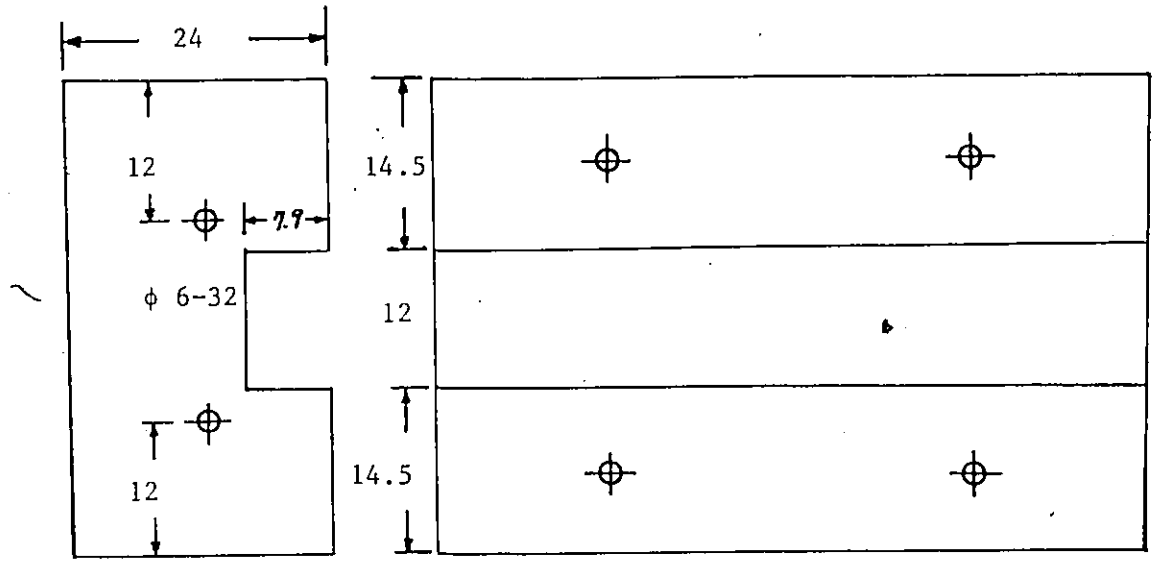

Figure 3-19(d). Mixer enclosure #4.

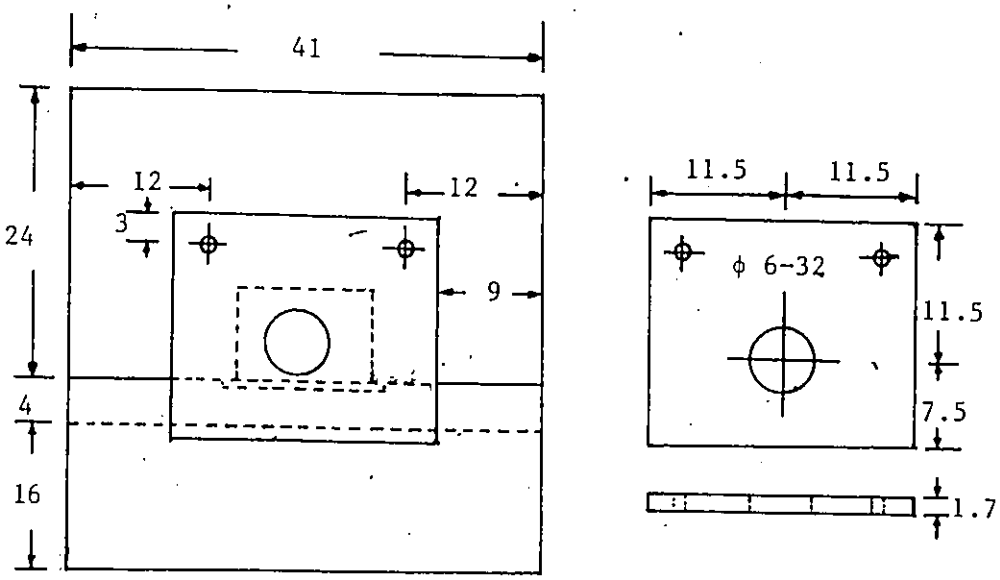

Material: Brass
unit : mm

Figure 3-19(e). Mixer enclosure #5.

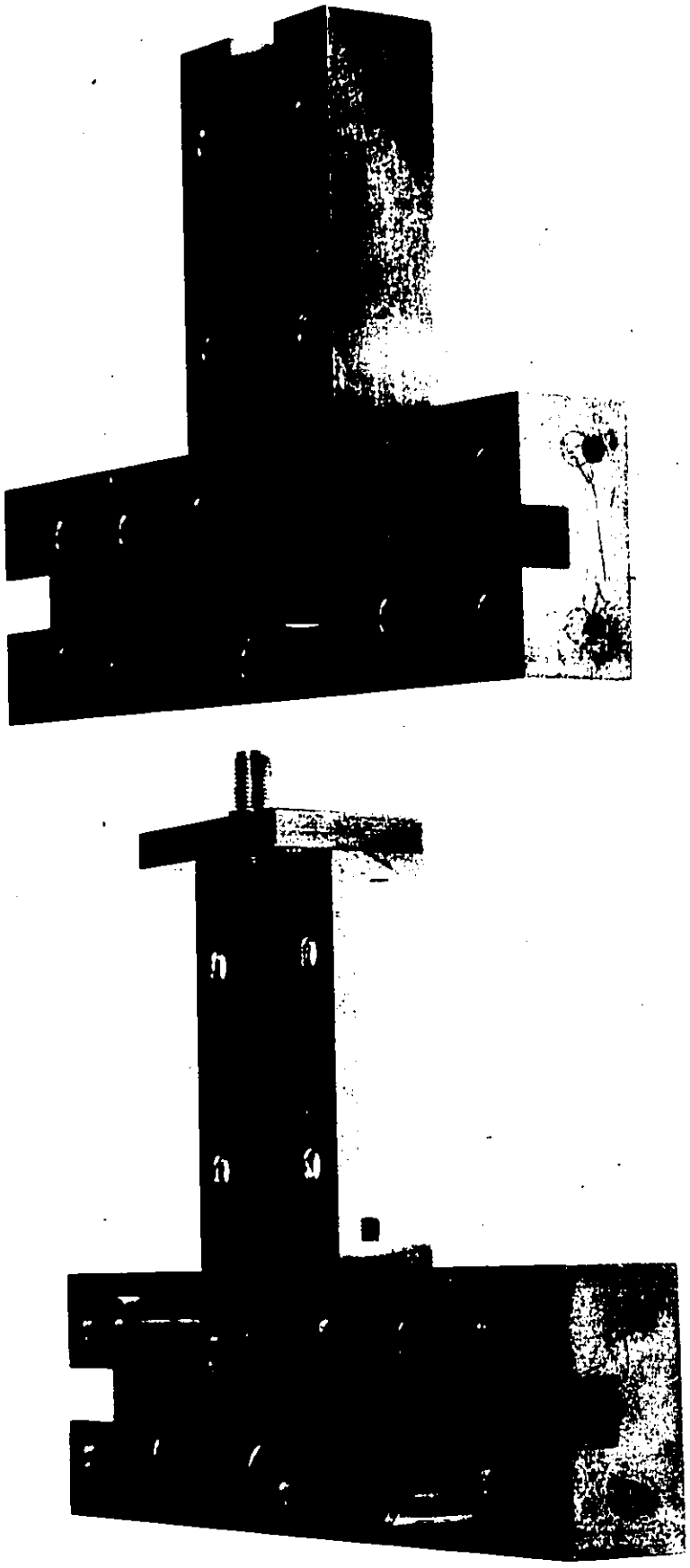

Figure 3-19(f). Two halves of the mixer enclosure.

CHAPTER 4

MEASUREMENT OF MIXER PERFORMANCE

This chapter demonstrates the measurement methods and the characteristics of the mixer we have realized. The conversion loss, noise figure, VSWR, isolation, and transfer characteristics were measured.

4.1 Introduction

After constructing the mixer, VSWRs were measured at the RF, LO, and IF ports. The isolation characteristic between the LO and RF ports will be discussed in Section 4.3. The LO power level and the tuning elements have been adjusted for minimum conversion loss.

The dynamic range and the signal power transfer characteristics were examined to ensure linear mixer operation. The noise characteristics of the mixer were obtained with the manual Y-factor method. At the end of this chapter an overall evaluation of the mixer is given.

4.2 Filter Characteristics

Before integrating the components designed in Chapter 3 on a single substrate, the BPF had been designed to keep the IF and its harmonics from the LO port. It was checked with a transmission measurement test set (HP8690 sweep oscillator main frame, HP8695B plug in, and HP8755A sweep amplitude analyzer).

At 16.05 GHz, a peak indicating resonance was shown in the first measurement without housing. The resonance was shifted down to a lower frequency when housing was added. Thus, the BPF with housing was tuned by reducing the capacitive components of the resonators.

29 dB attenuation at 17.0 GHz and 15.9 GHz was obtained with the housing. However, without the housing, 16 dB attenuation was obtained at the same frequencies. The 13 dB difference is due to radiation losses.

The LPF was designed and the response investigated at the LO frequency. 25 dB attenuation was measured at around the LO frequency as shown in Figure 4-1. This response ensures a good isolation characteristic between the LO and IF ports.

4.3 VSWR and Isolation

VSWRs at the three ports of the mixer depend on the degree of the match between diodes and the circuits of the three ports. The slotted line method was used to measure VSWRs.

VSWRs at the RF and LO ports were measured with a setup as shown in Figure 4-2. To measure the VSWR at the RF port, a 11 dBm LO signal was applied and the IF port was terminated in 50 Ω. The RF signal from the source was supplied at a -30 dBm power level.

Tuning was done by adjusting the stub length while measuring the VSWR at the RF port and watching the IF on a spectrum analyzer. Figure 4-3 shows the VSWR characteristic at the RF port. The best result, 1.45: 1, was obtained at around center frequency.

For VSWR measurement at the LO port, the same measurement setup was used under the same condition. But the equipment in the dotted rectangle shown in Figure 4-2 was placed between the mixer under test and the LO source instead of between the mixer and the RF source. The VSWR measured at the LO port with -30 dBm RF power and 11 dBm LO power was 1.65: 1.

The VSWR at the LO port is not a critical parameter in the mixer design.

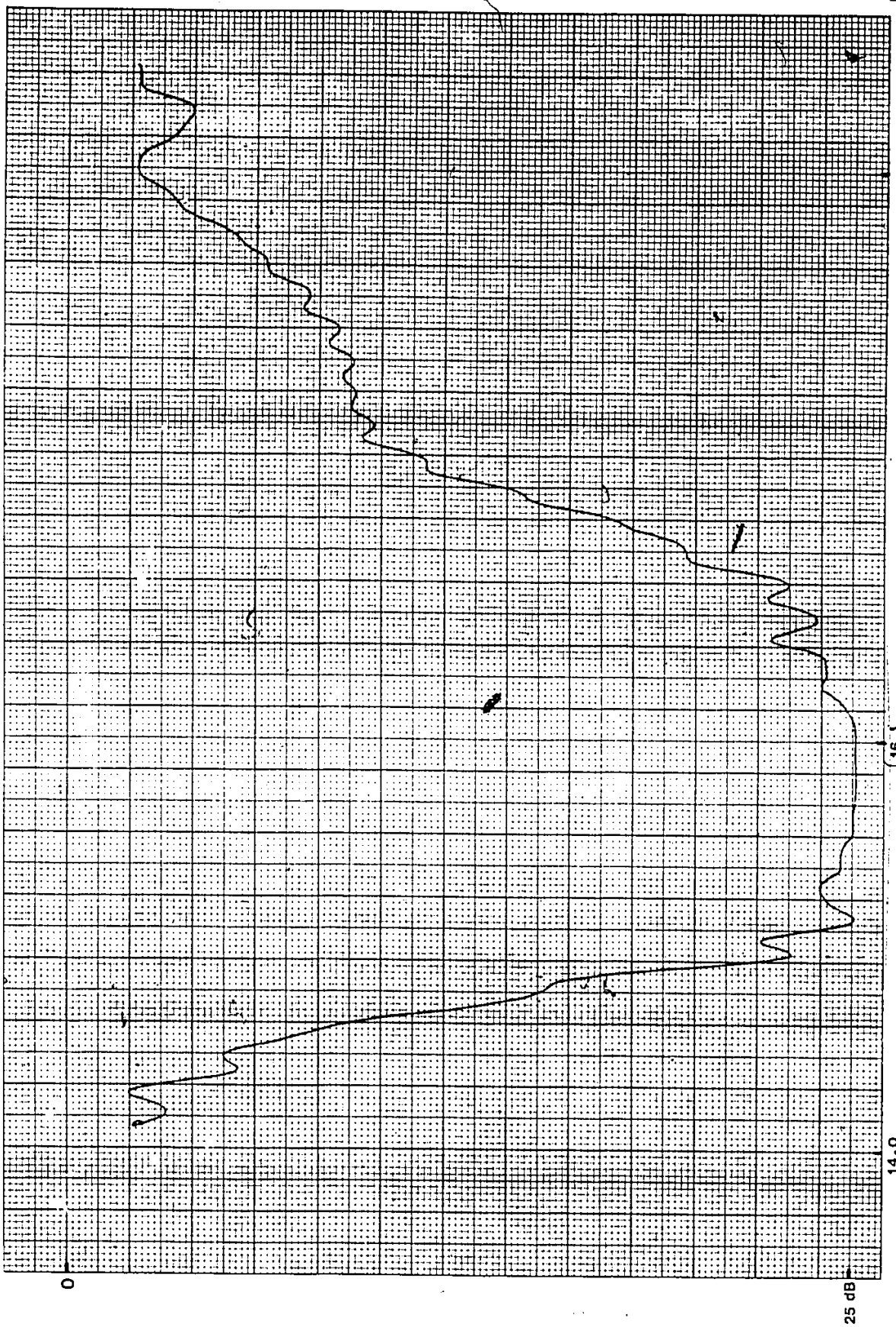

Figure 4-1. LPF response at the LO frequency.

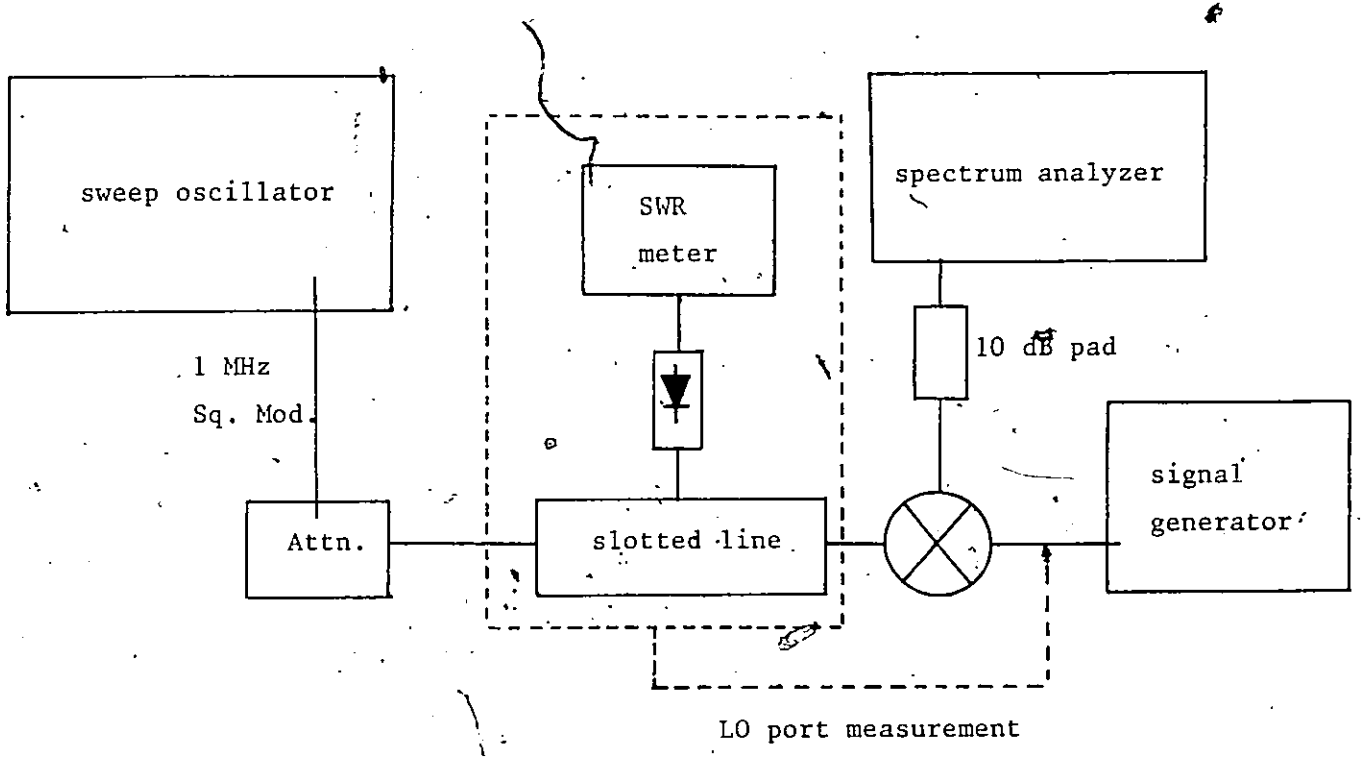

Figure 4-2. VSWR measurement setup for the RF and LO ports. The dotted rectangle shifts for the LO port VSWR measurement.

Figure 4-3. VSWR characteristics at the RF and IF ports.

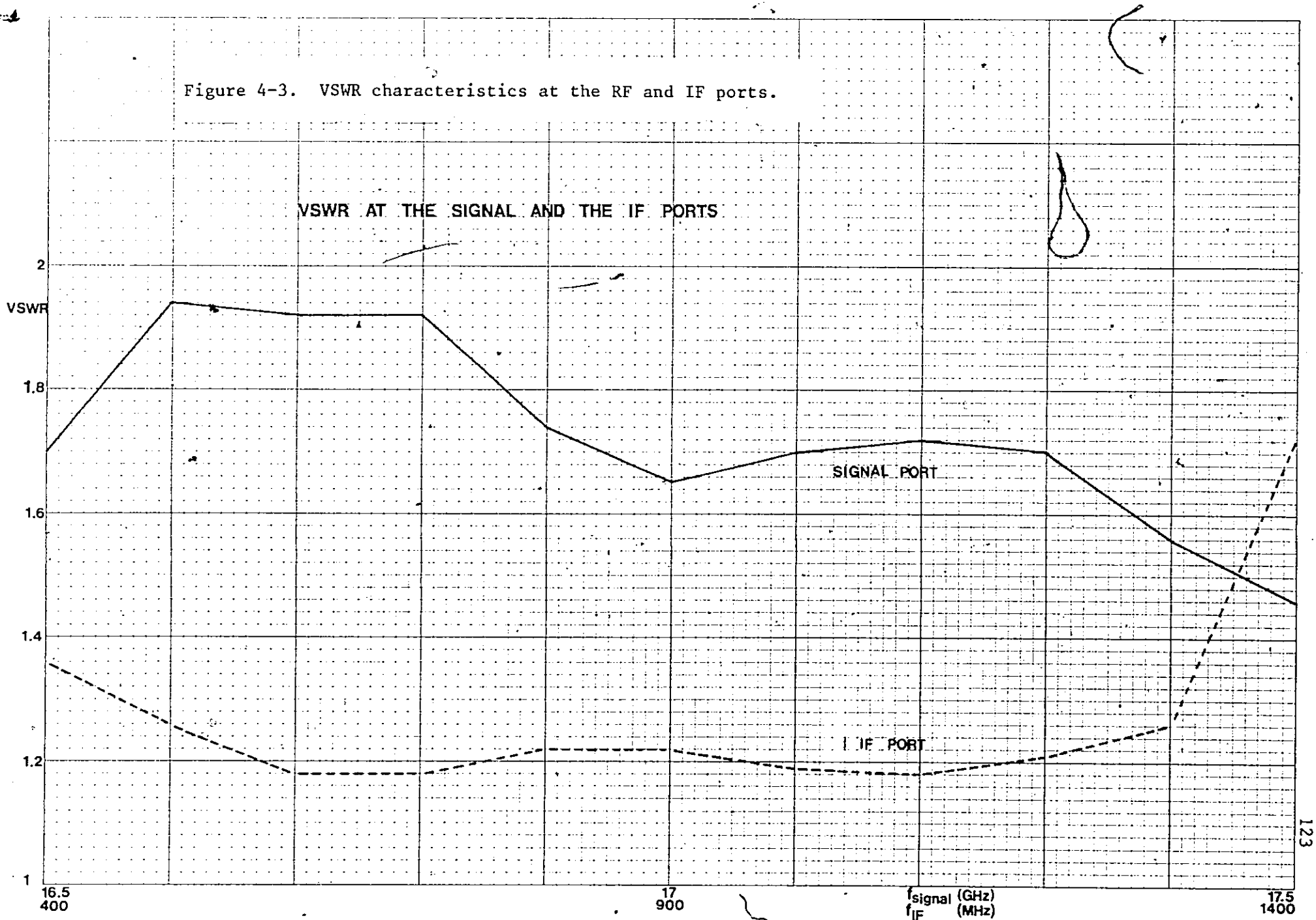

VSWR measurement at the IF port was accomplished with a waveguide termination at the RF port as shown in Figure 4-4. The IF signal (400 - 1400 MHz) was applied to the IF port for various LO power levels. The VSWR in the IF frequency band is shown in Figure 4-3. At 1.4 GHz, the worst result 1.6 : 1 was obtained because of the slope of the LPF characteristic. At 600 MHz, the best result 1.18 : 1 was obtained.

As a result of the VSWR measurement, it should be noted that a broad band mixer exhibits different VSWR characteristics at different frequencies. Factors causing this include circuit resonances and changes in diode impedance as the LO power level changes. Also of importance is the fact that the input impedances of the three different ports are load dependent, even though they are isolated from each other. At higher mm-wave frequencies, this effect is greater since isolation tends to drop as the frequency increases.

Isolation between the RF and LO ports determines the radiation of the LO fundamental and its harmonics, specially the 2nd harmonic, by the receiving antenna. Isolation was measured at a LO power level of 13 dBm with a setup shown in Figure 4-5. At the RF port, 30.5 dB isolation was measured at the fundamental and 22.5 dB isolation at its 2nd harmonic with the spectrum analyzer. This excellent isolation is an inherent characteristic of the hybrid junction. The isolation characteristic between the LO and IF ports was also measured with the same measurement setup except that a waveguide termination was placed

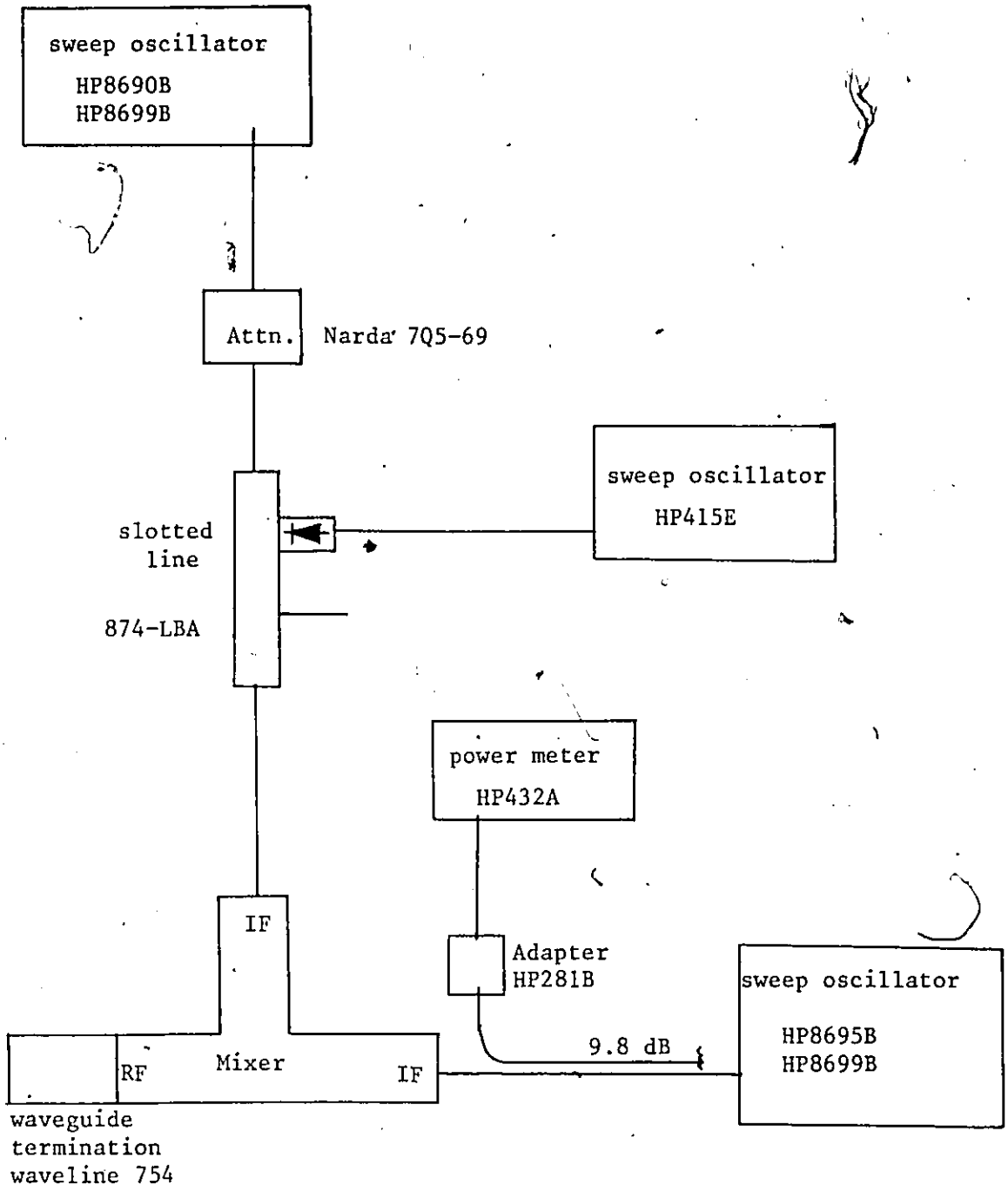

Figure 4-4. VSWR measurement setup at the IF port.

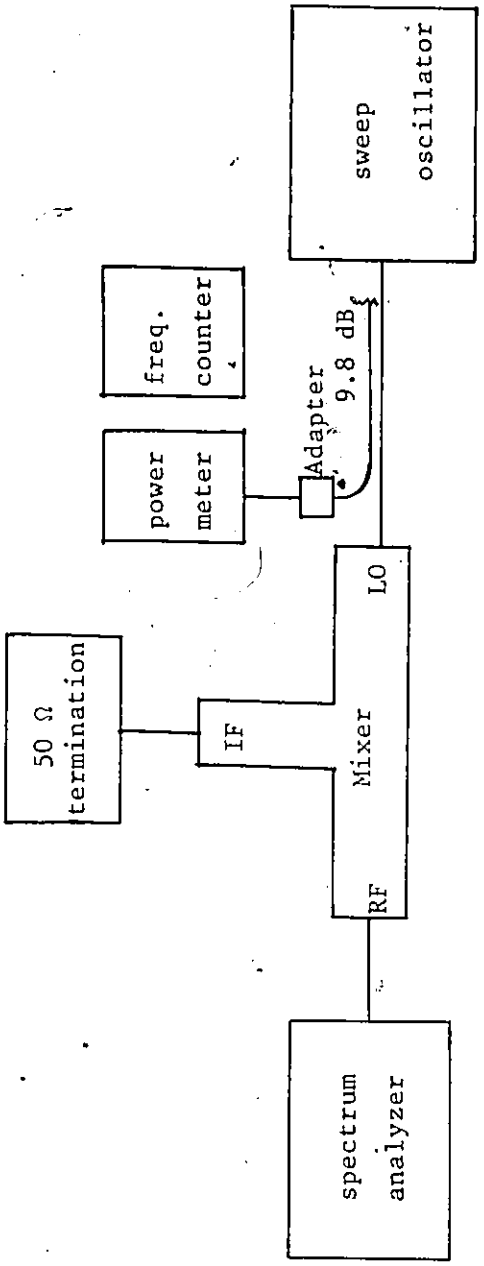

Figure 4-5. Isolation measurement setup.

at the RF port and the spectrum analyzer was connected to the LO port. A 21.3 dB isolation between the LO and IF ports was measured.

4.4 Conversion Loss Measurement

The conversion loss of microwave and mm-wave mixers depends on many factors as mentioned in Chapter 1. However, the conversion loss depends also on LO power level and RF signal power level in the pass band. The conversion loss measurement was done at various power levels of the LO and RF signals. The best conversion loss was obtained at a RF power level closest to the signal saturation level.

Before adjusting the tuning elements, a clear spectral information at the IF frequency was obtained by a measurement setup shown in Figure 4-6. Figure 4-7(a) and (b) represent the IF spectrum without and with tuning respectively. After calibration of the spectrum analyzer, the conversion loss measurement was done at 11 frequencies in the pass band at a LO power level of 13.5 dBm and a signal level of -30 dBm. Figure 4-8 presents the measured conversion loss vs. signal frequency. The conversion loss was typically 4 dB, reaching a minimum of 3.7 dB at the center frequency of 17 GHz. The cable loss between the spectrum analyzer and IF ports was considered. Figure 4-9 is a phtograph of the conversion loss measurement setup.

The full power range over which the mixer is usable can be investigated by a conversion loss measurement. It provides the transfer characteristic and determines 1 dB compression point and dynamic range of the mixer. These characteristics which are shown in Figure 4-10 were measured at three different LO power levels while increasing the RF

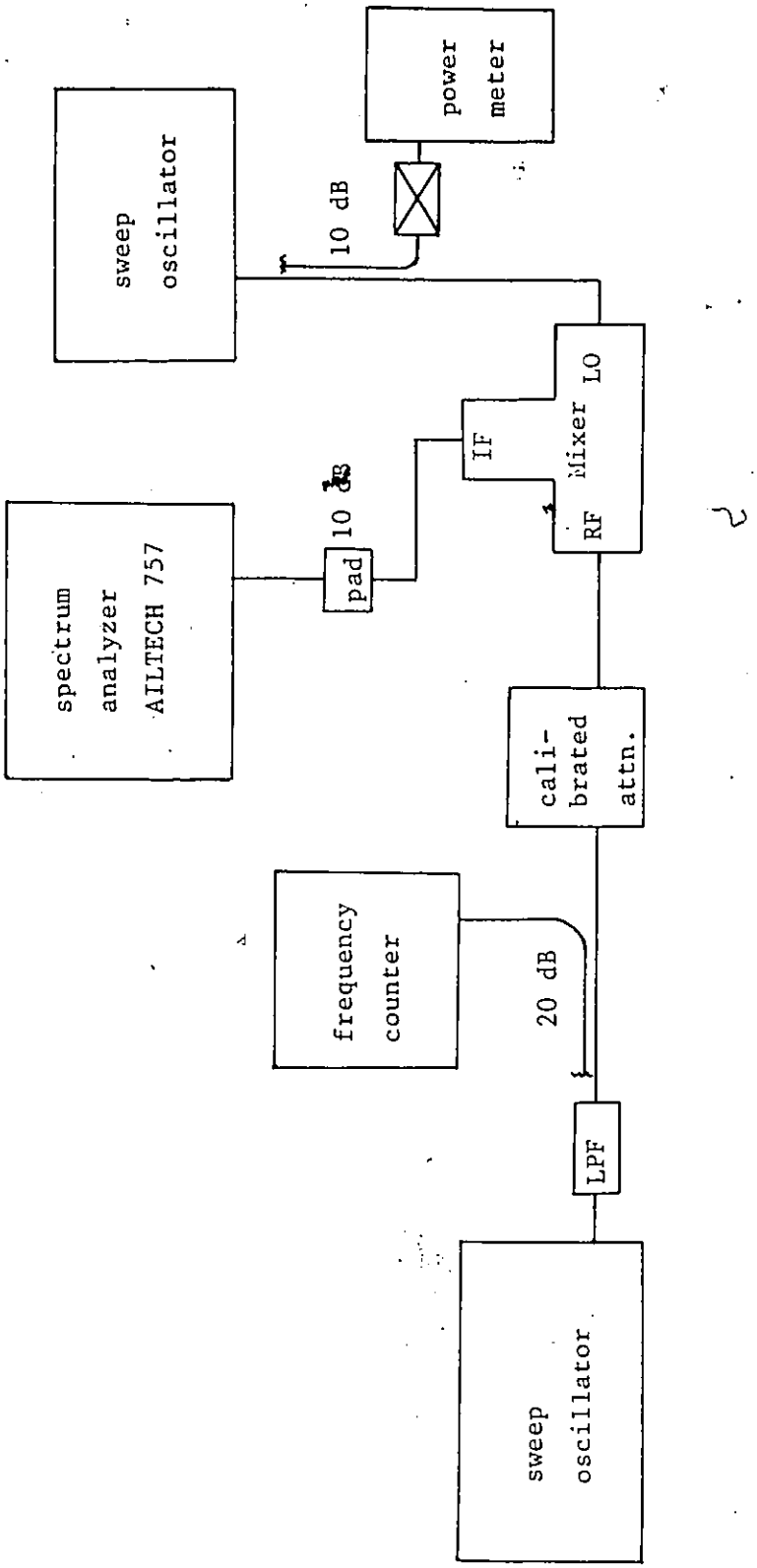

Figure 4-6. Conversion loss measurement setup.

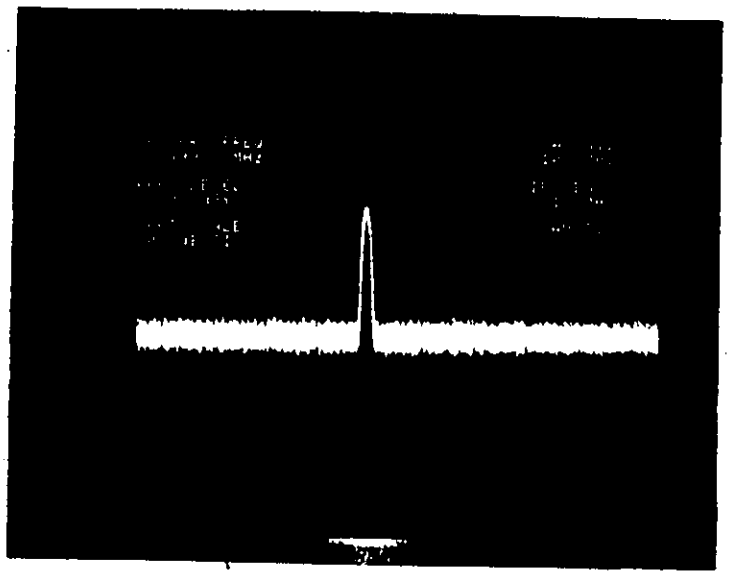

(a) IF spectrum without tuning

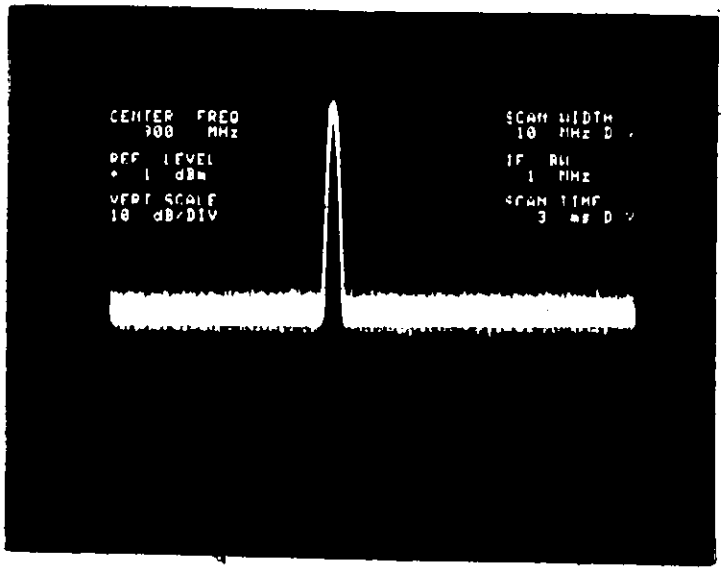

(b) IF spectrum with tuning

Figure 4-7. The output spectra of the mixer.

Figure 4-8. CONVERSION LOSS OF THE PLANAR MIXER

P_{signal} -30 dBm, P_{LO} 13.5 dBm

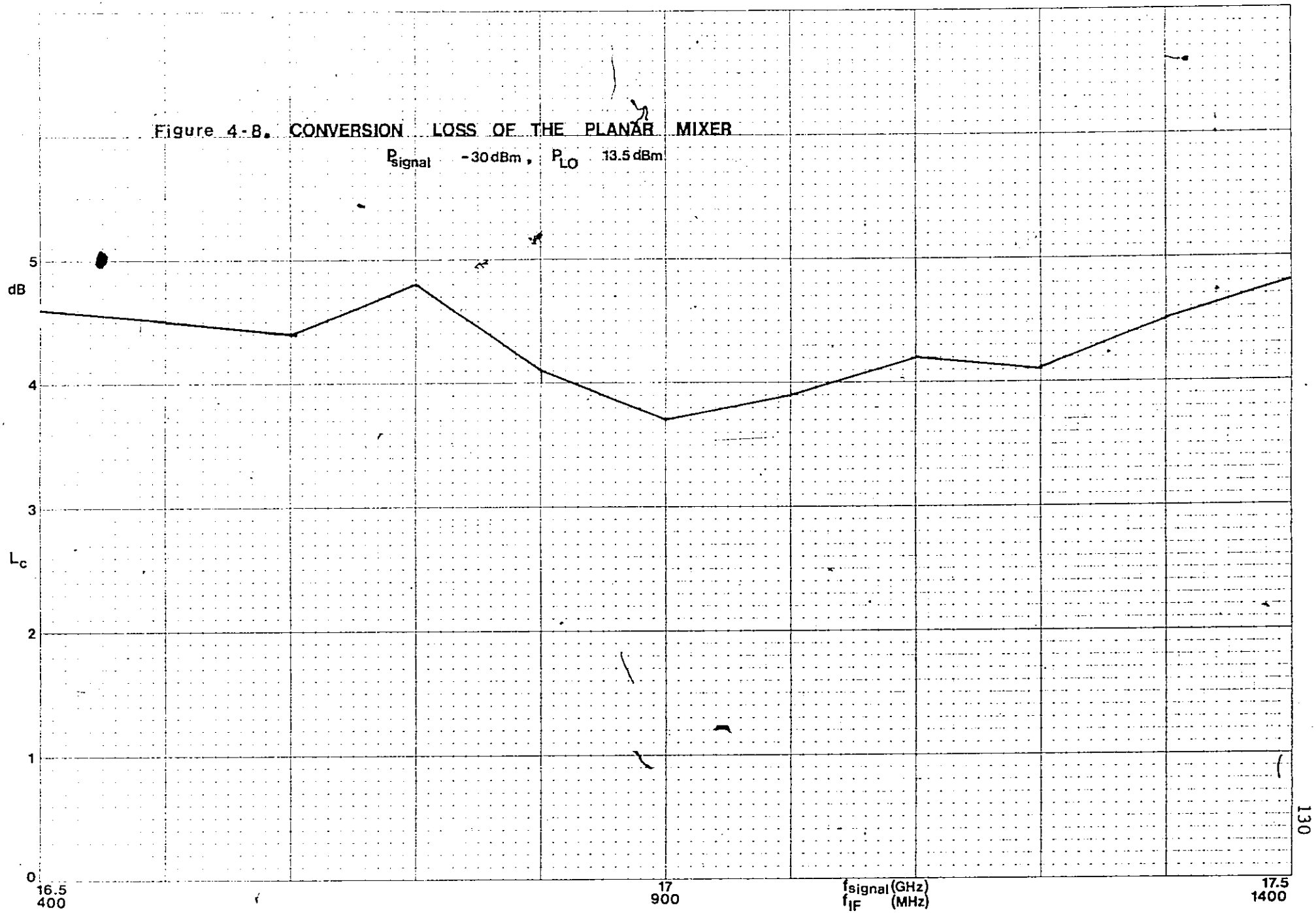

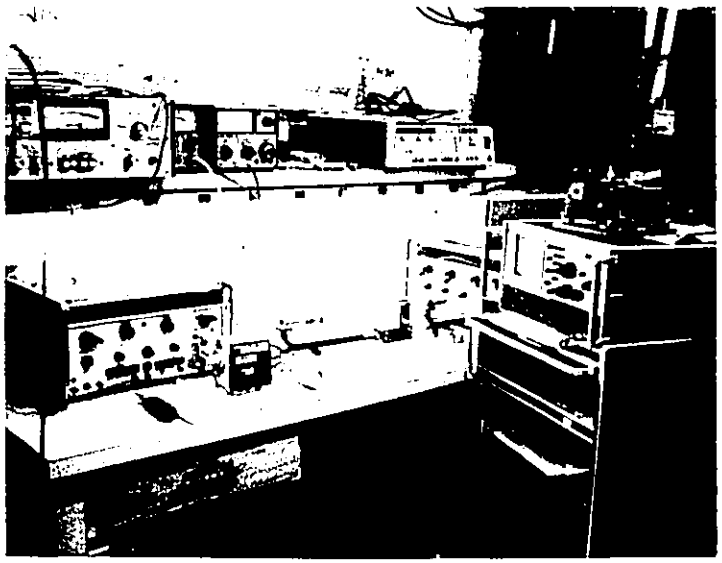

Figure 4-9. A photograph showing the conversion loss measurement setup.

Figure 4-10

TRANSFER CHARACTERISTICS

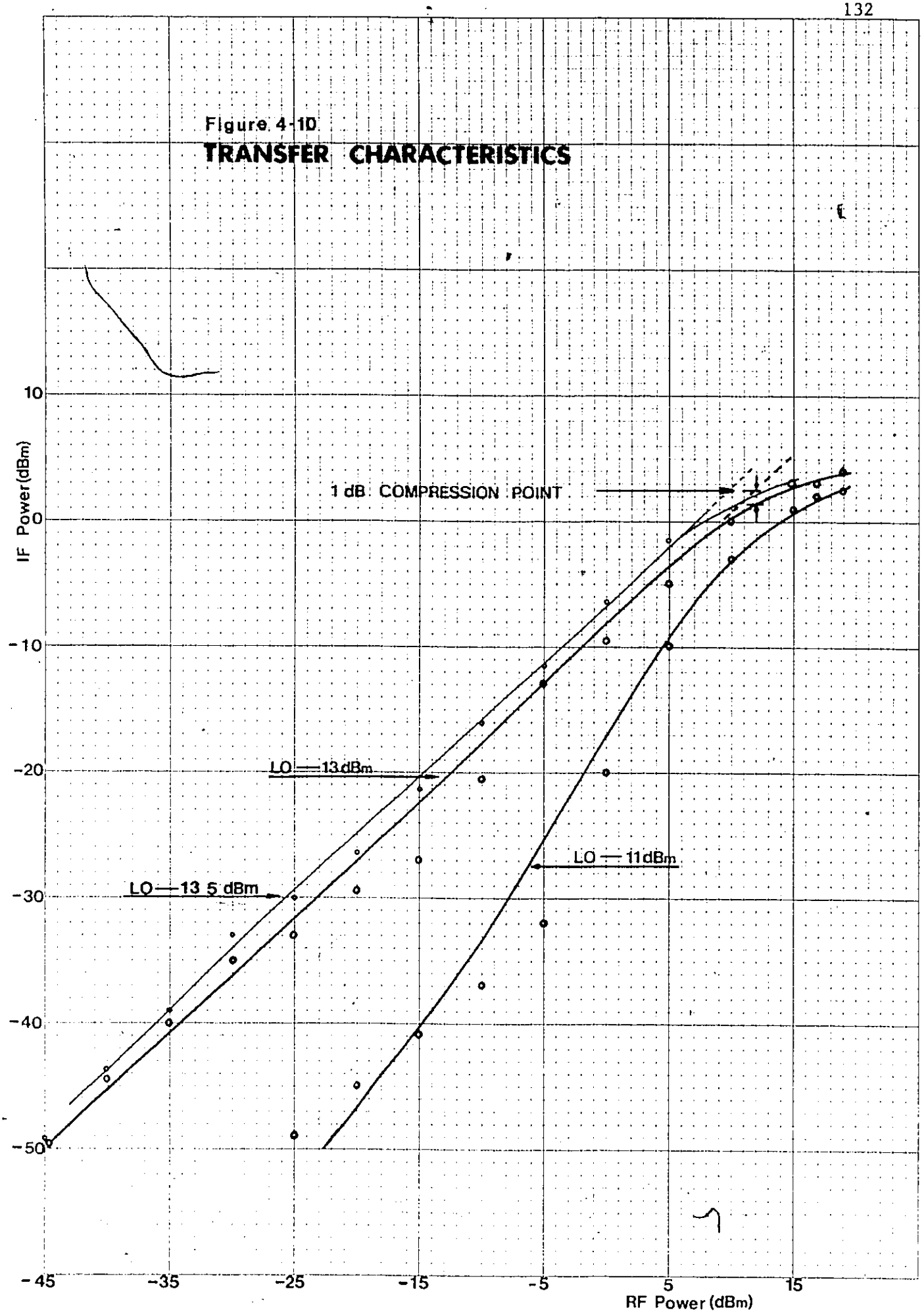

power level. Figure 4-10 shows the mixer dynamic range to be greater than 55 dB. Below a RF power level of -45 dBm, the linear dynamic range was no longer realistic because of the limitation of the measuring equipment. Also near the saturation level there is a 1 dB compression point that indicates the upper limit of the mixer dynamic range.

4.5 Noise Figure Measurement

The total output noise power includes contributions from the signal and image frequency bands. The single sideband noise figure of a mixer is

$$F_{SSB} = \frac{S_{in}/N_{in}}{S_{out}/N_{out}} = \frac{S_{in}}{\frac{1}{L_{sig}} \cdot S_{in}} \frac{\left[\frac{KT_o}{L_{sig}} + \frac{KT_o}{L_{im}} + \frac{KT_e}{L_{sig}} + \frac{KT_e}{L_{im}}\right]}{KT_o}$$

$$= \left(1 + \frac{L_{sig}}{L_{im}}\right)\left(1 + \frac{T_e}{T_o}\right) \qquad (4.1)$$

where KT_o is the input noise power per unit bandwidth from an input termination of T_o (290°K) and T_e is the noise contribution of the device to the total system output noise power, i.e., effective input noise temperature of the mixer. T_e is assumed to be constant over the frequency band that includes signal and image frequencies.

For the case where $L_{sig} = L_{im}$, the single sideband mixer noise figure is

$$F_{SSB} = 2\left(1 + \frac{T_e}{T_o}\right) \qquad (4.2)$$

The factor 2 would not appear in double sideband applications, where usable input signals are also received in the image frequency channel. Input noise power would contain equal contributions in the signal and image bands giving a total value in (4.2) of $2KT_o$. The 2's in the denominator and numerator cancel so that the double sideband mixer noise figure is

$$F_{DSB} = 1 + \frac{T_e}{T_o} \tag{4.3}$$

The noise figure of a mixer (single or double sideband) depends on its application. A particular mixer will have one noise figure when used in conventional communication and radar receivers and another when used for radio astronomy.

For many microwave and mm-wave mixers, the assumption of equal image and signal conversion losses is valid, and the difference in noise figure is 3 dB. If this assumption cannot be made, conversion losses must be measured at the signal and image frequencies.

The noise figure measurement of the mixer has been done basically by the manual Y-factor method using known excess noise ratio (ENR) of a solid state noise source at the LO power level 13.5 dBm.

The noise figure formula using the Y-factor is:

$$F = \frac{(T_2/T_o) - 1}{Y - 1} - \frac{Y[(T_1/T_o) - 1]}{Y - 1} \tag{4.4}$$

If $T_1 = T_o$, then

$$F = \frac{T_2/T_o - 1}{Y - 1} \tag{4.5}$$

But ENR can be defined by

$$ENR = \frac{T_2}{T_o} - 1 \tag{4.6}$$

Therefore, (4.7) yields the noise figure in dB.

$$F_{(dB)} = ENR_{(dB)} - 10 \log(Y - 1) \tag{4.7}$$

where the calibrated ENR is usually provided by the manufacturer [32] of the solid state noise source.

The measurement of the mixer noise figure was carried out with the setup shown in Figure 4-11. Since the input frequency (30 MHz) of the noise figure meter was too low to connect the output (900 MHz) of the mixer directly, another mixer to downconvert the IF was required. By switching the noise source on and off the Y-factor (8.2 dB) was obtained. And from the known ENR (14.8 dB) the mixer noise figure 6.6 ± .25 (DSB) was obtained by (4.7).

The single sideband mixer-receiver noise figure can be measured directly by inserting a filter between the noise source and the mixer. If the filter rejection at the image frequency is large enough, the term L_{sig}/L_{im} can be neglected. The SSB noise figure of the mixer

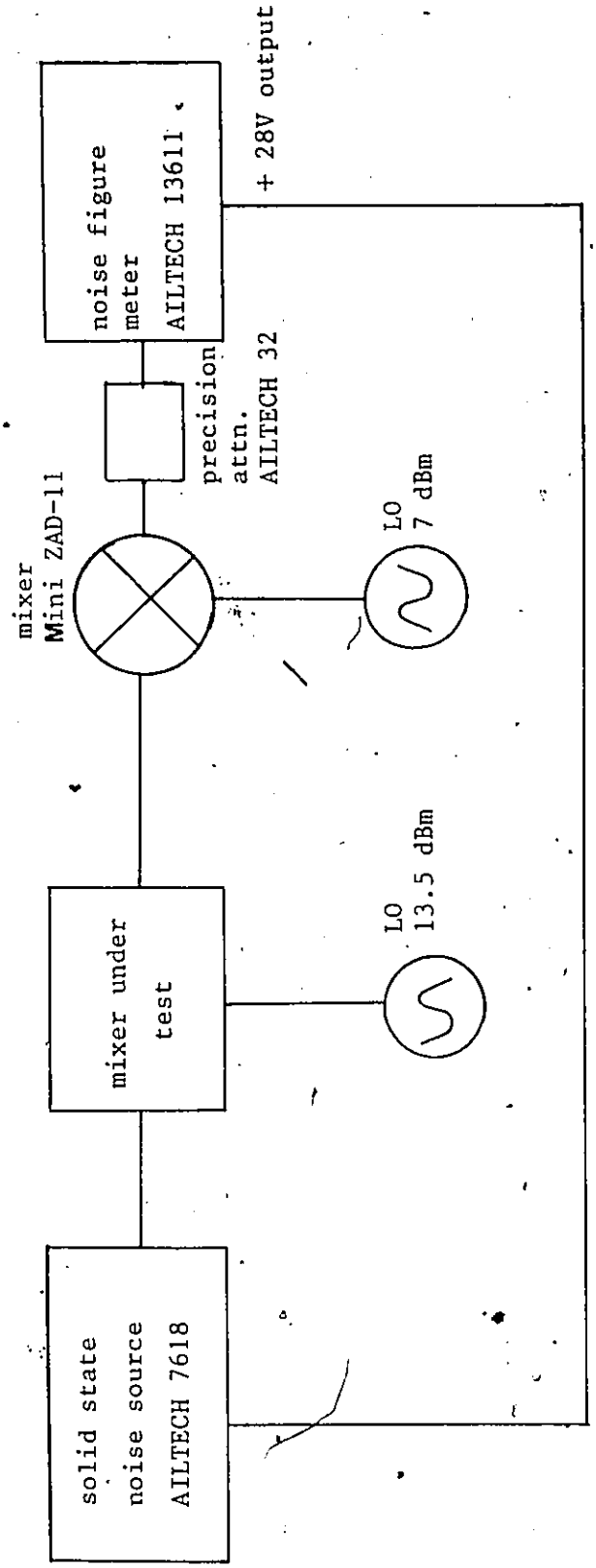

Figure 4-11. DSB mixer noise measurement setup.

is then assumed to be the measured noise figure minus the filter insertion loss. However, the impedance presented by the filter affects the mixer conversion loss at the signal frequency, the effective noise temperature and the impedance match at the IF terminal. In operation, with a broad-band resistive input termination, the termination provides a noise input at the image and other spurious frequencies that is not accounted for when measuring mixer noise figure with a filter. The effects of source impedance [33] on mixer performance is that insertion of the filter could change noise figure by several dB.

The only way to measure directly the noise figure of the SSB mixer having a resistive input termination is to use a filter and isolator with the Y-factor method using hot and cold loads.

4.6 Conclusion

The mixer characteristics were measured under various conditions in this chapter.

The low conversion loss (~4 dB) of the mixer is due to the use of high cutoff frequency (100 GHz) GaAs Schottky barrier diodes and to the low mismatch loss in the signal path.

In our noise figure measurement a source mismatch effect had to be considered when the noise source was switched on and off. Also to avoid the source mismatch effect an isolator was recommended by Mamola and Sannino [33].

CHAPTER 5

CONCLUSIONS

This chapter presents several special features of the mixer realized. Also future mixer design suggestions and trends for mm-wave receiver applications are briefly discussed.

5.1 Conclusions

The objective of this thesis was to design a single balanced mixer using planar technology at 17 GHz.

A planar mixer using a 180° hybrid has been realized with fin line and microstrip line components. The mixer presented can be fabricated at low cost in large quantities and shows very good performance particularly in terms of conversion loss. We expect that the circuit can be scaled down to 30 GHz without considerable degradation in performance.

Fin line transitions used in mixer design, unilateral and antipodal fin line transitions for input and LO ports, exhibit good VSWR characteristic. Compared with the other planar types of transitions, they have advantages, i.e., easy impedance transformation from waveguide to the other planar transmission line and to the active devices themselves.

The 180° hybrid combining the two planar transmission media also prevents to a high degree (30.5 dB isolation) of the radiation of the LO power through the RF port.

5.2 Suggestions and Trends

A balanced mixer configuration as described in this thesis is the preferred approach compared to a single-ended mixer since 20-30 dB of local oscillator noise suppression is provided as mentioned in Chapter 1. In radiometric receivers, where DSB mixers can be used, this suppression allows a lower IF band to be chosen, which generally reduces the system costs without degrading overall system performance.

However, for both communications and radar receivers, a preselector is required for image rejection and, therefore, a high IF frequency is normally selected to ease the design constraints that would be placed on this preselector. For this reason, single-ended mixers are very acceptable for the design of mm-wave systems.

It is possible to integrate a cavity-stabilized, solid state local oscillator with the mixer on the same substrate. A further step towards an increased degree of integration would be to construct the entire antenna/receiver subsystem on the same substrate. Therefore the entire integration of the mixer receiver subsystem including antenna and LO will clearly provide good cost effective design for applications requiring large quantities. The trend to integration of mm-wave subsystem or systems stimulates monolithic techniques.

One of the key elements that has attracted much attention in the mm-wave region has been the development of low noise mixers. The attainment of low noise performance has been accelerated by the availability of high cutoff frequency GaAs Schottky barrier mixer diodes and by the cryogenic cooling of mixer diodes.

At the time of writing, low noise GaAs FET amplifiers are available (up to around 30 GHz). If device technology is available, it is obvious that low noise GaAs FET amplifiers should be placed between the antenna and mixer to increase receiver sensitivity.

APPENDIX

CLOSED FORM EXPRESSIONS FOR FIN LINE DESIGN [37]

Meier's expressions for guided wavelength λ_g and characteristic impedance Z_o in fin line are [38]:

$$\lambda_g = \lambda[K_e - (\lambda/\lambda_{ca})^2]^{-1/2} \tag{A.1}$$

and

$$Z_o = Z_{o\infty}[K_e - (\lambda/\lambda_{ca})^2]^{-1/2} \tag{A.2}$$

where K_e is the equivalent dielectric constant, and λ is the free space wavelength. λ_{ca} and $Z_{o\infty}$ are the cutoff wavelength and characteristic impedance at infinite frequency of a ridged waveguide of the same dimensions. In order to determine K_e, we first obtain the cutoff wavelength of fin line (λ_{cf}) and the cutoff wavelength of the equivalent ridged waveguide (λ_{ca}). The equivalent dielectric constant at cutoff (K_c) is then simply given by

$$K_c = (\lambda_{cf}/\lambda_{ca})^2 \tag{A.3}$$

The equivalent dielectric constant K_e in (A.1) and (A.2) is assumed to have the following general form:

$$K_e = F(d/b,\ s/a,\ \lambda,\ \varepsilon_r) \cdot K_c \tag{A.4}$$

where the correction factor F must be determined such that (A.1) and (A.2) yield the results given in [39]-[43]. In the following, the analytical expressions for the required quantities are derived for a waveguide aspect ratio b/a = 0.5 containing dielectric substrates of ε_r = 2.22 and 3.0. They are valid in the normalized frequency range $0.35 \leq b/\lambda \leq 0.70$ suitable for most practical applications.

A. Cutoff Wavelengths

Meier's expressions require the knowledge of the cutoff wavelength λ_{ca} in an equivalent ridged waveguide, obtained by setting ε_r = 1.0. However, in order to keep the analytical expressions for λ_{ca} as simple as possible, we assume that the equivalent ridged waveguide is obtained by setting the substrate thickness equal to zero, which leads to identical expressions for λ_{ca} in the unilateral and bilateral case. The normalized cutoff frequency (b/λ_{ca}) is then given by

$$b/\lambda_{ca} = 0.245\ (d/b)^{0.173} \tag{A.5}$$

The normalized cutoff frequency (b/λ_{cf}) can be written in terms of the d/b and s/a:

$$b/\lambda_{cf} = A(d/b)^p(s/a)^q \tag{A.6}$$

For the range of structural parameters $1/16 \leq d/b \leq 1/4$ and $1/32 \leq s/a \leq 1/4$, the unknown constants in (A.6) are:

(i) For unilateral fin lines: ($\varepsilon_r = 2.22$)

$$A = 0.1748 \tag{A.7}$$

$$P = \begin{cases} 0.16\,(s/a)^{-0.07} & 1/32 \leq s/a \leq 1/20 \\ 0.16\,(s/a)^{-0.07} - 0.001\,\ln[(s/a) - (1/32)] & 1/20 \leq s/a \leq 1/4 \end{cases}$$

$$Q = -0.0836$$

(ii) For bilateral fin lines: ($\varepsilon_r = 2.22$)

$$A = 0.15 \tag{A.8}$$

$$P = \begin{cases} 0.225\,(s/a)^{-0.042} & 1/32 \leq s/a \leq 1/10 \\ 0.149\,(s/a)^{-0.23} + 0.1[(d/b) - (1/8)]^2 & 1/10 \leq s/a \leq 1/4 \end{cases}$$

$$Q = -0.14$$

The values of the normalized cutoff frequency for $\varepsilon_r = 3.0$ can be derived from the above results. We obtain:

(i) For unilateral fin lines: ($\varepsilon_r = 3.0$)

$$b/\lambda_{cf,\,3.0} = R(d/b,\, s/a)\cdot b/\lambda_{cf,\,2.22} + 0.1[(d/b) - (1/8)]^2 \tag{A.9}$$

(ii) For bilateral fin lines: ($\varepsilon_r = 3.0$)

$$b/\lambda_{cf,\ 3.0} = R(d/b,\ s/a)\cdot b/\lambda_{cf,\ 2.22} \qquad (A.10)$$

with

$$R = 0.9418 + 0.0754\ (d/b) - \\ - (s/a)[0.2813 + 0.35\ (d/b)^{.27} + (s/a)] \qquad (A.11)$$

Figures 1 and 2 compare the above expressions with numerical results obtained with the spectral domain technique. Results agree within ±1 % which inspires confidence in the above expressions.

B. Equivalent Dielectric Constant

Given the cutoff frequencies in fin lines and ridged waveguides of identical dimensions, the equivalent dielectric constant at cutoff K_c is calculated with (A.3). K_e is then obtained by multiplying K_c with a correction factor F. The expressions for F are:

(i) For unilateral fin lines: ($\varepsilon_r = 2.22$)

$$F = \begin{cases} [1.0 + 0.43\ (s/a)]\ (d/b)^{P_1} & 1/32 \le s/a \le 1/8 \\ [1.02 + 0.264\ (s/a)](d/b)^{P_1} & 1/8 \le s/a \le 1/4 \end{cases} \qquad (A.12)$$

where $P_1 = 0.096\ (s/a) - 0.007$ (A.13)

(ii) For unilateral fin lines: ($\varepsilon_r = 3.0$)

$$F = F' + 0.375\ (b/\lambda) - 0.2 \qquad (A.14)$$

with

$$F' = \begin{cases} 1.368\ (s/a)^{0.086}\ (d/b)^{P_1} & 1/32 \leq s/a \leq 1/8 \\ [1.122 + 0.176\ (s/a)]\ (d/b)^{P_2} & 1/8 < s/a \leq 1/4 \end{cases} \quad (A.15)$$

where $P_1 = 0.375\ (s/a) - 0.0233$

$$P_2 = 0.032 - 3.0\ [(s/a) - (3/16)]^2 \quad (A.16)$$

(iii) For bilateral fin lines: ($\varepsilon_r = 2.22$)

$$F = \begin{cases} 0.78\ (s/a)^{-0.098}\ (d/b)^{0.109} & 1/32 \leq s/a < 1/8 \\ [1.04 - 0.2\ (s/a)]\ (d/b)^{P_1} & 1/8 \leq s/a \leq 1/4 \end{cases} \quad (A.17)$$

where $P_1 = 0.152 - 0.256\ (s/a)$ (A.18)

(iv) For bilateral fin lines: ($\varepsilon_r = 3.0$)

$$F = \begin{cases} 0.975\ (s/a)^{-0.026}\ (d/b)^{P_1} & 1/32 \leq s/a < 1/8 \\ [1.0769 - 0.2424\ (s/a)]\ (d/b)^{P_2} & 1/8 \leq s/a \leq 1/4 \end{cases} \quad (A.19)$$

where $P_1 = 0.089 + 0.288\ (s/a)$

$$P_2 = 0.16 - 0.28\ (s/a) \quad (A.20)$$

Typical values of K_e computed with the above expressions at $b/\lambda = 0.3556$ are shown in Figures 3 and 4.

C. Characteristic Impedance

The definition of characteristic impedance in fin lines depends on the applications. We have used the voltage/current definition because it is practical in applications involving semiconductor devices [44]. It is given as follows:

$$Z_{o^{\infty}VI} = \frac{120\pi^2 \left(\frac{b}{\lambda_{ca}}\right)}{\frac{b}{d}\sin\frac{\pi s}{\lambda_{ca}} + \left[\frac{B_o}{Y_o} + \tan\frac{\pi(a-s)}{2\lambda_{ca}}\right]\cos\frac{\pi s}{\lambda_{ca}}} \qquad (A.21)$$

with $$\frac{B_o}{Y_o} = \frac{2b}{\lambda_{ca}}\left[\ln \csc\left(\frac{\pi d}{2b}\right) + \frac{Q\cos^4\left(\frac{\pi d}{2b}\right)}{1 + Q\sin^4\left(\frac{\pi d}{2b}\right)} + \right.$$

$$\left. + \frac{1}{16}\left(\frac{b}{\lambda_{ca}}\right)^2 \left[1 - 3\sin^2\left(\frac{\pi d}{2b}\right)^2 \cos^4\left(\frac{\pi d}{2b}\right)\right]\right] \qquad (A.22)$$

and $$Q = \left[1 - \left(b/\lambda_{ca}\right)^2\right]^{-1/2} - 1 \qquad (A.23)$$

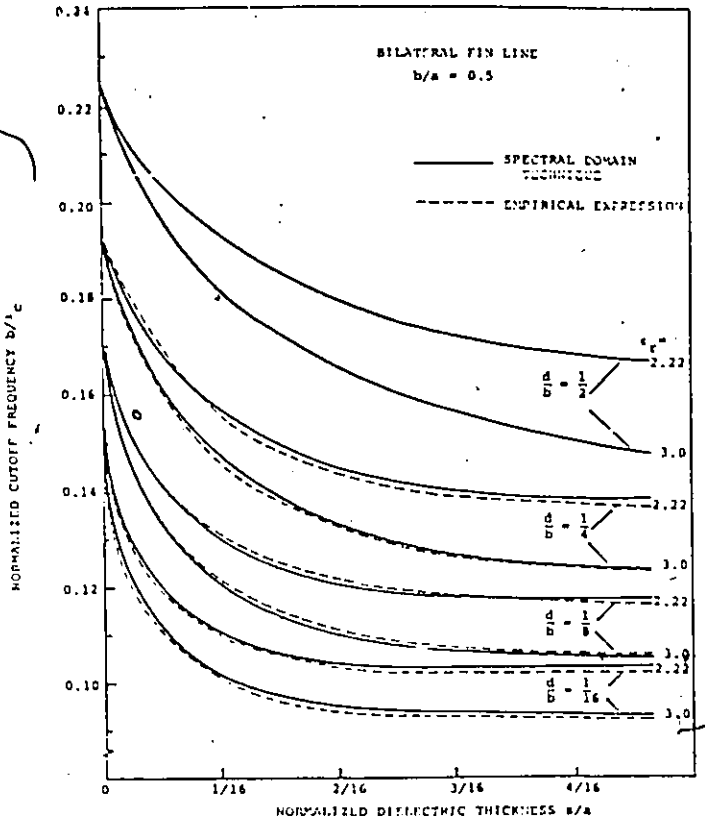

Fig. 1. Normalized cutoff frequency as a function of normalized dielectric thickness in bilateral fin lines.

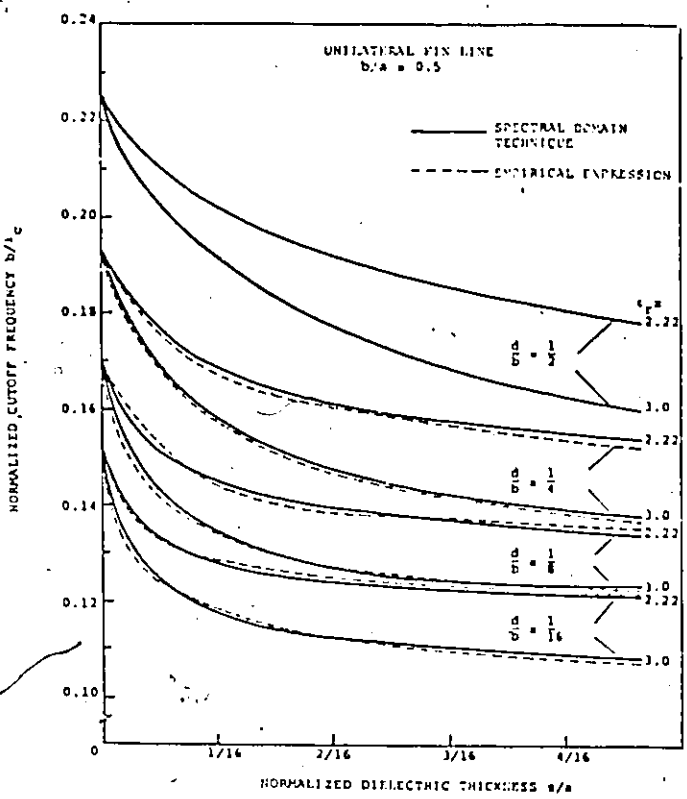

Fig. 2. Normalized cutoff frequency as a function of normalized thickness in unilateral fin lines.

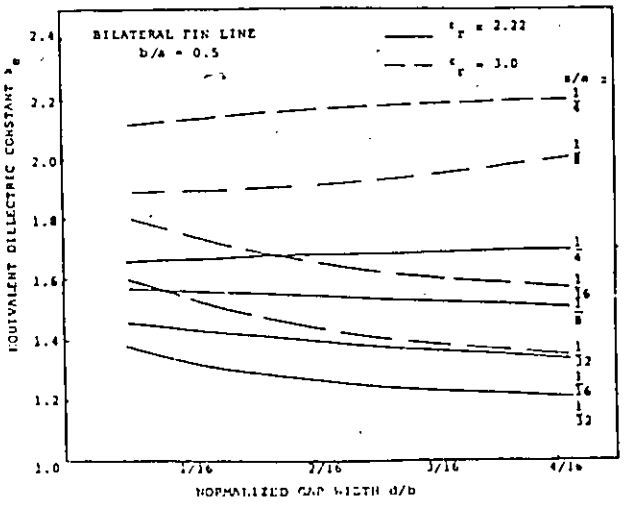

Fig. 3. Equivalent dielectric constant as a function of normalized gap width in bilateral fin line.

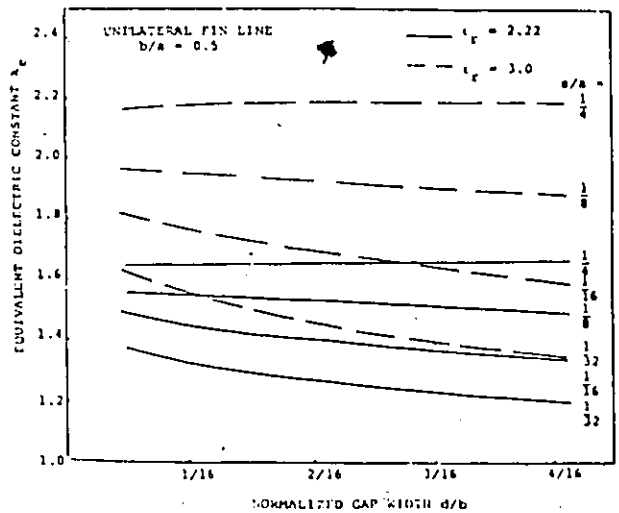

Fig. 4. Equivalent dielectric constant as a function of normalized gap width in unilateral fin lines.

REFERENCES

1. Torrey, H.C. and C.A. Whitmer, "Crystal Rectifiers", MIT Radiation Lab. Series, vol.15, New York, McGraw-Hill, 1947.

2. Messenger, G.C. and C.T. McCoy, "Theory and Operation of Crystal Diode as Mixers", Proc.IRE, vol.45, Sept. 1957, pp.1269-1283.

3. Howes, M.J. and D.V. Morgan, "Variable Impedance Devices", John Wiley & Sons, 1978.

4. Saleh, A.A.M., "Theory of Resistive Mixers", Research Monograph #64, MIT Press.

5. Abramowitz, M. and I.A. Stegun, "Handbook of Mathematical Functions with Formulas, Graphs, and Mathematical Tables, National Bereau of Standards— Applied Mathematics Series #55", Dover, New York, 1965, (Equation 9.7.1)

6. Reynolds, J.F., "Learn the Language of Mixer Specification", Microwaves, May 1978, pp.72-80.

7. Steiner, J.W., "An Analysis of Radio Frequency Interference due to Mixer Intermodulation Products", IEEE Trans. on Electromagnetic Compatibility, Jan. 1964, pp.62-68.

8. Bossard, B.B., P. Torrione, and S. Yuan, "Intermodulation Distortion in Mixers", U.S. Army Electronics Command, Contract DA-36-039-AMC-02345(E).

9. Anand, Y., "RF Burnout Dependence on Variation in Barrier Capacitance of Mixer Diodes", Proc. IEEE(Lett.), vol.61, Feb. 1973, pp.247-248.

10. Hackam, A. and J. Harrop, "Temperature Dependence of the Schottky Barrier Height in Gallium Arsenide", Solid State Communication, vol.11, Nov. 1972, pp.669-672.

11. Tyrrell, W.A., "Hybrid Circuits for Microwaves", Proc.IRE, vol.35, Nov. 1947, pp.1294-1306.

12. Robin, W.P., "Phase Noise in Signal Sources", IEEE Telecommunication Series 9, Peter Peregrinus Ltd., 1982.

13. Wrixon, G.T., "Select the Best Diode for Millimeter Mixers", Microwaves, vol.15, no.9, Sept. 1976, pp.56-60.

14. Saul, D.L., "Design a K_a-Band Polar Frequency Discriminator", Microwaves, April 1976, pp.74-80.

15. Kajfez, D. and S. Govind, "Effects of Difference in Odd- and Even-Mode Wavelengths on a Parallel-Coupled Band Pass Filter", Elec. Letters, March 6, 1975, pp.117-118.

16. Rubin, D., "Millimeter Wave Microstrip Varactor Tuned Oscillator", IEEE Trans. MTT, vol.MTT-24, Nov. 1975.

17. Krage, M.K. and G.I. Haddad, "Frequency-Dependent Characteristics of Microstrip Transmission Lines", IEEE Trans. MTT, vol.MTT-20, no.10, Oct. 1972, pp.678-688.

18. Akhtazad, S., T.R. Rowbotham, and P.B. Johns, "The Design of Coupled Microstrip Line", IEEE Trans. MTT, vol.MTT-23, no.6, June 1975, pp.486-492.

19. Hinton, J.H., "On Design of Coupled Microstrip Line", IEEE Trans. MTT, vol,MTT-28, no.3, March 1980, pp.272.

20. Gysel, U.H., "Circuit Aspects of Broadband Planar Millimeter Wave Mixers", 1973 IEEE International Symposium on Circuit and System Proceeding, pp.542-545.

21. Meier, P.J., "New Developments with Integrated Fin Line and Related Printed Millimeter Circuits", IEEE Symp. Digest MTT-S, 1975, pp.143-145.

22. Begemann, G., "An X-Band Balanced Fin Line Mixer", IEEE Symp. Digest MTT-S, 1978, Ottawa, pp.24-26.

23. Bates, R.N. and M.D. Coleman, "Millimeter Wave Fin Line Balanced Mixers", 9th EuMC, Brighton, 1979, Symp. Digest, pp.721-725.

24. Menzel, W. and H. Callsen, "Millimeterwellen-Empfänger in Finleitungstechnik", Wiss. Ber. AEG-Telefunken 54, Nr.4-5, 1981, pp.251-253.

25. Private Communication with Mr. John Pierre, Dept. Elect. Eng., Univ. of Ottawa.

26. Walker, R.M., "Waveguide Impedance Too Many Definitions", Electronic Communicator, vol.1, May/June 1966, pp.13.

27. Program for Fin Line Design in FORTRAN IV, Dept. Elect. Eng., Univ. of Ottawa.

28. Matthaei, G., L. Young, and E.M.T. Jones, "Microwave Filters, Impedance Matching Network, and Coupling Structures", Artech House Inc., 1980

29. Edwards, T.C., "Foundation for Microstrip Circuit Design", John Wiley & Sons, 1981.

30. Benedek, P. and P. Silvester, "Equivalent Capacitances for Microstrip Gaps and Steps", IEEE Trans., vol.MTT-20, no.11, Nov. 1972, pp.729-733.

31. Held, D.N., "An Approach to Optimal Mixer Design at Millimeter and Submillimeter Wavelengths", Microwave Symposium 1979, pp.25-27.

32. Operation and Service Manual of AIFTECH 7600 Series Noise Generators.

33. Mamola, G. and M. Sannino, "Source Mismatch Effects on Measurements of Linear Two-Port Noise Temperatures", IEEE Trans. Instrumentation and Measurement, vol.IM-24, no.3, Sept. 1975.

34. March, S., "Microstrip Packaging: Watch the Last Step", Microwaves, Dec. 1981, pp.83-98.

35. March, S., "Final Corrections", Microwaves, July 1982, pp.8.

36. Hammerstad E. and O. Jensen, "Accurate Models for Microstrip Computer-Aided Design", 1980 IEEE MTT-S International Symposium Digest, June 1980, pp.407-409.

37. Sharma, A.K. and W.J.R. Hoefer, "Empirical Analytical Expressions for Fin Line Design", 1981 IEEE MTT-S International Symposium Digest, pp.102-104.

38. Meier, P.J., "Integrated Fin Line Millimeter Components", IEEE Trans. MTT, vol.MTT-22, Dec. 1974, pp.1209-1216.

39. Hofmann, H., "Dispersion of Planar Waveguides for Millimeter Wave Applications", AEÜ, vol.31, Jan. 1977, pp.40-44.

40. Knorr, J.B. and P.M. Shayda, "Millimeter Wave Fin Line Characteristics", IEEE Trans. MTT, vol.MTT-28, July 1980, pp.737-743.

41. Schmidt, L.P. and T. Itoh, "Spectral Domain Analysis of Dominant and Higher Order Modes in Fin Lines", IEEE Trans. MTT, vol.MTT-28, pp.981-985.

42. Beyer, A. and I. Wolff, "A Solution of the Earthed Fin Line with Finite Metallization Thickness", 1980 IEEE MTT-S Int. Microwave Symposium Digest, Washington, D.C., pp.258-260.

43. Sharma, A.K., G.I. Costache, and W.J.R. Hoefer, "Cutoff in Fin Lines Evaluated with the Spectral Domain Technique and with the Finite Element Method", 1981 IEEE AP-S Int. Antenna and Propagation Symposium Digest, Los Angeles.

44. Meinel, H. and B. Rembold, "New Millimeter Wave Fin Line Attenuators and Switches", 1979 IEEE MTT-S Int. Microwave Symposium Digest, Orlando, pp.249-252.